3-12-2004

Evaluating the Navigation Potential of the National Television System Committee Broadcast Signal

Ryan J. Eggert

AFIT/GE/ENG/04-08

EVALUATING THE NAVIGATION POTENTIAL OF THE NATIONAL TELEVISION SYSTEM COMMITTEE BROADCAST SIGNAL

THESIS

Ryan J. Eggert
Second Lieutenant, USAF

AFIT/GE/ENG/04-08

DEPARTMENT OF THE AIR FORCE

AIR UNIVERSITY

AIR FORCE INSTITUTE OF TECHNOLOGY

Wright-Patterson Air Force Base, Ohio

APPROVED FOR PUBLIC RELEASE; DISTRIBUTION UNLIMITED.

The views expressed in this thesis are those of the author and do not reflect the official policy or position of the United States Air Force, Department of Defense, or U.S. Government.

AFIT/GE/ENG/04-08

EVALUATING THE NAVIGATION POTENTIAL OF THE NATIONAL TELEVISION SYSTEM COMMITTEE BROADCAST SIGNAL

THESIS

Presented to the Faculty

Department of Electrical and Computer Engineering

Graduate School of Engineering and Management

Air Force Institute of Technology

Air University

Air Education and Training Command

In Partial Fulfillment of the Requirements for the

Degree of Master of Science in Electrical Engineering

Ryan J. Eggert, B.S.E.E.

Second Lieutenant, USAF

March, 2004

AFIT/GE/ENG/04-08

EVALUATING THE NAVIGATION POTENTIAL OF THE NATIONAL TELEVISION SYSTEM COMMITTEE BROADCAST SIGNAL

Ryan J. Eggert, B.S.E.E.
Second Lieutenant, USAF

Approved:

//SIGNED//	12 Mar 04
Dr. John F. Raquet Thesis Advisor	Date
//SIGNED//	12 Mar 04
Dr. Michael A. Temple Committee Member	Date
//SIGNED//	12 Mar 04
Dr. Meir Pachter Committee Member	Date

Acknowledgements

First and foremost, I want to extend my thanks to everyone who has supported me and my efforts during this thesis. Many of you will go unnamed individually, but your support is far from unappreciated.

I extend my utmost gratitude and appreciation to my fiancée. She has encouraged and supported all of my efforts, and I certainly would not have experienced the success I've had without that support. She has always found the ways to make everything seem possible. No words can ever do justice to what she deserves, but I hope she knows how much it all means to me.

I also thank and cherish the support from all of my family. They too have stood by my side and provided all they could. A part of everything I am is, and will always be, because of you.

I owe much thanks to my advisor, Dr. John Raquet. His insights and guidance were instrumental in the success of this research, despite the frustration that has seemed to follow our meetings (especially those recently during the writing).

I certainly cannot exclude my fellow students, especially the guys from the lab: José, Jonathan, and Jacque. Working together with each of you has provided some warm memories surrounding the past 18 months.

I thank and value the guidance and insights from my thesis committee.

I thank the United States Air Force for providing the time and financial resources of my educational experiences.

Finally, I cannot exclude the two gent's who have been with me through it all. Together, we made sure none of us would falter. Never did we let each other lose sight of what was truly important, no matter how bad it got. So in case I've never stated it, thanks for everything.

Ryan J. Eggert

Table of Contents

Page

List of Figures

List of Tables

Abstract

The accuracy and worldwide availability of the Global Positioning System (GPS) make it the dominant system for navigation and precise positioning. Unfortunately, many situations arise in which GPS may not be adequate, e.g., urban navigation. This research evaluates the navigation potential of the National Television System Committee (NTSC) broadcast signal using a time-difference-of-arrival (TDOA) algorithm. TDOA measurements are made using NTSC broadcast signals collected from low and high multipath environments. These measurements are then used to evaluate the severity and dynamic effects of NTSC broadcast multipath signals. Three data reduction algorithms were developed–one that modifies the classical cross-correlation TDOA approach, and two that difference the signals' time-of-arrival at each receiver. Each algorithm was evaluated for consistency and accuracy in each environment. Multipath mitigation was demonstrated using a locally fabricated antenna.

Collected NTSC broadcast signal samples reveal TDOA measurement errors ranging from 1 to 200 meters, with typical errors between 10 and 40 meters. Multipath was shown to be the dominant error source. However, errors due to the particular hardware configuration used in this research were also significant. Simple multipath mitigation techniques were able to reduce these errors, and analyses of the received waveforms provide the foundation for developing additional active multipath mitigation techniques.

Simulations using eight television station locations near Dayton, Ohio reveal 40 meter position accuracy with the typical range errors found in this research. Extreme measurement errors from high multipath areas reduced this accuracy to 100 meters. Additionally, using the same transmitter geometry, simulation results showed that TDOA measurement accuracies of 5 to 10 meters were required to provide position estimates with 10 meter accuracy–the accuracy of readily available single frequency GPS receivers.

EVALUATING THE NAVIGATION POTENTIAL OF THE NATIONAL TELEVISION SYSTEM COMMITTEE BROADCAST SIGNAL

I. Introduction

This chapter provides the necessary background for researching the navigation potential of the National Television System Committee (NTSC) broadcast signal, including background, problem definition, and assumptions made to limit the scope of the research. Following this, a review of other similar research is made, and, finally, the remaining chapters in this Thesis are outlined.

1.1 Background

The accuracy and worldwide availability of the Global Positioning System (GPS) makes it the dominant system for navigation and precise positioning. Unfortunately, many situations arise in which GPS may not be adequate. First, the low signal power does not provide reliable reception indoors, under dense foliage, or in large urban areas. Second, despite many security measures, including encrypting one of the two coding waveforms, local or widespread degradation could result from intentional or unintentional interference. Finally, GPS is only a single system; an unexpected system failure could render the system inoperable. While other systems, such as an inertial navigation system (INS), can provide accurate short-term navigation solutions, they can not provide any absolute position capabilities. Additional systems must be employed to ensure the current capabilities are not degraded in any environment or under any circumstances.

One category of sources with navigation potential are signals of opportunity, or signals with another purpose that could be exploited for navigation with no affect on their primary users. Two readily available signals with characteristics suitable for navigation are the IS-95 Digital Cellular Network [1] and the NTSC broadcast signal [2].

The IS-95 Digital Cellular Network utilizes many signals, including a forward channel (transmissions from the cellular tower to the individual users), a reverse channel (transmissions from the users to the cellular tower), and a pilot channel (a coded signal allowing the users to synchronize with the system). The pilot channel offers the best navigation potential. It repeatedly transmits a 32,767 bit pseudorandom "short" code 37.5 times a second [3]. Because the bit pattern and modulation techniques of this signal are known, correlation properties can be used to estimate the signal's time of reception. If four or more independent signals are available, this data can be used to determine position. Unfortunately, the IS-95 network requires GPS for time-synchronization, so it is not practical as an alternative for GPS.

The NTSC television broadcast does not require GPS for time-synchronization. Rather, each television station is independent and transmits its own alignment (or synchronization) data. Specifically, a vertical blanking field is transmitted 60 times a second to reset the display to the top of the screen, along with a series of horizontal synchronization pulses to indicate the start of each line [4]. As these two pieces of the signal are known, they can be exploited for passive navigation. Specifically, the received signal can be correlated with a copy of the analytic signal to estimate the time of arrival. These times can then be processed to determine ranges and, ultimately, position through multi-lateration techniques.

In comparison to GPS, the NTSC broadcast signals have many advantages. First, NTSC broadcast signals are transmitted with more power than GPS signals. GPS satellites use approximately 50 Watts of power for all transmitted signals [5]. NTSC transmitters can transmit in excess of 5 MegaWatts, depending on channel

selection and height above ground [4]. Second, the NTSC transmitters primarily use stationary land-based locations, whereas GPS uses up to 32 satellites in a medium earth orbit [5]. This not only provides stronger signals indoors and in large urban areas where buildings and other large structures can block signals, it eliminates some of the errors introduced by space-vehicle position and atmospheric affects. Next, the NTSC video signal has an approximate bandwidth of 4 MHz [4], while the unclassified course/acquisition (C/A) code has a bandwidth of only 2 MHz [5]. The higher the bandwidth, the sharper the edges and corners of a waveform can be. As the intent of this research is to use the sequences of analog pulses transmitted in a correlation algorithm, the sharpness of the signal is important for accurate measurements. Finally, the NTSC broadcast is available at many frequencies ranging from 54 to 800 MHz; GPS signals are only available at 1227.6 and 1575.42 MHz. The wide range of frequencies improves system operability by giving the potential to avoid interference at a single frequency.

1.2 Problem Definition

The time-difference-of-arrival (TDOA) navigation system is a range-based method of determining position. To eliminate the need for any time synchronization in the signal, two receivers are used: a reference receiver and a target receiver. The reference receiver is stationary at a known location; the target receiver is at the point of interest. Initially, both receivers acquire the desired signals (from sources with known points of origin). Then, the reference receiver provides the time-tagged data to the target receiver so it can determine how much more or less time the signal took to get to the target receiver than the reference receiver. Then, using the speed of light, this time difference is converted to distance. These measurements, described as TDOA measurements in this research, tell how much nearer to or farther from the signal source the target receiver is compared to the reference receiver. However, because both the signal source and reference receiver have known locations, these

TDOA measurements can be converted to the actual distance between the signal source and target receiver. In reality, there is normally a differential receiver clock error that must also be accounted for, so the distance (or range) is actually a "pseudorange" (combination of range plus clock error). These pseudoranges can then be processed in a multi-lateration algorithm to determine position and clock errors. While receiver clock error is often not a desired system output, it must be estimated to accurately determine the difference in propagation times to each of the receivers.

The primary goal of this research is to analyze the feasibility of using the NTSC broadcast signal in a TDOA navigation system. Specifically, the signal's availability and performance in indoor and outdoor environments are studied. Performance is studied by analyzing the correlation results and the accuracy of the time-difference data. These results are then used to determine potential navigation accuracy from a TDOA navigation system.

A second research goal is to optimize the data transmitted from the reference receiver to the target receiver. As discussed above, the reference receiver must provide the target receiver with the time-tagged data so it can determine the time difference and, ultimately, range. As this research uses a signal with known characteristics, the actual signal does not have to be time-tagged and sent to the target receiver. Rather, both receivers only need to record the time at which the predefined events occur. Then, the reference receiver provides the times at which the events occurred to the target receiver, which then differences the arrival times for the predefined events to provide the time difference. Unfortunately, potential data (and accuracy) is lost using this technique. This research aims to evaluate how much improvement can be gained by transmitting segments of time-tagged data to the target receiver (at the cost of more dataflow), compared to just providing signal's time of arrival.

1.3 Assumptions

As with any research, countless topics of interest could be studied. To focus on the main objective (analyzing the navigation potential of the NTSC broadcast signal), many assumptions are made concerning different parts of the system. Each of these are discussed below, along with the potential effects to the system.

1.3.1 Errors. To achieve a perfect estimate of position, all data must not contain any errors. Potential error sources dismissed in this research are:

1.3.1.1 NTSC Transmitter Location. Transmitter location is used to calculate the range between the transmitter and reference receiver. As the final pseudorange estimate is then based upon this range calculation, transmitter location errors may or may not affect the final position estimate depending on the system's geometry. To better understand this, an illustration for one transmitter and both receivers is shown in Figure 1.1, where "R" represents the true ranges between the transmitter and receivers, "r" represents the assumed ranges, and the error in the projection of the assumed range onto the true range is shown by the heavy lines. Ultimately, if these projection errors have equal magnitudes, the transmitter location error will not affect the final position estimate. Furthermore, if the transmitter location error (B) is much smaller than the range between the transmitter and receivers, the amount of error introduced into the final position estimate is negligible. Both of these claims are developed below.

First, the relationship between the true ranges, assumed ranges and transmitter location error is defined using the notation corresponding to Figure 1.1.

$$R_{TAR} = r_{TAR}cos(\Theta_1) + Bsin(\Phi_1) \tag{1.1}$$

$$R_{REF} = r_{REF}cos(\Theta_2) + Bsin(\Phi_2) \tag{1.2}$$

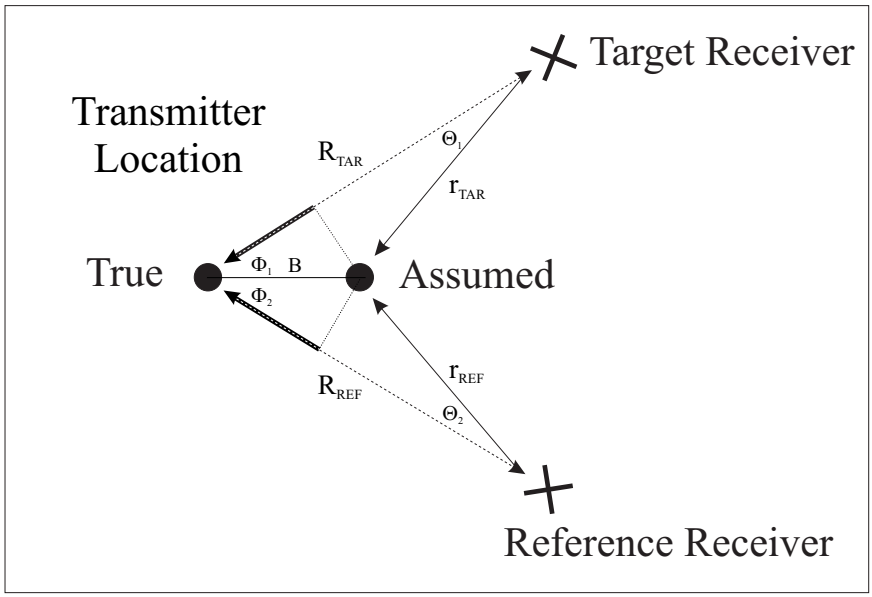

Figure 1.1: Transmitter Location Error Scenarios

Then, the TDOA measurement is computed from the assumed ranges and defined in terms of the true ranges and errors.

$$\begin{aligned}\widehat{TDOA} &= r_{TAR} - r_{REF} \\ &= \frac{R_{TAR} - Bsin(\Phi_1)}{cos(\Theta_1)} - \frac{R_{REF} - Bsin(\Phi_2)}{cos(\Theta_2)}\end{aligned} \tag{1.3}$$

where the error free TDOA measurement is $R_{TAR} - R_{REF}$, the projection from the true position to the assumed position is $\frac{1}{cos(\Theta)}$, and the range error is $Bsin(\Phi)$. Thus, if the range error term is equal, there an no affects on the final position (again because the pseudorange is based on the assumed position, not the true position). And if the transmitter location error, B, is small, the differences between the calculated TDOA measurement and the true TDOA measurement are negligible. (Using the Law-of-Sines, if B is much less than than r, angles Θ and Φ must be small. Thus, the sine term is approximately zero and the cosine term is approximately one.)

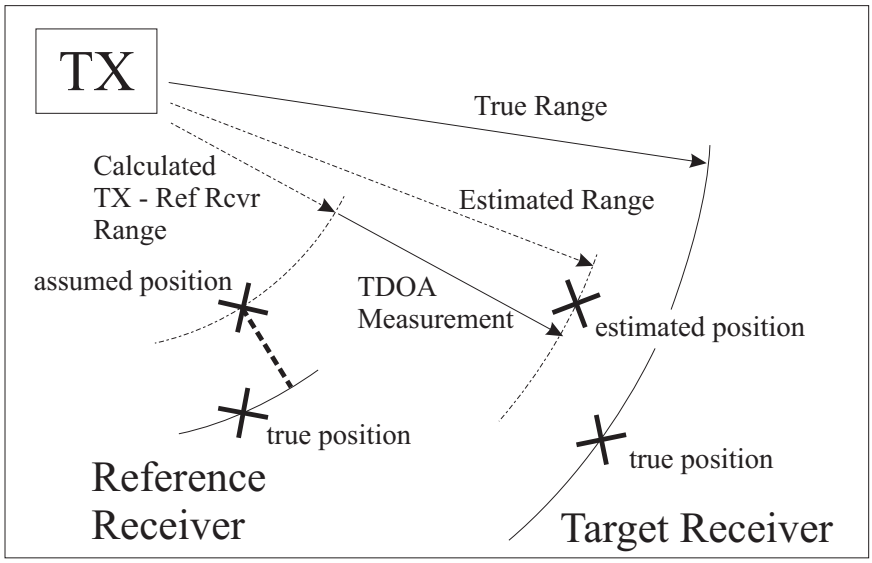

Figure 1.2: Reference Receiver Errors

The baselines used in this research are considerably less than the distance to the transmitters. Therefore, dismissing the error caused by the transmitter location error is justified.

1.3.1.2 Reference Receiver Location. Unlike the errors in transmitter location, reference receiver location errors can significantly affect the final position estimate of the target receiver. To determine the significance of this error, it must be separated into two components: (1) the portion perpendicular to the radial of the transmitter, and (2) the portion about this radial (or pointing away from the transmitter), see Figure 1.2. The amount of reference receiver error in this second component (shown by the heavy dashed line) directly carries into the pseudorange estimate between that transmitter and the target receiver.

All reference receiver locations used in this research are calculated using differential GPS techniques with millimeter level accuracies. The magnitude of the errors caused by this data, therefore, is negligible.

1.3.1.3 Processing Delays. Time delays are introduced by the processing and propagation delays inside each receiver. The reference and target receivers have the same hardware and test setups, thus these delays are nearly identical. The delay common to both receivers is directly removed by the differencing in the algorithm. The slight difference between the delays, however, is not eliminated. The algorithm estimates this difference, but errors in this estimate produce an error in the TDOA measurements. To the extent possible, these delays will be compensated for in processing. After compensation, this research will assume all processing and propagation delays are the same and do not induce any time errors.

1.3.2 Secure Data Link. The data link between the reference receiver and the target receiver is assumed real-time and error free. Thus, the target receiver has the implied ability to determine errors in the reference receiver data. However, to ensure the target receiver remains passive, a method of requesting erroneous data be repeated was not designed; rather, the data is simply dismissed and processing resumes with the next set of data. If a data repeat system were to be implemented in a real time navigation system, the process of determining errors, requesting the data be repeated, waiting for the reference receiver to process the request and retransmit the data, and then finally processing the data would all have to be accomplished in less time than the interval between measurements. The rapid availability of signal measurements justifies dismissing errors and continuing processing with the next data set.[1]

1.3.3 Synchronization. All levels of synchronization required are assumed and performed manually during analysis. Most notable is the target receiver's ability to difference the proper measurements for the TDOA calculations.

[1]Reference Section 2.2 for a detailed description of the NTSC Television Broadcast Signal

1.3.4 Coordinate Frame. Three-dimensional calculations requiring a specific location use the Earth-Centered Earth-Fixed (ECEF) coordinate frame. Two-dimensional calculations, performance comparisons, and error analysis results are converted to a local level (East-North-Up) reference frame to provide more intuitive results for the reader.

1.4 Related Research

Many methods of providing navigation data have been implemented using various techniques. This section first outlines other navigation systems that use TDOA methods and then describes other radio-location and non-radio-location techniques. It concludes by detailing the work done by others for using television signals as a navigation source.

1.4.1 Other TDOA Systems. TDOA position estimation systems have been successfully implemented in the past. This section will discuss two implementations of the TDOA algorithm: (1) a single receiver with two synchronized transmitters, as used by the Long Range Navigation (LORAN) system [6], and (2) a single transmitter with multiple receivers, as used by the NAVSYS Corporation's GPS Jammer and Interference Location System [7].

1.4.1.1 LORAN. Loran is a radio-navigation system that was developed in the 1940s by the Radiation Laboratory of the Massachusetts Institute of Technology for aircraft navigation and ships navigating coastal waters [6]. Users estimate the TDOA of low-frequeny pulses from multiple synchronized transmitters to determine a set of possible position estimates. Then, provided enough measurements are available, the intersection of the possible positions is the final position estimate [6, 8].

The possible position estimates from each measurement form one of two hyperbolas about the transmitters. While the mathematics of this curve are not discussed,

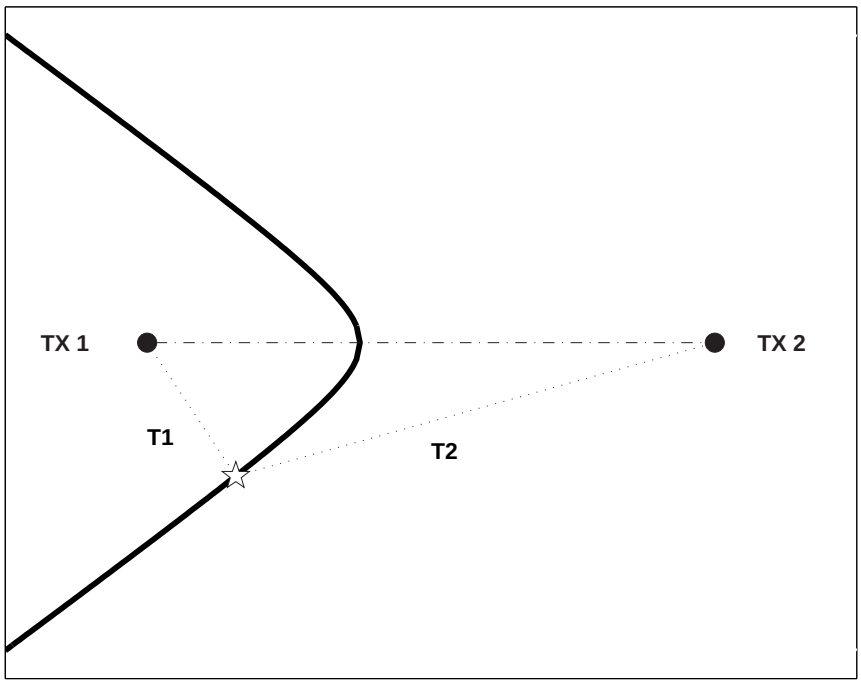

Figure 1.3: Locus of Possible Positions from Single Time-Difference Measurement in a Hyperbolic Navigation System

the only information needed to create the curve are the baseline between the transmitters and the TDOA measurement (converted to distance). Inherent in the TDOA measurement is knowledge about which signal arrived first. This determines which of the two hyperbolas must be used. When the constant time-difference, T2-T1 in Figure 1.3, is plotted for all transmitter pairs in the system, the point where all the hyperbolas intersect (not shown), is the final position estimate.

1.4.1.2 GPS Jammer and Interference Location System. The GPS Jammer and Interference Location System developed by NAVSYS uses multiple receivers at known locations to estimate the position of a single transmitter. In this scenario, two aircraft use modern GPS equipment with the ability to record "a snapshot of GPS data when in the presence of a jammer signal" [7]. This data can then be processed to isolate and cross-correlate the interfering signal from both receivers. The resulting TDOA and FDOA (Frequency-Difference-of-Arrival) mea-

surements allow the receivers, when enough measurements from additional aircraft or by the aircraft moving (assuming a stationary source) are available, to estimate the interfering source's (or sources') position estimate [7].

1.4.2 Other Radiolocation Position Estimation Methods. Three additional radiolocation techniques for estimating the position of a mobile receiver are: (1) signal strength measurement, (2) time of arrival (TOA), and (3) angle of arrival (AOA) – with TOA and AOA being the more feasible methods. [9]

1.4.2.1 TOA. TOA is a multi-lateration technique that calculates a range estimate based upon the propagation time of a signal. Specifically, the receiver knows a priori what time the signal is transmitted and uses the local clock to determine propagation time. One constraint to the TOA system, however, is that all transmitters must be time synchronized. With all transmitters synchronized, the receiver clock does not have to be synchronized for the error is the same for all transmitters. Thus, adding an additional measurement beyond those required for the position estimates allows this value to be calculated and eliminated from the measurements.

One example of this system is GPS. Each of the satellites transmit the Course/Acquisition code every millisecond on the millisecond. To ensure time synchronization, very stable clocks are used on each satellite, and a "Control Segment" monitors and corrects any clock errors [5].

1.4.2.2 AOA. The AOA technique estimates the direction (or azimuth) to at least two known signal sources (for a two-dimensional position estimate) and then triangulates the user's position based upon these estimates. The principal benefits of this system are: (1) it is passive, (2) it does not require extremely accurate time synchronization, and (3) it can easily combine many different signals of opportunity. Unfortunately, its accuracy is very range sensitive. As the signal source

becomes farther away from the target receiver, errors in the direction measurement produce larger position estimate errors. [10]

Each signal direction is estimated by comparing either the carrier-phase or signal amplitude at multiple calibrated antennas, known as an interferometer [11]. While the phase comparison method is generally more complex than the amplitude method, it is more accurate. A two antenna phase-comparison interferometer can produce an angle estimate with sub-degree accuracy. Furthermore, the results from this system are unambiguous; a one-to-one relationship exists between the signal phase and azimuth angle [11]. Thus, the user does not have to account for the possibility of tracking the back-azimuth (or the vector pointing away from instead of towards the source).

An example of this system is another approach NAVSYS has taken in the GPS Jammer and Interference Location System. This approach uses a Controlled Radiation Pattern Antenna (CRPA) to identify and eliminate (or reduce) the antenna gain in the direction of an interfering source (inherently providing a bearings measurement from the antenna to the source as well). Then, as the receiver antenna moves, the bearing to the source will also change and provide the additional bearings necessary to estimate the source's position (assuming it is stationary) [7].

A more historic example of this type of system is how a ship determines it's position in coastal waters. Bearings (or compass headings) are measured to at least two lighthouses or stationary bouyes (whose locations are indicated on navigation charts). These bearings are then plotted on the navigation chart to estimate position. As stated above, two bearings will provide a position estimate in the two-dimensional case (assuming they intersect). However, errors in both the measurement and plotting process will degrade the accuracy. To help reduce this error, a third bearing is often measured and plotted. Assuming that all measurements and plots are equally accurate, the center of the resulting triangle is the estimated position, see Figure 1.4.

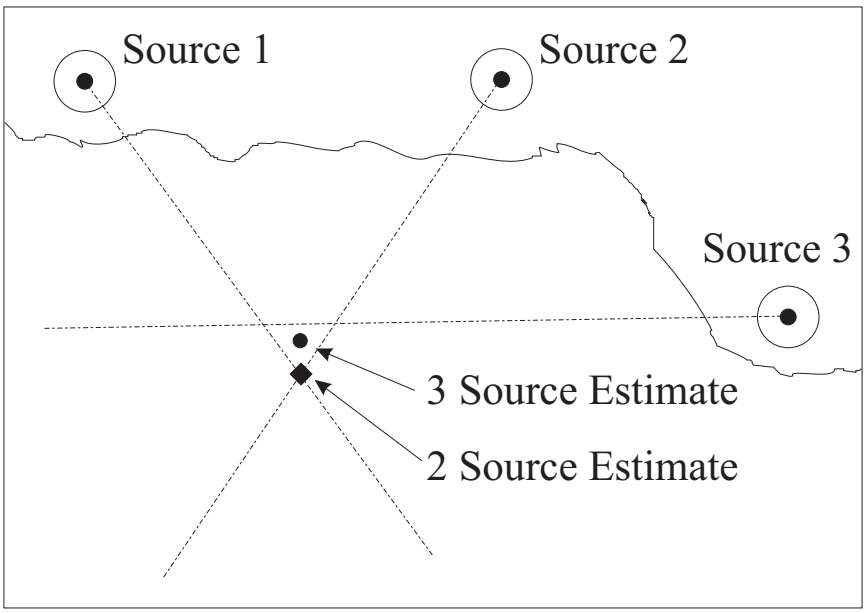

Figure 1.4: AOA Position Estimate Technique using 2 or 3 Bearing Measurements

1.4.2.3 Hybrid Systems. While the systems discussed above are capable of functioning independently, research has shown that hybrid systems using AOA and either TOA or TDOA perform better than a system using only one type [12]. One distinct advantage is the potential decrease in processing time. The iterative techniques often used to solve the multi-lateration systems require an initial location estimate and could take several iterations to achieve the desired accuracy. Besides taking many iterations, if the initial estimates are not accurate enough, the system may not be able to converge on a single solution. However, if the AOA position estimate can be solved quickly, it can provide the initial estimate for the multi-lateration algorithm. The two results can then be combined to form the final position estimate. [10, 13]

In general, a system using two independent and equally accurate estimates of the same parameter can expect a $1/\sqrt{2}$ factor of improvement in accuracy, compared to just one estimate. While the multi-lateration and triangulation techniques are not completely independent (many sources of error could affect both), they do use

different parameters to derive the position estimate. The multi-lateration techniques use information embedded in the signal (predefined bit patterns, waveform structure, etc), while the triangulation techniques use the carrier-phase–regardless of the data modulated onto the carrier. Thus, a proper combination of these two estimates improves the accuracy of the overall position estimate.

1.4.3 Non-Radiolocation Position Estimation Systems. Each of the systems discussed in Section 1.4.2 have all used data transmitted by radio signals. Many other "signals" can be used to navigate and/or estimate position. For example, we all perform our daily lives by the images seen by our eyes, sounds heard by our ears, and, possibly, the scents detected by our nose. This section discusses two other methods of generating position estimates: terrain reference navigation (TRN) and optical measurements.

1.4.3.1 TRN. TRN is primarily intended for airborn navigation and involves correlating the current terrain under the aircraft with prestored terrain data. The current terrain data can be calculated many ways depending on the object being positioned, but usually involves altitude measurements from a barometric altimeter or similar device. Unfortunately, this system only performs well in terrain with a unique known profile [14]. Large areas with similar characteristics, such as flat fields, generally don't allow high accuracy. One way to overcome this situation is to use scene matching area correlation [15]. This technique is an automated method of finding distinct features of the terrain and locating them on a map. Unfortunately, both of these systems require much a priori information about the environment. Additionally, some of the data-collection may require active sensors which compromises the ability for passive navigation. [14, 16]

1.4.3.2 Optical Measurements. Visual navigation, or position estimation using optical measurements, includes map based, natural landmark based,

and artificial landmark based forms [17]. After detecting the desired object, azimuth and/or elevation angle measurements are taken to triangulate the position estimate. More recent research extends this method for use with objects of unknown location [18]. While this new method provides only relative position information, if the initial position is known, this method also estimates the absolute position. Advantages of this method are that it is passive and nearly any discernable object (corner of a building, distinct landscape, etc) produces the needed measurements. Unfortunately, the measurements are easily impaired by clouds, smoke, or a bright light "blinding" the camera.

1.4.4 Other Navigation Systems Using Television Signals. This research is not the first attempt at using television signals as a navigation source; other methods have been proposed and/or attempted. This section discusses three of these attempts, with emphasis placed on the most recent attempt by the Rosum Corporation.

1.4.4.1 TELENAV. Exploiting television signals for navigation was first proposed in the TELENAV system [2]. This system sought to implement a TDOA system using synchronized transmitters and a single receiver (similar to LORAN), and chose to exploit television signals for their radiated power levels, typical placement of antennas on high ground, decreased financial burden by using the existing system, and rapid availability of measurements. TELENAV's TDOA measurements were made by correlating with the known color burst signal to avoid potential problems with the rectangular synchronization pulses and allowed tolerances. Specifically, the television signal (after synchronization) was to be gated–allowing only the color burst signal–and then correlated against a known signal to find the TOA. The TDOA measurement was then calculated from the synchronized sources and the hyperbolic curve of possible position estimates was created. Again, after enough measurements were available, the final position could be estimated [2].

TELENAV was never fully implemented, but testing was performed using two pairs of television transmitters in the Palm Beach and Miami, Florida areas. The resulting TDOA measurements, generated by averaging 1000 measurements from successive color-burst correlations, had spreads of 10.1 and 14.2 nanoseconds, or 3.0 and 4.3 meters, respectively. Most of the individual measurements also fell within this range. The outliers were analyzed and generally attributed to multipath interference from aircraft on flight paths within a mile of the receiver.

1.4.4.2 Tokyo University. Antoher exploitation of television signals for navigation was the evaluation of a single receiver system for ship locations in Tokyo Bay by the Laboratory of Communication Engineering, Tokyo University of Mercantile Marine [19]. This system used television signals from geostationary satellites as well as a land-based tower to calculate relative positions. The differences in propagation time were derived from a gated counter that used a local oscillator to start the counter and the rising edge from the received signal to stop the counter. Specifically, when active, the gated counter counted the zero-crossings of a 60 MHz sinusoid to determine the change in propagation time with a resolution of 2.5 meters per measurement. The gate stopping signal was the eleventh rising edge of the synchronizing pulses and was extracted from the signal by dedicated hardware.

The RMS error of 240 position estimates of a moving ship, using GPS data as truth, was 9.7 meters longitudinally and 6.4 meters latitudinally. For comparison, the RMS error of a static location was 2.9 meters longitudinally and 14.5 meters latitudinally.

1.4.4.3 Rosum Corporation. The Rosum Corporation's TDOA algorithm for estimating user position (namely a cellular telephone) uses the start of each digital television (DTV) segment as a timing signal (known as synchronization segments). Due to the lower frequency and higher power (compared to GPS and cellular signals), these signals are well suited for both indoor and "urban canyon"

environments - two environments where GPS has degraded performance. The Rosum algorithm, when combined with a GPS system, provides a highly accurate system in rural and urban areas alike [20, 21].[2]

A DTV signal transmits 520,832 symbols, grouped into 626 segments, with a symbol rate of 10.762237 MHz. Thus, the synchronization segments occur at a rate of $\approx$ 12.935 kHz.

In addition to the DTV synchronization segments, the Rosum Corporation claims that digital synchronization signals included with some analog television stations can be used in the same fashion. These synchronization signals are not the same as the synchronization pulses in the NTSC broadcast for controlling the picture output, but are digital signals for information that some stations transmit in addition to the NTSC broadcast.

The main advantages the Rosum Corporation lists for using the DTV signal are:

- Megawatt transmission power at "prime" UHF frequencies
- Stationary ground-based transmitters
- Faster chipping rates (greater frequency spreading) than military GPS

The Rosum Corporation, using the DTV algorithm, avoids some of the real-time errors inherent in the GPS positioning system–namely space vehicle position errors, ionospheric delay in signal propagation, and doppler shift of the frequency spectrum. The Rosum Corporation also claims the synchronization signals can be received and processed up to 100 miles from the signal source, despite the signal being too weak for accurate television demodulation.

Despite the same objective, the first two systems had very different implementations. The required synchronized transmitters or use of satellites and hardware added complexity and error sources that this research hopes to avoid. Furthermore,

[2]Much of the information on the Rosum Corporation, including one of the cited references, has come from the company website: http:\\www.rosum.com

both of these approaches used very limited pieces of the signal. This research investigates ways to improve accuracy by using much more of the signal structure.

The Rosum Corporation, with much of the same motivation for the research in this Thesis, chose the digital signals from DTV as a timing signal. This Thesis aims to use patterns in the NTSC analog waveform as the timing signal. Thus, despite the many similarities, the two approaches are fundamentally different. Additionally, the emphasis of this research aims for as precise a position estimate as possible, while the goal of the Rosum Corporation aims to develop a system realistically capable of providing E-911 service for cellular phones and other mobile devices.

1.5 Thesis Overview

Chapter 2 describes the background theory used in this research through studies of the TDOA positioning algorithm, the NTSC broadcast signal, and the concepts of correlation and matched filters. *Chapter 3* begins with a discussion of the hardware used during signal acquisition and model validation. It then discusses development of the algorithms used to reduce the dataflow from the reference receiver to the target receiver. *Chapter 4* then analyzes each of the algorithms' ability to accurately calculate the TDOA measurement. It concludes with an example of processing received data from acquisition to a final position estimate using the TDOA algorithm. *Chapter 5* gives the overall system recommendations towards a feasible system, followed by recommendations for further research in using NTSC broadcast signals in a TDOA algorithm.

II. Background

This chapter provides the necessary background for the major topics in this research: TDOA position estimation, the NTSC broadcast signal, signal detection using matched filters, and multipath. First, the TDOA algorithm is developed both conceptually and rigorously with the necessary equations. Then, the NTSC broadcast signal is outlined in both the time and frequency domains. Next, the ability of a matched filter to detect a known signal is discussed. As a foundation to this discussion, the principles of autocorrelation and cross-correlation are discussed. Finally, multipath effects, both in a general sense and those specific to the television signal, are discussed.

2.1 TDOA Positioning

The TDOA algorithm is an extension of multi-lateration, or using distances from known locations to estimate position [5]. The following TDOA algorithm is developed from that used in the LORAN system (see Section 1.4.1.1), but differs in that it will use a single transmitter with two receivers to estimate the range between one of the receivers and the transmitter. This range provides a sphere (or a circle in 2 dimensions) of possible points for the target receiver about that transmitter. Again, provided enough measurements are available, the intersection of these points is the final position estimate.

To illustrate this TDOA concept, first the case of two synchronized receivers is presented. Then, the position estimate is rigorously developed for the unsynchronized case (when a bias exists between the receivers' clocks) by first developing the TDOA measurement and then using it to estimate position.

2.1.1 Range Estimation Using Synchronized Receivers. The two receiver TDOA system requires that the transmitters and one of the two receivers be static

at known locations. For real-time operation, one receiver (normally the reference receiver) must also have a real-time data link to the second receiver at the location of interest (normally the target receiver). Given this setup, the transmitted signal–whatever it may be–is received and time tagged at both receivers. Then, the reference receiver sends this time of arrival to the target receiver which calculates the TDOA between the signals. This is converted to distance by multiplying by the speed of light. As the distance between the transmitter and reference receiver is known, the TDOA measurement is the only measurement needed to estimate the range between the transmitter and target receiver.

Figure 2.1 illustrates how the TDOA algorithm produces the range estimate for a single transmitter using the propagation time to each of the receivers, as opposed to the actual time when the signal was received. Furthermore, it does not convert the times to distance; this conversion is just a scale factor of the speed of light. One can see that if the propagation time (or true range in the actual algorithm) from from the signal source to reference receiver is known, the difference in propagation times (or arrival times) can be used to calculate the propagation time (or range) from the signal source to the target receiver. Then, if at least three signal sources are available, multi-lateration techniques can be used to estimate the target receiver's position, as shown in Figure 2.2.

A general assumption for the system illustrated in Figure 2.2 is that all signals are measured at the same time or with a known time offset [13]. Otherwise, the range estimates from each transmitter could be for different positions. If the target receiver is stationary, however, this assumption is no longer required for the synchronized receiver scenario.

2.1.2 Developing the TDOA Measurement. The concept of the TDOA algorithm and how the range estimates to each signal source are derived was described in the previous section. The following two sections will mathematically develop the

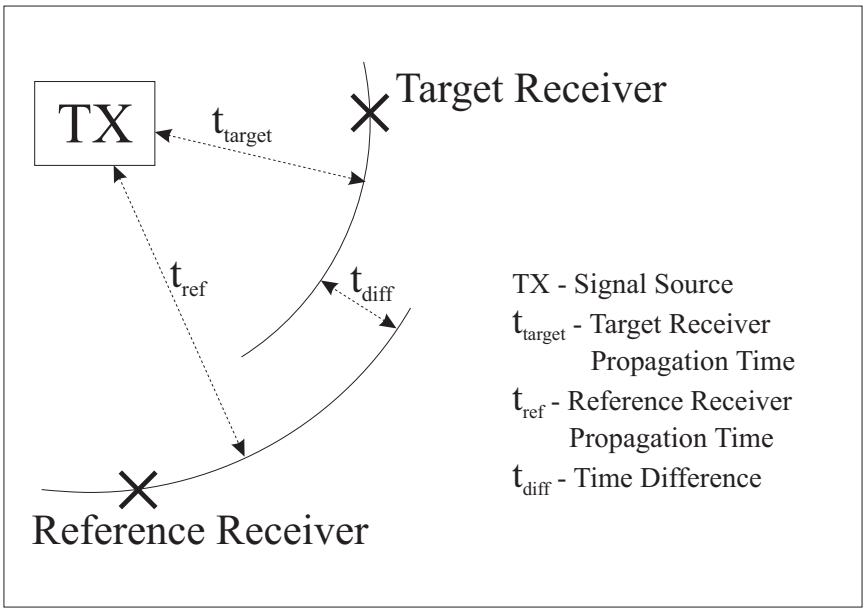

Figure 2.1: Illustration of TDOA Range Estimates

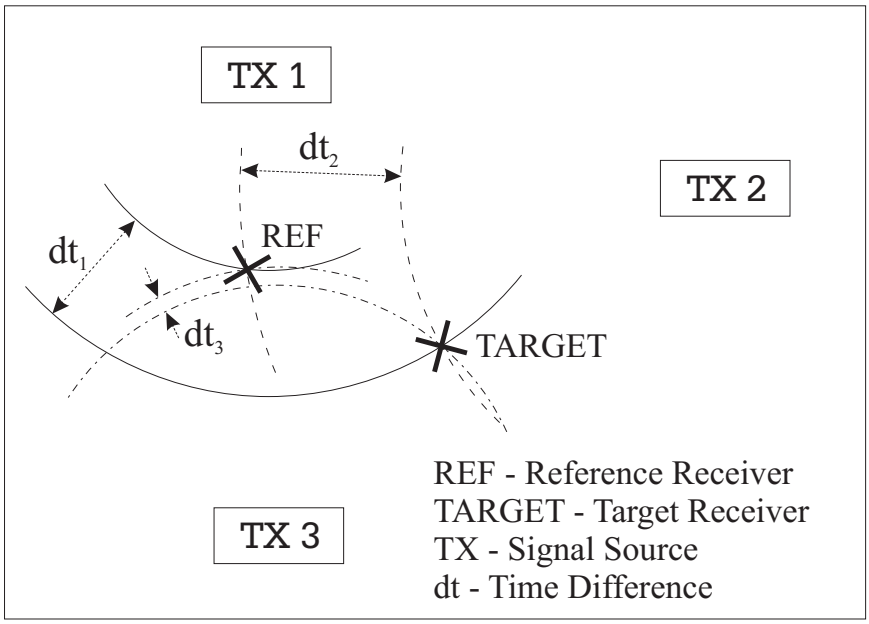

Figure 2.2: Illustration of TDOA System with Three Signal Sources

solution to this system, but the synchronized receivers assumption is removed. First, to understand the effects of removing the synchronized receiver assumption, the local time for each receiver is defined in terms of some universal true time:

$$\hat{t}_{REF} = t_{REF} + \epsilon_{REF} \tag{2.1}$$

$$\hat{t}_{TAR} = t_{TAR} + \epsilon_{TAR} \tag{2.2}$$

where

$\hat{t}_{REF}$ is the time according to the reference receiver clock
$\hat{t}_{TAR}$ is the time according to the target receiver clock
t_{REF} and t_{TAR} are the actual receive times at the respective receivers
ϵ_{REF} and ϵ_{TAR} are the respective clock errors in each receiver

The TDOA measurement, incorporating these errors, then becomes:

$$\begin{aligned} TDOA &= \hat{t}_{TAR} - \hat{t}_{REF} \\ &= (t_{TAR} + \epsilon_{TAR}) - (t_{REF} + \epsilon_{REF}) \\ &= (t_{TAR} - t_{REF}) + (\epsilon_{TAR} - \epsilon_{REF}) \\ &= \frac{RANGE_{TAR} - RANGE_{REF}}{c} + \delta t \end{aligned} \tag{2.3}$$

where

$\hat{t}_{TAR}$ and $\hat{t}_{REF}$ are the TOAs according to the respective receiver clock
t_{TAR} and t_{REF} are the true TOAs
$RANGE_{TAR}$ and $RANGE_{REF}$ are the actual ranges between the transmitter and receivers
δt is the difference in clock errors
c is the speed of light

Thus, the individual clock errors have created an error in the TDOA measurement. More specifically, the TDOA measurement error is the difference between the

receiver clock errors. (If both errors were the same, the measurement error would be zero.) This difference in local clock error will be referred to as the clock bias and must also be estimated by the TDOA algorithm. Therefore, as this adds another unknown, the required number of range estimates is increased to four (for a three-dimensional position estimate).

Another subtle constraint added by the clock bias is all measurements must be taken simultaneously. The clock error for each receiver could change over time, and the TDOA algorithm only estimates a single value for all measurements. Fortunately, the drift rate statistics of many types of clocks are known [5]. If the potential increase in error caused by this drift over the period in which samples are taken is acceptable, then the individual measurements can be taken sequentially.

Equation (2.3) defined the TDOA measurement in terms of actual values when the errors were known. The parameters as known to a physical system can be defined by rearranging that equation.

$$\begin{aligned} TDOA &= \frac{RANGE_{TAR} - RANGE_{REF}}{c} + \delta t \\ cTDOA &= RANGE_{TAR} - RANGE_{REF} + c\delta t \\ cTDOA + RANGE_{REF} &= RANGE_{TAR} + c\delta t \end{aligned} \tag{2.4}$$

where

$cTDOA + RANGE_{REF}$ is the "pseudorange"-like measurement
$RANGE_{TAR}$ is the actual range
$c\delta t$ is the clock bias in units of meters

Note that the $cTDOA + RANGE_{REF}$ (which as shown in Equation (2.4) is comprised of measured values and known quantities), is essentially equivalent in

form to a GPS pseudorange measurement, which is the combination of true range and clock error [5].

2.1.3 Position Estimation Using Unsynchronized Receivers. With the system parameters defined by Equation (2.4), multilateration techniques can be used to convert these parameters to a position estimate. The following derivation for estimating the target receiver position closely follows a similar development for GPS positioning given in [5]. First, the range from each signal source to the target receiver is expressed in terms of the signal source and target receiver position:

$$r^{(k)} = \sqrt{(x^{(k)} - x)^2 + (y^{(k)} - y)^2 + (z^{(k)} - z)^2} \tag{2.5}$$

where

$r^{(k)}$ is the true range from signal source k to the target receiver
$(x^{(k)}, y^{(k)}, z^{(k)})$ is the signal source position
(x, y, k) is the target receiver position

Following the form of Equation (2.4), the estimated range from the TDOA algorithm is

$$\rho^{(k)} = r^{(k)} + c\delta t \tag{2.6}$$

where

$\rho^{(k)}$ is the estimated range from signal source k to the target receiver
$c\delta t$ is the clock bias in units of meters

From Equations (2.5) and (2.6), four unknowns exist: the three position coordinates and the clock bias. A simple approach for solving these unknowns (when at least four measurements are available) is to linearize about an initial guess and iteratively improve the solution until the combined error magnitude is below a preset threshold. This method is generally referred to as the *Newton-Raphson method* and will be summarized here. The reader is referred to [5] for more details.

Let the initial guess for the target receiver position and clock bias be defined as (x_0, y_0, z_0) and $c\delta t_0$, respectively. The range from each signal source (again designated by the superscript (k)) to this initial position (including the effects of clock error) is:

$$\rho_0^{(k)} = \sqrt{(x^{(k)} - x_0)^2 + (y^{(k)} - y_0)^2 + (z^{(k)} - z_0)^2} + c\delta t_0 \tag{2.7}$$

The range estimate error for each signal source is then

$$\delta\rho^k = \rho^{(k)} - \rho_0^{(k)} \tag{2.8}$$

A vector of the range estimate error for all signal sources is then created as

$$\delta\boldsymbol{\rho} = \begin{bmatrix} \delta\rho^{(1)} \\ \delta\rho^{(2)} \\ \vdots \\ \delta\rho^{(K)} \end{bmatrix} \tag{2.9}$$

where K is the number of signal sources available.

The corrections to the initial estimates are now calculated using the least-squares solution. For simplicity, the three coordinate (x, y, z) will be represented by $\mathbf{x}$.

$$\begin{bmatrix} \delta\hat{\mathbf{x}} \\ \delta(\hat{c\delta t}) \end{bmatrix} = (\mathbf{G}^T\mathbf{G})^{-1}\mathbf{G}^T\delta\boldsymbol{\rho} \tag{2.10}$$

where

$$\mathbf{G} = \begin{bmatrix} (-\mathbf{e}^{(1)})^T & 1 \\ (-\mathbf{e}^{(2)})^T & 1 \\ \vdots & \\ (-\mathbf{e}^{(K)})^T & 1 \end{bmatrix} \tag{2.11}$$

$$\mathbf{e}^{(k)} = \frac{1}{\sqrt{(x^{(k)} - x_0)^2 + (y^{(k)} - y_0)^2 + (z^{(k)} - z_0)^2}} \left(x^{(k)} - x_0, y^{(k)} - y_0, z^{(k)} - z_0\right) \tag{2.12}$$

The position and clock bias estimates for the next iteration are then calculated using the initial estimates and results from Equation (2.10):

$$\hat{\mathbf{x}} = \mathbf{x}_0 + \delta\hat{\mathbf{x}} \tag{2.13}$$

$$c\hat{\delta}t = c\delta t_0 + \delta(c\hat{\delta}_t) \tag{2.14}$$

This process of iterating to the solution continues until the magnitude of the errors from Equation (2.10) are less than a predetermined threshold. The resulting position and clock bias estimates are then the system estimates.

In many situations, a 3-dimensional position estimate is not practical. Many users only require 2-dimensional positioning, and the 3-dimensional processing adds unneeded complexity. Furthermore, if four sources are not available, the system can not be solved [22]. In either of these situations, the known coordinates can be transformed to a local level frame and a 2-dimensional position estimate is possible by removing the "z" component from Equation (2.12).

2.1.4 Accuracy of the Position Estimate. The accuracy of the position estimate is affected by two things: (1) the errors in each of the range measurements, and (2) the geometry between the transmitters and receivers. The geometry portion of the errors along with the expected position error is discussed below. One of the main goals of this research is to derive the errors in the TDOA measurement from this kind of system and this is discussed in Chapter 3.

2.1.4.1 Geometry Between Transmitters and Receivers. The part of the position accuracy affected by the geometry between the transmitters and receivers is accounted for in a dilution of precision (DOP) matrix. Depending on what type of accuracy estimate is desired (horizontal position accuracy, 3-D position

accuracy, etc), different terms of the DOP matrix are used. Because this research uses ground-based transmitters and receivers, the main concern is the horizontal accuracy. Thus, the horizontal DOP (or HDOP) will be used. Fortunately, HDOP is generally lower with transmitters that have lower elevation angles and good azimuthal coverage about the receiver. Thus, provided the transmitters are spread around the location of interest, the horizontal uncertainty of a ground-based system should be minimal. [5]

The HDOP derivation is not critical to this research; readers are referenced to [5] for additional information. The results in terms of Equation (2.11) are:

$$\widetilde{\mathbf{H}} = \left(\widetilde{\mathbf{R}}_L \mathbf{G}^T \mathbf{G} \widetilde{\mathbf{R}}_L^T\right)^{-1} \tag{2.15}$$

where

$$\widetilde{\mathbf{R}}_L = \begin{bmatrix} \mathbf{R}_L & \mathbf{0} \\ \mathbf{0} & 1 \end{bmatrix} \tag{2.16}$$

and $\mathbf{R}_L$ is the direction cosine matrix that rotates coordinates from the ECEF to a local level frame, see below.

$$\mathbf{R}_L = \begin{bmatrix} -sin\lambda & cos\lambda & 0 \\ -sin\phi cos\lambda & -sin\phi sin\lambda & cos\phi \\ cos\phi cos\lambda & cos\phi sin\lambda & sin\phi \end{bmatrix} \tag{2.17}$$

$$\begin{aligned} \lambda &= tan^{-1}\ \tfrac{y}{x} \\ \phi &= tan^{-1}\ \tfrac{z}{y} \end{aligned} \tag{2.18}$$

with (x, y, z) the ECEF coordinates of the target receiver.

HDOP is then defined as:

$$\text{HDOP} = \sqrt{\widetilde{H}_{11} + \widetilde{H}_{22}} \tag{2.19}$$

where $\widetilde{H}_{\text{XX}}$ is the x$^{\text{th}}$ element of the diagonal of $\widetilde{\mathbf{H}}$.

2.1.4.2 Combining To Calculate Estimated Position Accuracy. The horizontal planar root sum square (RSS_{2D}) uncertainty is calculated as [5]

$$RSS_{2D} = \text{HDOP x } \sigma_d \tag{2.20}$$

where σ_d is the standard deviation of the TDOA measurement errors (assumed to be zero-mean and Gaussian).

2.2 NTSC Television Signal

The NTSC broadcast is a structured method of transmitting the images shown on a television. This section outlines some of the NTSC broadcast parameters. First, general specifications and the frequency spectrum of the NTSC broadcast are discussed. Then, the composite video signal is outlined. As this signal has many different parts to it, it is discussed in two sections: (1) the signal structure that contains the picture information, and (2) the synchronization pulses. Because these pulses are the main part of the signal used in this research, they are covered in detail in Section 2.2.3.2. After both structures are discussed, the combined signal, as a whole, is discussed. Finally, the suggested filter performance for bandlimiting the signal is discussed. As the actual picture information (chrominance, luminance, etc) is not used in this research, the NTSC method of transmitting this is not discussed. Readers are referenced to [4, 23–25] for additional information on this topic.

2.2.1 General Specifications. Television screens are divided into 525 horizontal lines, which are alternately grouped into two fields. The first field contains 263 lines; the second contains the remaining 262 lines. Television screens divide the lines between the two fields by alternating the field of each line from top to bottom (causing them to be interlaced). When a television screen refreshes, each field alternately refreshes at 60 Hz, giving a complete refresh rate of 30 Hz. Thus, using

Table 2.1: NTSC Broadcast Frequency Assignments

Channels	Frequency	Band
2-6	54-88 MHz	VHF
7-13	174-216 MHz	VHF
14-69	470-806 MHz	UHF

the 30 Hz refresh rate and the 525 lines to be updated, the approximate duration of each line is 63.5 microseconds. Stated differently, the line-scanning frequency is 15.750 kHz [4].

2.2.2 Frequency Spectrum. The NTSC broadcast signals occupy both the very high frequency (VHF) and ultra high frequency (UHF) bands. Each station is allocated a bandwidth of 6 MHz for all audio and video signals. Table 2.1 shows the general frequency spectrum for each channel. The allocation of the bandwidth between audio and video signals is shown in Figure 2.3. The video spectrum uses vestigial sideband modulation and is centered 1.25 MHz above the lower bandwidth edge. The audio signals use a combination of frequency modulation (FM) and double side band, suppressed carrier, amplitude modulation (AM). The audio carrier is transmitted 4.5 MHz above the video carrier, or 5.75 MHz above the lower bandwidth edge. The remaining bandwidth is left as a guard band to assist interference suppression among television transmitters. [26]

2.2.3 NTSC Composite Video Signal. The video signal containing the picture data and all necessary synchronization pulses is known as the composite video signal. While a clear distinction can be made between the two different signal structures present, there aren't distinct starting and ending points in the signal. This research uses the lower level of the falling edge that occurs every 63.5 microseconds as a starting point for both signals.

The pulses used in the NTSC broadcast are negative pulses (i.e., the "active" pulse is below the blanking level). Many references, including [4, 23], illustrate pos-

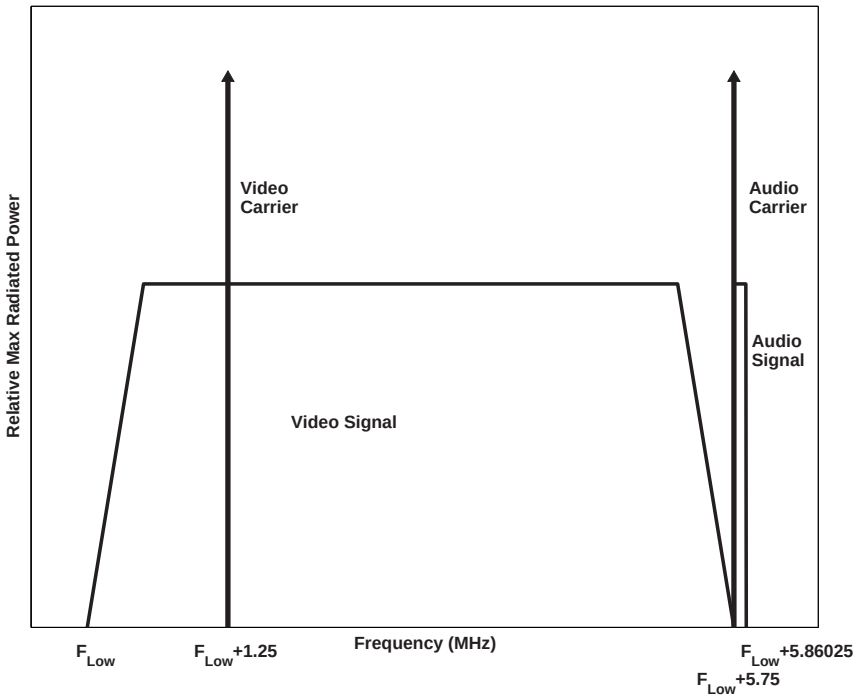

Figure 2.3: NTSC Bandwidth Allocations for a Particular Station

itive pulses. The concepts are identical, but this research will only discuss negative pulses.

2.2.3.1 Picture Line Structure. The picture line structure is actually used by two different parts of the signal in the NTSC broadcast: (1) each of the 525 horizontal lines on a television screen, and (2) the blank lines transmitted between fields that allow time for the electron gun to move back to the top of the screen. The only difference between these lines is the picture information is omitted from the blanking lines; the signal remains at the blanking level.

Figure 2.4 shows a picture line with the individual sections labeled. The front porch, sync tip, and back porch make up the horizontal synchronization pulse that "wraps" the electron gun from the previous line and aligns it to the beginning of the current line. Both the front porch and back porch are at the blanking level and last for 1.5 and 4.7 microseconds, respectively. The sync tip is well below the blanking

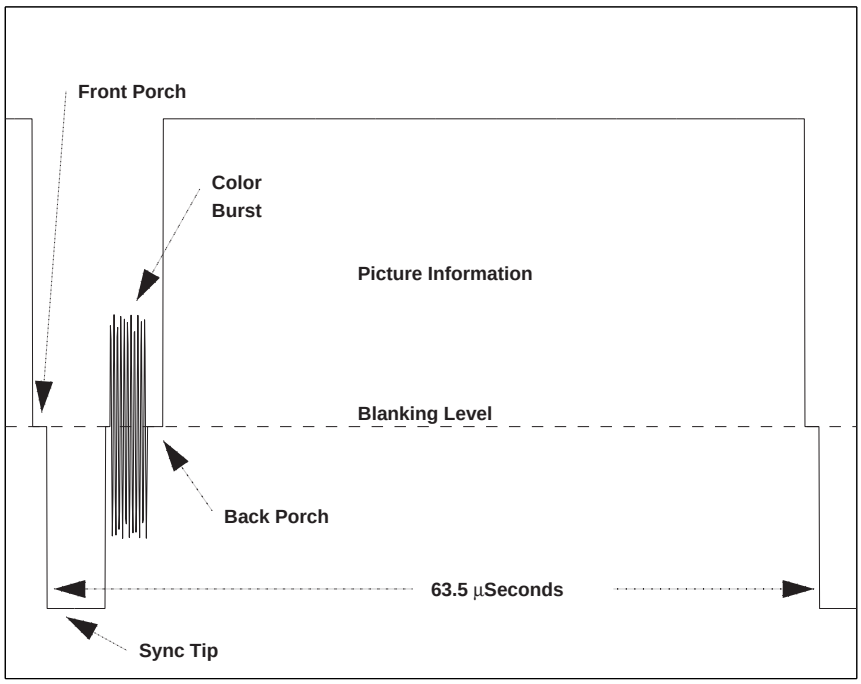

Figure 2.4: NTSC Picture Line Structure

level and lasts for 4.7 microseconds. The color burst "re-tunes" an ongoing reference signal within the receiver for decoding the picture information and is interjected on the back porch. It is 8-10 cycles of a 3.5795 MHz sinusoid, thus has a duration of approximately 2.5 microseconds [25]. The picture information contains the picture for the individual line. Pieces of the picture are contained not only in the amplitude of the signal, but in the differential phase as well, as compared to the reference signal controlled by the color burst [4].

One interesting characteristic of the color burst frequency is it is the 455th harmonic of one-half the line scanning frequency (15.750 kHz) [4]. Therefore, the phase-offset will be the same in every other pulse and the inverse (180° shift) in the remaining pulses (i.e. they will alternate).

2.2.3.2 Synchronization Pulses. Besides the picture line structure, the synchronization pulses are the other primary structure. As this part of the signal aligns the electron gun to the top of the screen for both fields, it is not data dependent

and, therefore, does not change. Furthermore, despite starting on different lines of the television, the same set of pulses is used by both fields. The only difference is that the synchronization pulses for field 2 are delayed by one half of a horizontal line, or 31.75 microseconds. The other half of this line is inserted after the synchronization pulses, ensuring two things: (1) the synchronization pulses of field 1 align at the proper time, and (2) both fields have the timing of 263 picture lines (ensuring the same duration for both fields) [23]. The implementation of this delay is described in Section 2.2.3.3 below.

The synchronization pulses contain two different types of pulses: (1) equalizing pulses, and (2) vertical sync pulses, as shown in Figure 2.5 [24]. The equalizing pulses are inserted to correct vertical retrace inconsistencies in successive scans. Furthermore, to ensure the horizontal refresh trigger is maintained, the frequency of these pulses is exactly double the horizontal refresh rate. Thus, even when delayed by one half the horizontal line, the falling edge of one of the pulses aligns with the horizontal retrace pulse (maintained in the television receiver). These pulses are narrower than the horizontal sync pulses with a pulse width of 2.54 microseconds. The vertical sync pulses provide the vertical refresh trigger and are differentiated from the others by the wider pulse width of 29.21 microseconds. In fact, the original desire was to make the vertical sync pulses one wide pulse. Difficulties associated with this method, specifically in maintaining the horizontal refresh trigger, made it impractical, however [4]. The vertical refresh trigger is determined by applying the entire set of synchronization pulses to a resistance-capacitor integrator (an integrator that has a natural damping trend). The narrow pulses of the equalizing pulses only excite the output slightly, and the response is damped prior to the next pulse. In contrast, the wider sync pulses have a significant effect on the output, and the narrow time between pulses does not allow the response to become damped. Thus, the successive pulses integrate to a discernable peak [23].

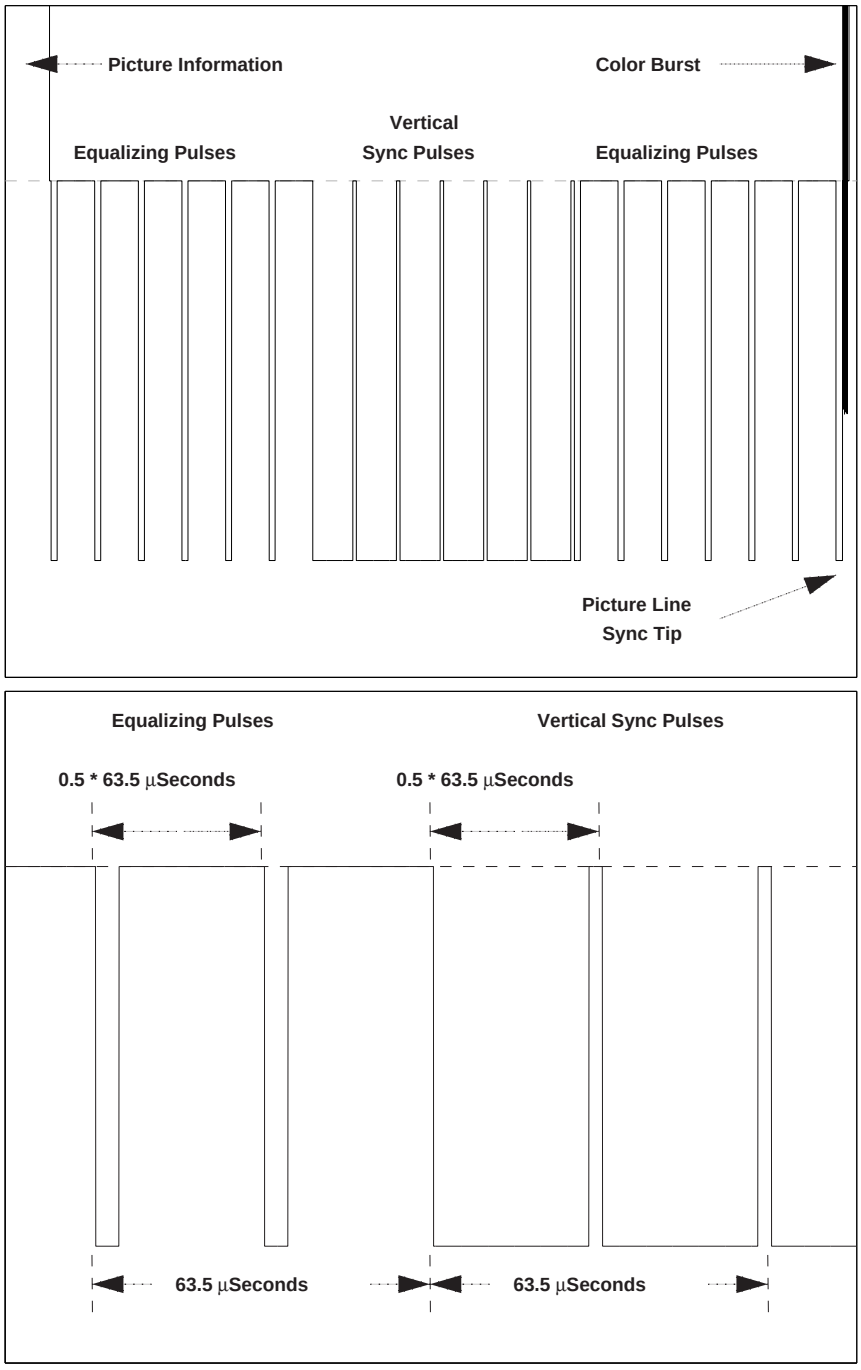

Figure 2.5: Upper: NTSC Synchronization Pulses Structure
Lower: Synchronization Pulses Detail

2.2.3.3 Combined Signal Structure. The combined video signal, despite having many pieces, is now just a piecewise combination of the two structures defined above. A listing of the successive pieces comprising a single 525 line television screen is shown below [4].

- Synchronization pulses
- 8-10 blanking lines
- 263 picture lines
- 31.75 microseconds of a blanking line (first half)
- Synchronization pulses
- 31.75 microseconds of a blanking line (second half)
- 8-10 blanking lines
- 262 picture lines

Figure 2.6 shows how the different parts of the signal listed above connect together. Note the half blanking line leading the synchronization pulses in the lower signal. This shifts the synchronization pulses such that the second pulse aligns with the 63.5 microsecond time interval and indicates frame 2. While not shown, the second half of the blank line structure follows this same set of synchronization pulses (it simply looks like the last pulse has been extended by 31.75 microseconds).

2.2.3.4 Bandlimited Signal Structure. The signals thus far have been theoretical in the fact they did not account for the limited bandwidth available. This section briefly discusses the video signal's bandlimiting filter.

The general frequency content of the video signal was shown in Figure 2.3, but did not provide enough detail to create an appropriate filter. The following video signal filter performance is suggested in [4]:

- Passband: 0-4 MHz
- Stopband: >5.5 MHz
- Stopband Rejection: 60 dB
- Passband Ripple: <2 dB
- Linear Phase Offset from 0-3 MHz: $\approx$ 0-85°
- Maximum Phase Offset at 3.58 MHz: $\approx$ 220°

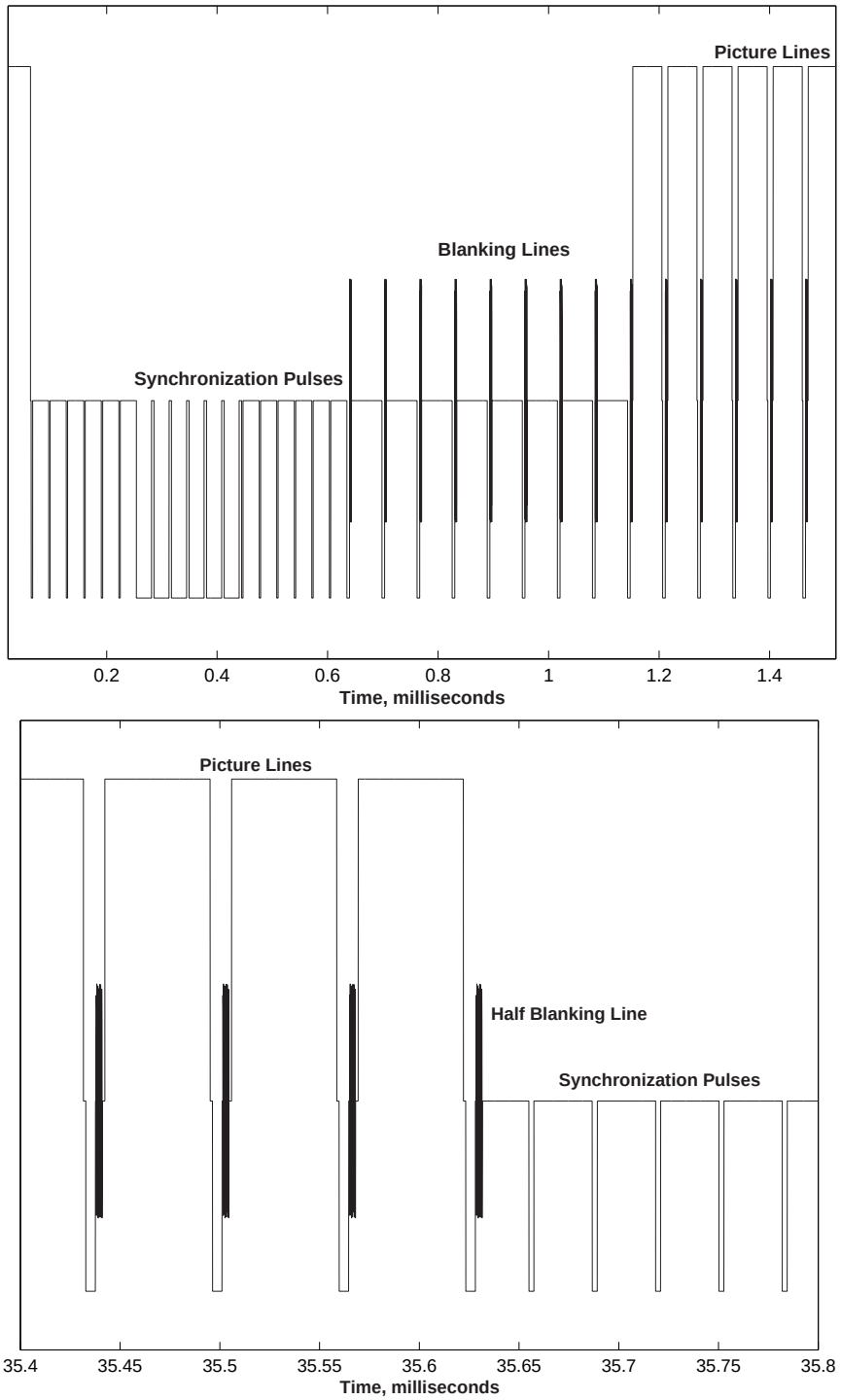

Figure 2.6: Upper: Video Signal with Frame 1 Synchronization Pulses

Lower: Frame 2 Synchronization Pulses Offset

The passband and stopband parameters provide the general frequency envelope, or how much frequency content the signal can have. The phase parameters provide the amount of distortion and delay that can be added to the remaining signal. These factors were suggested to prevent crosstalk and visually noticeable degradation in the picture information. As this part of the signal is not the focus of this research, these factors have a lower priority than the frequency content.

2.3 Signal Detection

Section 2.1 developed the TDOA algorithm using a signal's time of arrival at two receivers. As the NTSC broadcast is transmitted continuously, an arbitrary part (or parts) of this waveform must be considered the start so that it's time of arrival can be considered the signal's time of arrival. This section will develop how a particular signal can be detected within a longer signal. First, the concepts of autocorrelation, cross-correlation, and matched filtering are defined. These processes are then applied to detecting a signal corrupted by additive white Gaussian noise (AWGN). Finally, the correlation properties of random signals are discussed.

2.3.1 Theoretical Development. Two basic forms of correlation exist: autocorrelation and cross-correlation. As the names suggest, autocorrelation is "the product integration" of a signal with itself, and cross-correlation is "the product integration" of a signal with another signal [27]. Thus, the operations are identical – only the inputs are different. Nonetheless, both provide very different information and have unique notation [27, 28]:

$$R_{xx}(T) = \int_{-\infty}^{\infty} x(\tau)x(T+\tau)d\tau \tag{2.21}$$

$$R_{xy}(T) = \int_{-\infty}^{\infty} x(\tau)y(T+\tau)d\tau \tag{2.22}$$

where

$R_{xx}(T)$ is the autocorrelation of signal x at time offset T
$R_{xy}(T)$ is the cross-correlation of signals x and y at time offset T

Autocorrelation correlates a signal with itself, whereas matched filtering convolves a signal with the theoretical signal's impulse response [27]. As this operation attempts to detect a signal within another signal, it imparts time bounds on the signal (caused either by synchronization or when detection began) and provides the limits of integration for the matched filter response:

$$z(T) = \int_{0}^{T} r(\tau)h(T-\tau)d\tau \tag{2.23}$$

where

$z(T)$ is the matched filter output at time T
$r(\tau)$ is the received signal
$h(\tau)$ is the impulse response of the theoretical signal

Despite matched filtering using convolution (instead of correlation), if the same time constraints are imposed, the theoretical outputs of a correlator and a matched filter at time T are identical. From Equations (2.21) and (2.23), one can see the only difference between convolution and correlation is the time reversal of one of the signals. However, because the matched filter uses one signal's impulse response, which is also derived using convolution, a double time reversal is created. Therefore, calculating the cross-correlation of a signal with a replica of the theoretical signal is identical to using a matched filter (for some time T). Refer to [27] for a detailed

development of this comparison, but since the two produce identical results, the terms correlation and matched filtering are used interchangeably.

2.3.2 Detection of Corrupted Signals. While it is often convenient to assume the transmitter, receiver, and medium through which a signal travels are perfect and don't distort the signal, this is a gross oversight. All of these components, along with other interference, can corrupt the signal. If these errors only slightly distort the signal, they should not cause signal detection problems. However, detection problems can arise if they distort the signal so much that it no longer resembles the original signal. Fortunately, the correlation process detects signals that have been corrupted to some extent. Often, correlation can accurately detect signals where the original signal is so distorted it is no longer discernable in the received waveform [27].

The distortions caused on a signal are random in nature. While many different sources affect the signal, each possibly having very different characteristics (strength, mean, time-constant, etc), AWGN often provides an adequate model for the overall effects [15]. The amount of average noise power corrupting each signal can be expressed as the signal-to-noise ratio (SNR) and is defined as [27]

$$\text{SNR} = \frac{\text{Average Signal Power}}{\text{Average Noise Power}} \tag{2.24}$$

The following examples demonstrate the ability of correlation to detect a signal corrupted by AWGN. First, the theoretical signal is correlated with an uncorrupted waveform, as shown in Figure 2.7 (where the correlation results are compensated to indicate the start of the desired signal). The shaded area of the top plot indicates the desired waveform (i.e., the correlation period), and one can see the (normalized) peak of the correlation results indicates the start of this waveform.[3] Furthermore, when looking at the "Correlation Detail" plot, one can see that the peak of the

[3]For comparison, the normalizing factor used in this correlation result will be maintained for the remaining sets of correlation results.

correlation results aligns with the actual start (indicated by the dashed line). Figures 2.8 through 2.10 show correlation results for decreasing SNR values. In Figure 2.8, noise has clearly been added to the signal, but one can still visually see patterns of the desired waveform in the signal. The correlation results from this signal are nearly identical to those of the theoretical waveform, including those from the "Correlation Detail" plot. In Figure 2.9, the desired waveform is no longer visible in the signal, but the correlation results still appear to accurately detect the signal. However, the "Correlation Detail" shows the geometry of the peak is slightly degraded. In this case, the peak has been skewed approximately 2 samples to the right of the known true value. In Figure 2.10, the signal has been too badly corrupted for accurate detection. First, the largest peak of the correlation results is near the middle of the desired waveform, not the start. Furthermore, even if some form of synchronization were present to detect the proper peak, the "Correlation Detail" shows the correlation peak has been skewed approximately 4 samples to the right.

One potential way to reduce the effects of noise on the correlation peak is to find the intersection of trend lines fit to both sides of the peak value. Figure 2.11 shows the trend lines applied to the correlation peaks of Figures 2.9 and 2.10. One can see that the intersection of the trend lines more accurately determines the correlation peak, as compared to the highest sample in the plot.

It should also be noted the required SNR values for accurate waveform detection vary from waveform to waveform. The desired waveform used in the above examples had a unique structure compared to the rest of the signal. Many other signal constellations may not have this structure and may require higher SNR values.

2.3.3 Correlation Properties of Random Signals. The previous section demonstrated how correlation can mitigate the effects of noise (or random signals). This section will investigate correlating random signals. First, as motivation for the ideas presented in this section, the theoretical properties of white noise are

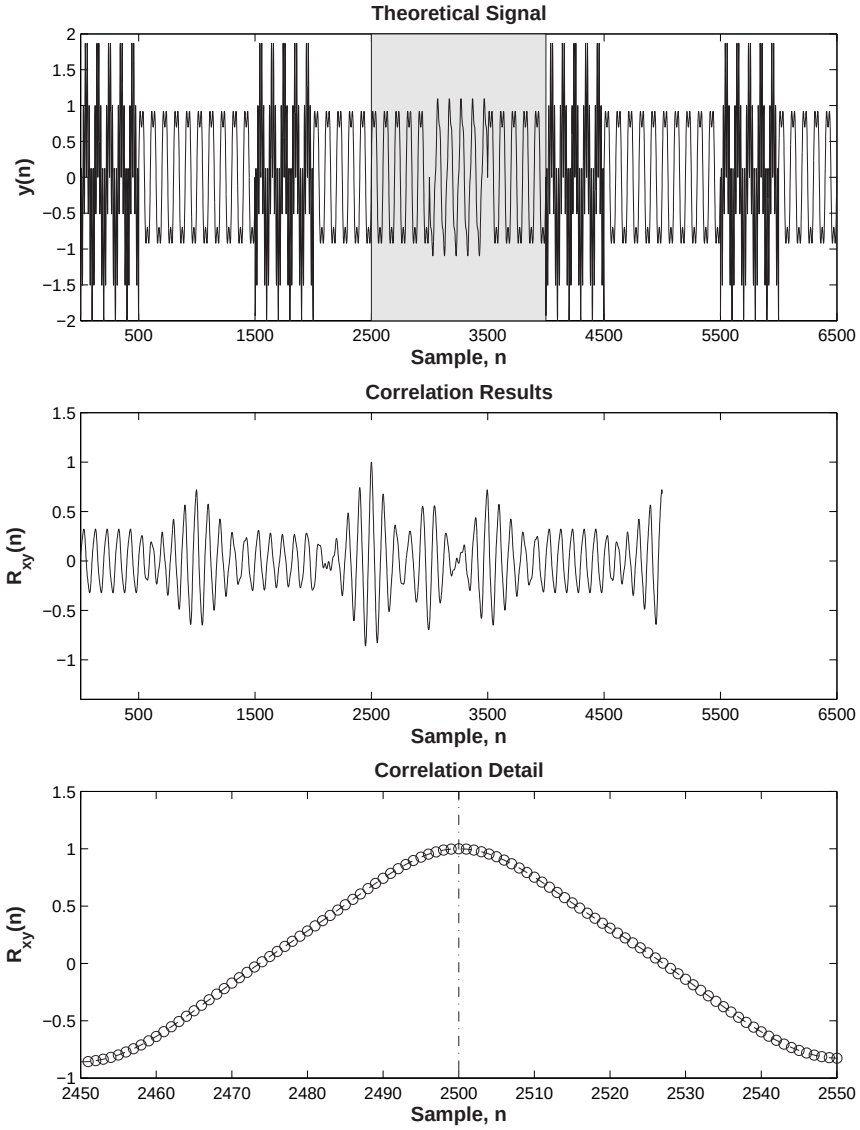

Figure 2.7: Correlation Results of Theoretical Signals (Compensated to Indicate the Start of the Desired Signal)

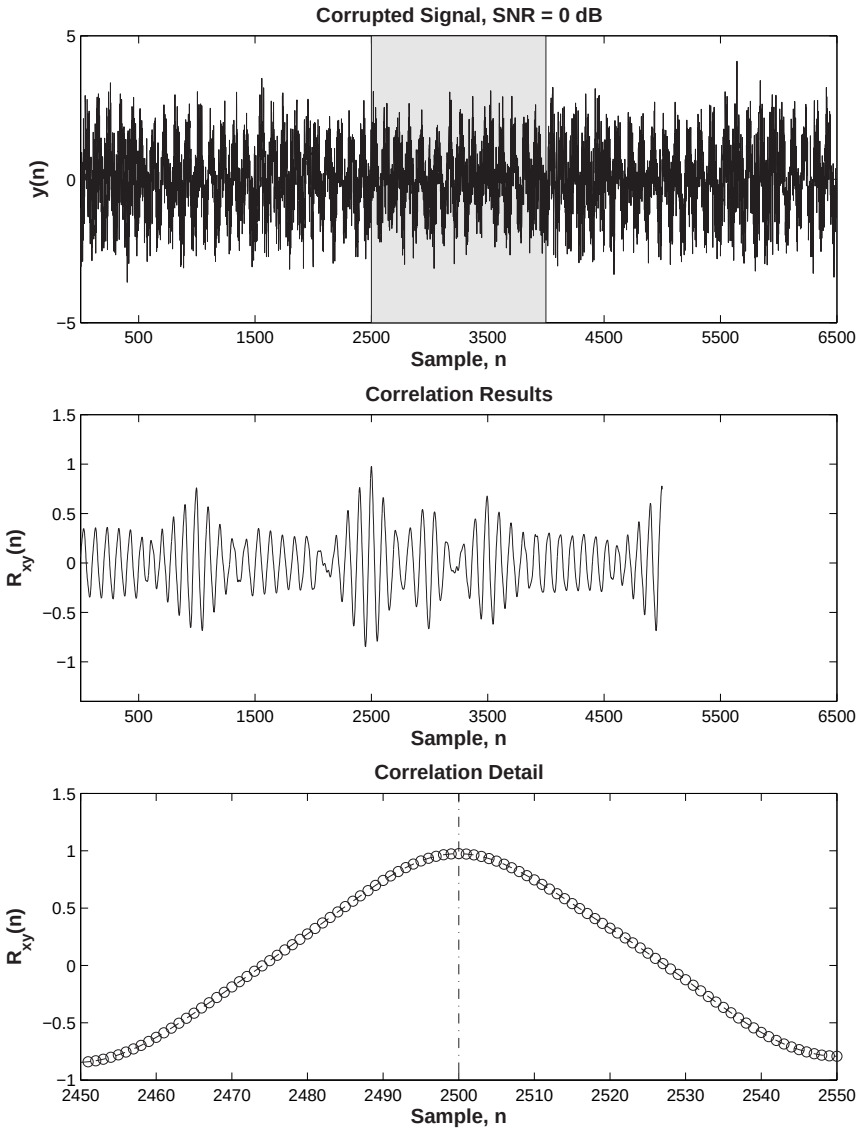

Figure 2.8: Correlation Results, SNR = 0 dB (Compensated to Indicate the Start of the Desired Signal)

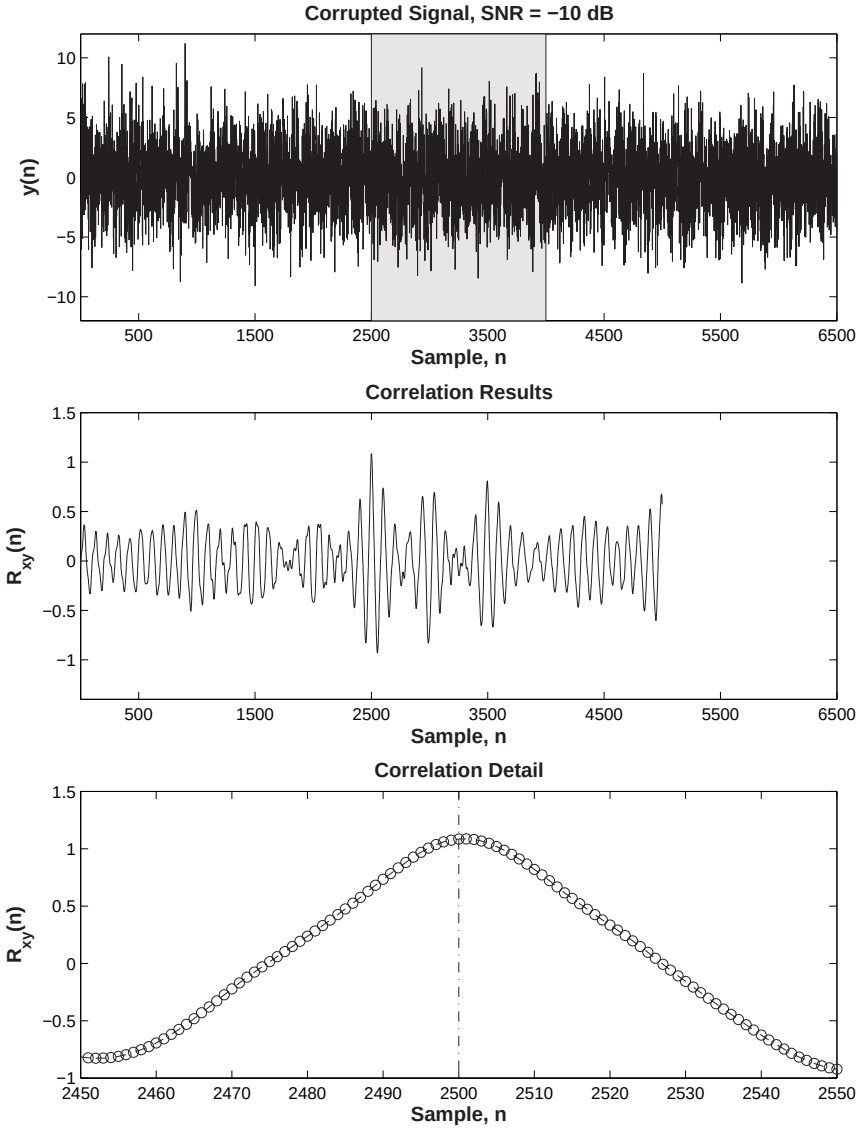

Figure 2.9: Correlation Results, SNR = -10 dB (Compensated to Indicate the Start of the Desired Signal)

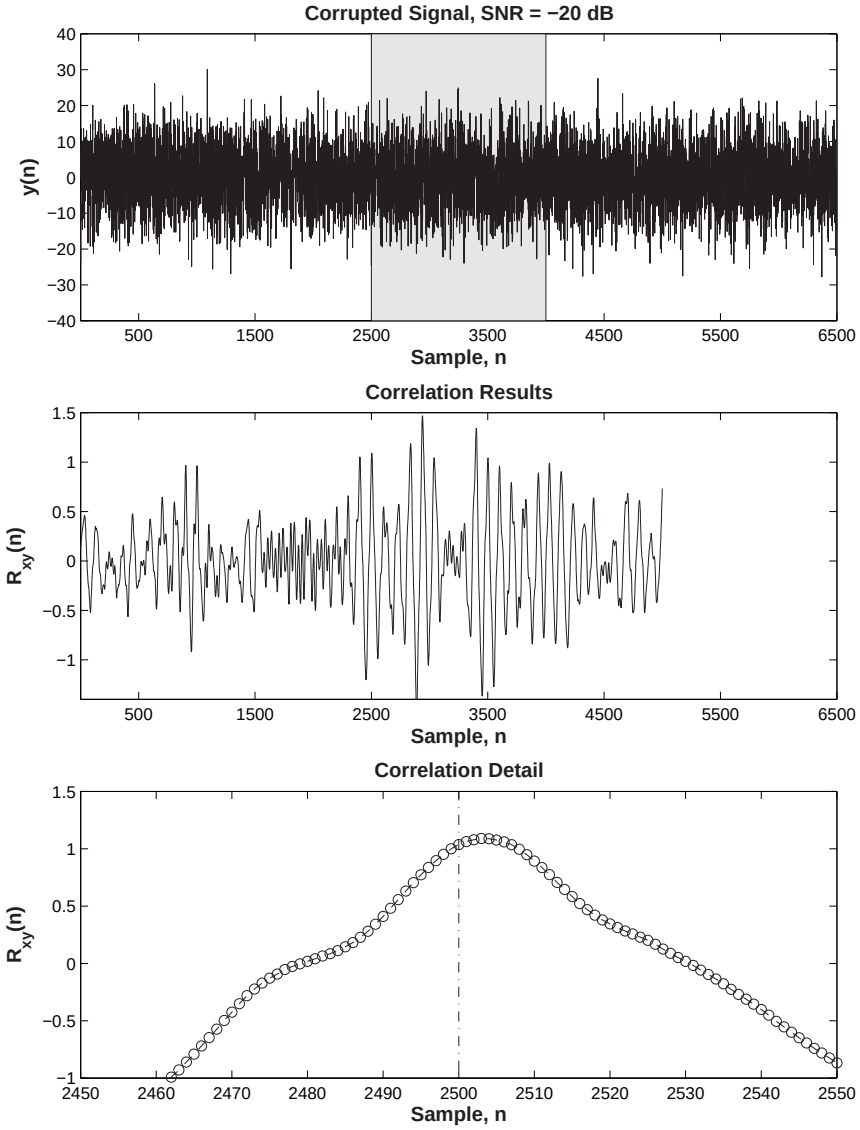

Figure 2.10: Correlation Results, SNR = -20 dB (Compensated to Indicate the Start of the Desired Signal)

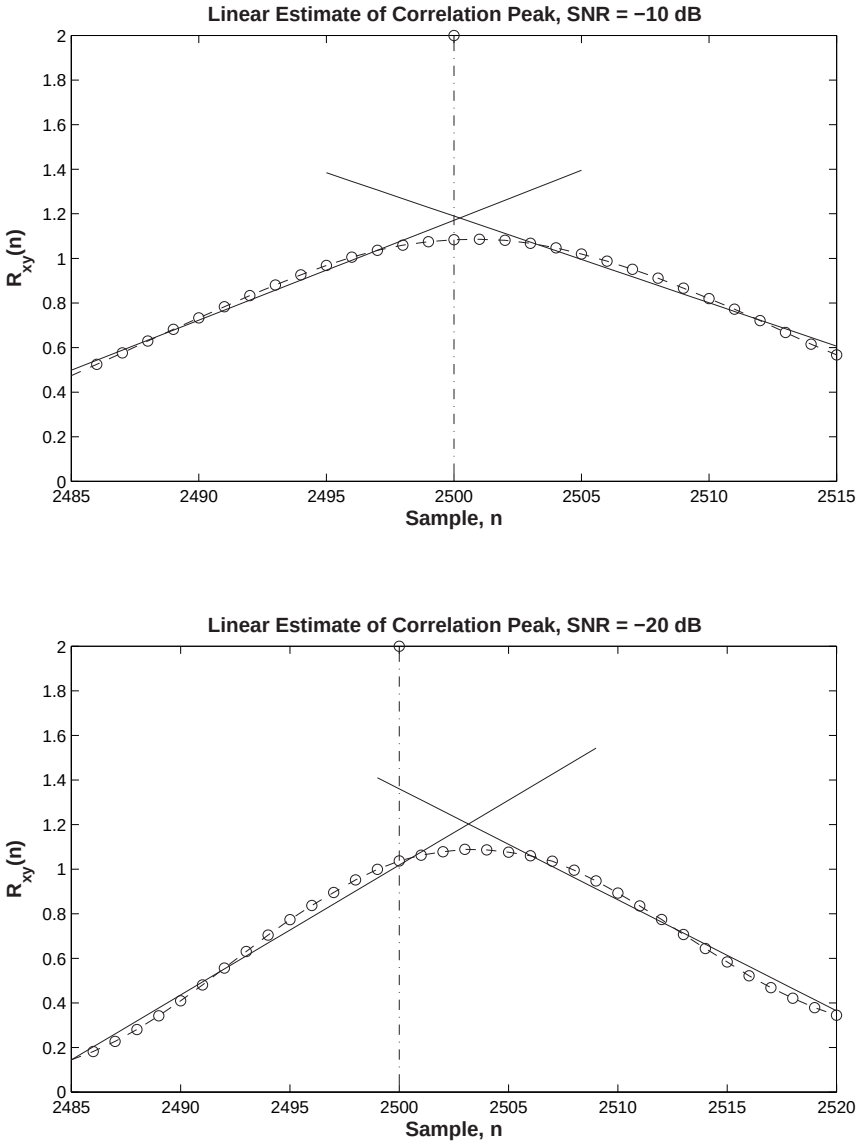

Figure 2.11: Linear Fit Peak Estimator

discussed. Then, practical solutions to the impracticalities associated with white noise are discussed.

By definition, white noise has a uniform spectral density over all frequencies [28]:

$$S_{NN}(f) = \frac{\eta}{2} \tag{2.25}$$

The resulting autocorrelation is the inverse Fourier transform of Equation (2.25) given by

$$R_{NN}(\tau) = \frac{\eta}{2}\delta(\tau) \tag{2.26}$$

which implies any realization of white noise is uncorrelated over all time (except when $\tau = 0$) [28]. Putting this into the context of signal detection, the output of a correlator performing a white noise autocorrelation would remain at zero except for the one instant when the signal was perfectly aligned with itself.

Unfortunately, white noise, as described in Equation (2.25), is not realizable – this would require an infinite amount of energy. Fortunately, any realizable system has an associated bandwidth (B) from physical elements such as component selection, component layout, and – if applicable – sampling rates. Therefore, the spectral density required for the noise to appear white over the system bandwidth and the resulting autocorrelation are [28]:

$$S_{NN}(f) = \begin{cases} \frac{\eta}{2}, & |f| \leq B \\ 0 & else \end{cases} \tag{2.27}$$

$$R_{NN}(\tau) = \eta B \frac{\sin 2\pi B\tau}{2\pi B\tau} \tag{2.28}$$

Therefore, a set of uncorrelated samples can be realized for the above system if the sampling rate is $T_s = \frac{n}{2B}$.

While the above development is realizable, many situations either require different sampling rates or do not need noise samples to be perfectly uncorrelated.

Stated differently, $R_{NN}(\tau) \approx 0,\ \tau \neq 0$ will provide adequate noise samples for the system. This "approximately zero" result is easily obtained using a random number generator (RNG). An additional benefit of the RNG is repeatability. The same signal can be generated multiple times with complete independence of the other generations. Figure 2.12 shows a signal generated by a RNG and the correlation results from a segment of this signal (again, indicated by the shaded region) with the entire signal. The correlation results clearly show how well a random signal performs in a correlation function – the next highest "peak" is approximately $1/10^{th}$ (-10 dB) that of the main peak. An SNR analysis similar to that of the previous section could also be performed here, but it is not necessary – the unique ability of random signals has already been demonstrated.

2.4 Multipath

The previous section discussed signal detection and the effects distortion can have on this process. This section elaborates on one of those distortions: multipath. The general concepts of multipath are discussed first, followed by specifics on how multipath affects television signals.

2.4.1 Multipath Concepts. Multipath occurs whenever multiple signal paths exist between a source and destination, namely a transmitter and receiver [29]. All other signals besides the dominant signal, typically the line-of-sight signal, are classified as multipath, see Figure 2.13. Exceptions to the line-of-sight case occur when the line-of-sight signal is obstructed, and a reflected signal becomes dominant [30]. Nonetheless, the multipath signals combine with and distort the dominant signal either constructively or destructively by adding signals with various attenuations, time-delays, and phase shifts [31]. The amount of distortion depends on a number of factors, including strength of the dominant signal, variation in delays experienced by the multipath signals, and the surface of the reflecting body [30, 32]. Furthermore, via the superposition principle, individual sources of multipath may

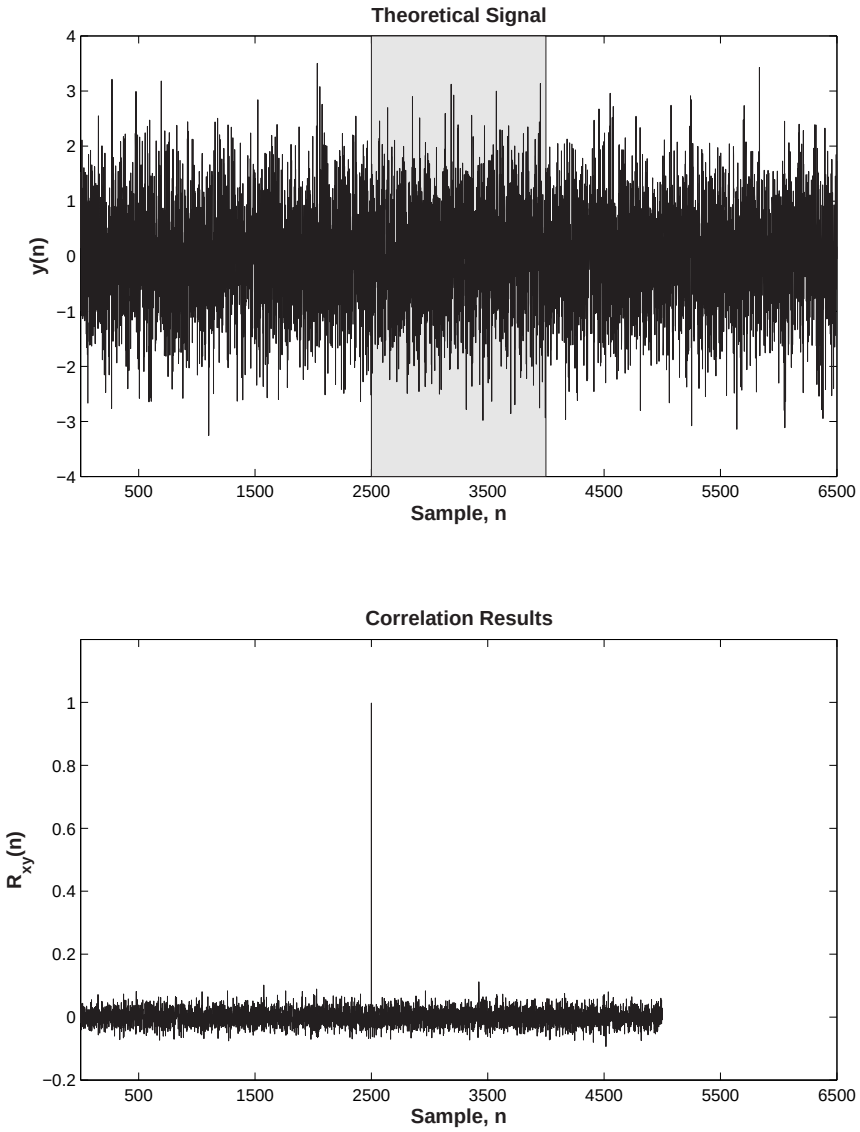

Figure 2.12: Correlation Results, Random Signals (Compensated to Indicate the Start of the Desired Signal)

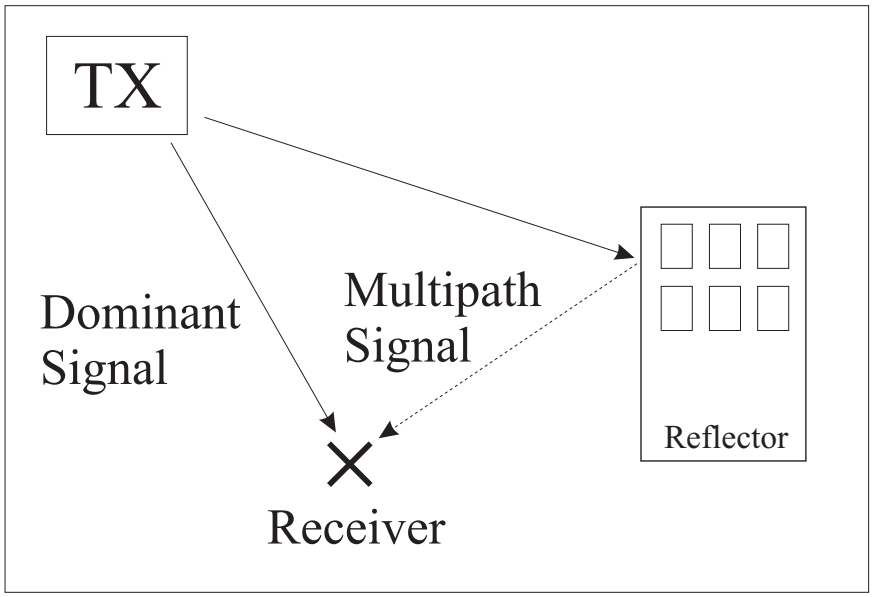

Figure 2.13: Multipath Signal

not affect system performance, but the multipath signals combined effects may cause severe degradation (or elimination) in system performance.

In a signal detection environment, the constructive or destructive nature of multipath can alter the shape of a correlation peak [5]. Depending on the amount of multipath, the delay associated with the multipath, and the method in which the correlation peak is estimated, these changes can cause the correlation peak to be advanced or delayed [30]. Furthermore, the constructive and destructive nature of multipath can alternate if the relative phase of the multipath signal changes with respect to the phase of the dominant signal. If the multipath is in phase with the dominant signal, the distortions will be constructive; if the multipath is out of phase with the dominant signal, the distortions will be destructive [5]. Figure 2.14 shows a dominant autocorrelation peak along with autocorrelation peaks from constructive and destructive multipath signals. The geometry of the combined peaks is the fundamental cause of the delay or advance in estimated correlation peak.

Lessening the effects of multipath, or multipath mitigation, can be performed using either passive or active techniques. Passive techniques involve preventing mul-

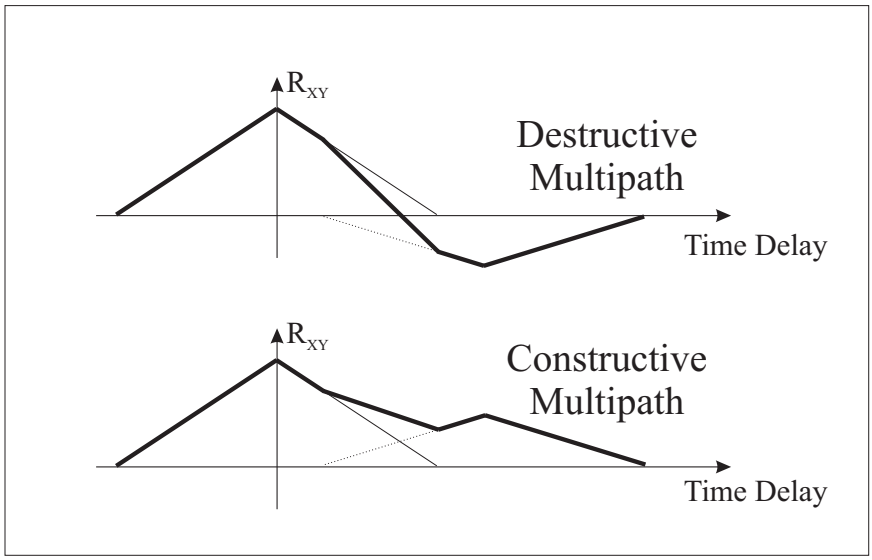

Figure 2.14: Multipath Effects on the Correlation Peak

tipath signals from entering the receiver by use of directional antennas [29]. Studies involving these "smart antennas", including those in [33, 34], have found them to be very effective – reducing multipath by a factor of 2 in some cases. Active techniques reduce the effects of multipath by characterizing the received signal and correcting detected multipath signals [29]. This approach is dependent on the signal structure used, but a study in [35] showed that a technique of this sort reduced the strength of multipath signals by over 30 dB.

2.4.2 Television Multipath Effects. The high power and close proximity of television transmitters causes the multipath signals from nearby buildings, mountains, or even moving objects such as vehicles and airplanes to have significant energy compared to the dominant signal [31,35]. As these signals generally have longer propagation times than the dominant signal, they often cause replica images to appear slightly "behind" and to the right of the main image, known as a ghost image [36]. Additional television image degradation, specifically in the color content, occurs by very short delayed multipath signals corrupting the color burst signal [31]. Multipath signals can also make the television image completely unattainable by either

destructively combining with the dominant signal [31] or constructively distorting the signal to an extent that receiver synchronization is no longer possible [4, 31].

Television multipath mitigation techniques include both passive and active varieties. Passive techniques have been demonstrated in systems that impose different delays on multiple instances of the signal such that the combined signal has reduced multipath effects [35]. Active mitigation techniques have been implemented where an additional "training" signal is inserted into the vertical blanking interval. The receiver compares this to a local version of the signal and adjusts a multi-tap "deghoster" filter to lessen the multipath effects [35].

2.5 Summary

This chapter provided an overview of the TDOA algorithm implemented in this research. The NTSC broadcast signal was presented, focusing on the synchronization structures used. Signal detection was presented both from a theoretical and practical point of view. The section on multipath highlighted the multipath problems associated with television signals.

III. NTSC Signal Acquisition and Algorithm Development

This chapter describes the test system used to evaluate the navigation potential of the NTSC broadcast signal, including the hardware, the NTSC broadcast model, the dataflow reduction algorithms, and the environments where testing occurred. Section 3.1 discusses the hardware test setup along with the motivation for each piece. Section 3.2 explains and validates how the specifications in Section 2.2 were implemented to create an analytic copy of the NTSC broadcast. Section 3.3 develops the methods for dataflow reduction for both the matched filter and cross-correlation approaches. Finally, Section 3.4 describes the two test environments used in this research.

3.1 Hardware

The hardware used in this research was solely for the purpose of signal acquisition. Thus, the two areas affected were video signal generation and analog-to-digital conversion. Following a discussion of each of these, the complete acquisition process is discussed.

3.1.1 Signal Sources. The video signals used were collected from the video out terminal on different video sources from both local and propagated data. Specifically, samples were generated from the output of a DVD player, two different VCRs not using the built-in television tuner, and two identical VCRs using the television tuner. The motivation for each source is discussed below, followed by a description of all the hardware in Table 3.1.

The DVD player was chosen as the first sample set because its video signal had the least amount of distortions and was best suited for model validation and initial algorithm development. The DVD player video signal originated from local digital data. Thus the distortions caused during signal propagation were avoided, namely

multipath, antenna effects, and other signal interference. Furthermore, the digital data maximized the signal's integrity, not only from more accurate measurements (compared to analog), but from improved processing techniques as well.

The VCRs not using the television tuner were used because they provided a video signal from local data that was based on analog processing (unlike the digital DVD player). Therefore, the signals again avoided distortions from propagation, but not those inherent in the analog data and associated processing.

The two identical VCRs using the television tuner were then used for acquisition of the real, propagated television signals used in the TDOA algorithm. As the video signal output required real-time processing, signals used in this test were restricted to those with enough signal strength to produce video outputs from the VCRs. For signal reception, each VCR was connected to either of two antennas: a passive antenna (i.e., "rabbit ears") or a locally fabricated antenna using a stripped piece of coaxial cable. The "rabbit ears" antenna (shown in Figure 3.1) was used because it was designed for television signal reception. The wire antenna was used as a preliminary attempt to reduce multipath and variations in the antenna gain pattern. The coaxial cable was cut approximately one-half meter in length (quarter wavelength for Channel 7) and attached to a dowel to hold it vertical at all times, as shown in Figure 3.2. To allow separation of the antennas, each antenna was connected to the VCR using a coaxial cable 200 feet in length. Thus, when extended in opposite directions, the maximum separation was near 400 feet (121 meters).

As mentioned above, the wire antenna was maintained in a vertical orientation. Similarly, the rabbit-ears antenna was maintained in the "slant" orientation shown in Figure 3.1. Both of these orientations were mismatched to the transmitters' horizontal polarization, but this mismatch was constant so any losses were assumed to be uniform throughout this research.

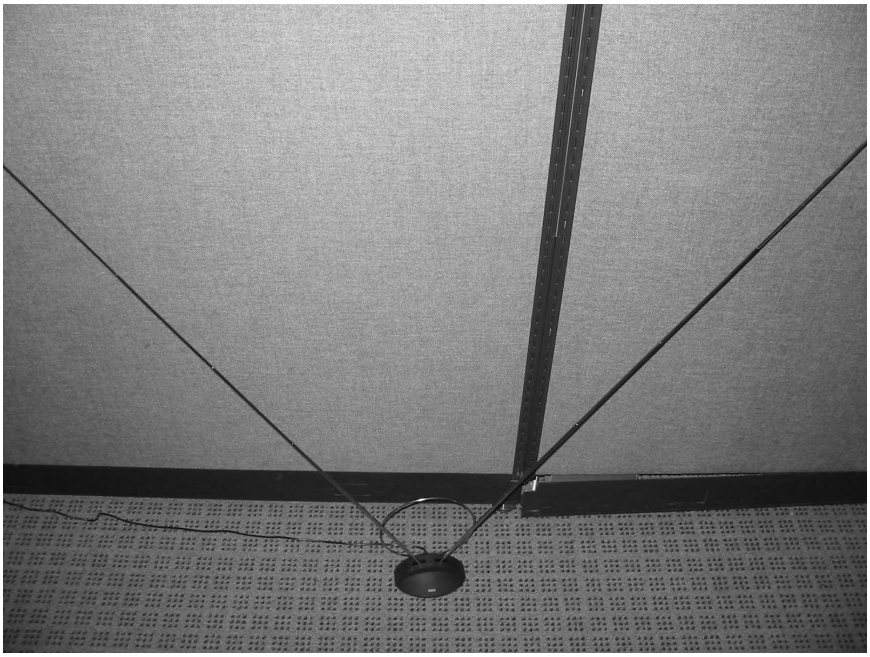

Figure 3.1: Rabbit Ears Antenna

Table 3.1: Description of Hardware Used

Function	Manufacturer	Model
Digital Signal Source	Panasonic	DVD-LV60
Analog Signal Source	Sony	SLV-70HF
	JVC	HR-J692U
Propagated Signal Sources	JVC	HR-J692U
Antennas	RCA	ANT110
	N/A	wire

Figure 3.2: Wire Antenna

3.1.2 Analog-to-Digital Conversion. After the signals had been generated, they needed to be captured and digitized for analysis. For this task, a four channel, 20 MHz sample rate, 10 bit, ±1 volt analog input range analog-to-digital converter (ADC) from Adlink Technologies, Inc (Model PCI-9810) was installed in a computer. The four channels enabled simultaneous sampling of the two input signals. The sample rate had to provide enough points in the desired portion of the signal that was the shortest duration, without excessive amounts of data. The shortest pulses were the equalizing pulses described in Section 2.2.3.2. They have a duration of 2.54 microseconds, so approximately 50 samples would be taken in this time period with a 20 MHz sample rate. Lastly, the number of bits and input range needed to capture the signal and provide enough quantization levels that the signal be distinguishable, but not necessarily a perfect replica. The correlation function would account for the minor differences quantization imposed.

The sample rate and number of bits of the ADC used in this research was probably more than needed. However, this research wanted to evaluate the best possible navigation performance of the NTSC broadcast signal. Additional research needs to evaluate the feasibility of using slower sampling rates and fewer quantization bits.

3.1.3 Signal Acquisition. The previous two sections discussed the major hardware components used during signal acquisition. For the TDOA measurements, all connections between components were made using the same types of cables with matched lengths. Therefore, all processing delays should have been nearly equal. The validity of this assumption will be evaluated later in Section 4.1.

The complete acquisition process for the propagated signals is shown in Figure 3.3. For the locally generated signals, the process is the same, except the antennas are removed and the appropriate video encoder replaces the VCR block.

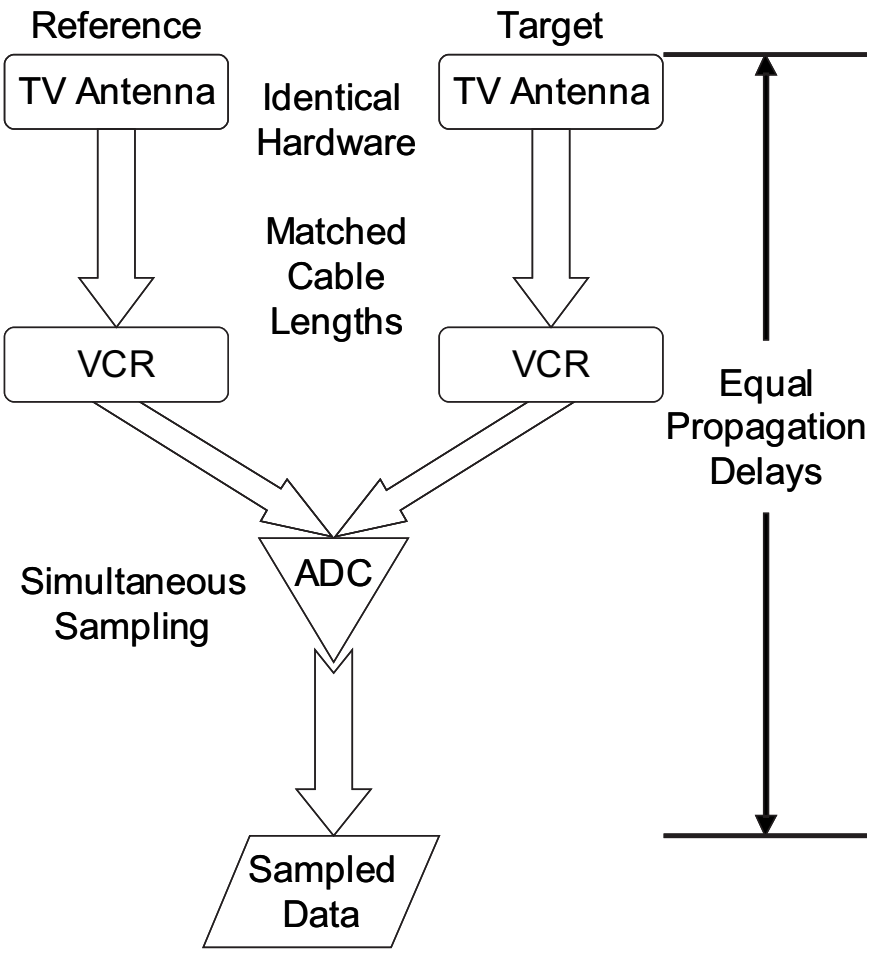

Figure 3.3: Signal Acquisition Flowchart

3.2 Model Development

The first step in analyzing the acquired signals and evaluating their navigation potential was developing an accurate model. This section discusses the creation and validation of the model used in this research.

3.2.1 Model Creation. The NTSC broadcast parameters described in Section 2.2 were used to create analytical models for all parts of the signal. This way, any combination of signal structures desired could easily be created without having to revalidate the model. The only segment not based on these parameters was the picture information (previously depicted by the elevated rectangle). The parameters chosen for the model were not critical because this research did not use this portion of the signal. To make the signal more realistic, however, this region used a first-order Gauss-Markov data set.[4] The power (or amplitude) of this data set was adjusted to match empirical results gathered from the video encoder, and the time constant was set to approximately 20 microseconds (1/3 of a line). The true time constant would be highly dependent on a particular line of any particular image. This value was chosen to allow dynamic picture information (as opposed to a black line, for example), but still provide a degree of structure to the signal (as opposed to an uncorrelated random signal).

After developing all of the signal segments, a bandlimiting filter needed to be designed to approximate the bandwidth limitations imposed by the signal specifications. This research chose to implement a finite impulse response (FIR) filter with a Hamming window for this task. This type of filter (a weighted combination of sequential samples) was chosen for it's ease of implementation, both in simulation and hardware. More advanced filters could outperform this filter, with sharper transitions from passband to stopband, more attenuation and less ripple in the stopband,

[4]A Gauss-Markov process is one that is both a Gaussian process (or has a normal probability distribution) and a Markov process (or any sample is dependent only on the value of white noise input and the previous sample). [15]

and less phase delay (while still being linear). This performance was not necessary for this research, however; the analytical model only needed to be similar to, not an exact replica of, the broadcast signal. The frequency response for the 25 tap FIR filter used in this research is shown in Figure 3.4. The two areas that did not meet the performance suggestions in Section 2.2.3.4 were: (1) the stopband did not begin until approximately 6.2 MHz (whereas the suggested stopband started at 5.5 MHz), and (2) the phase offset was approximately 700° at 3 MHz (whereas the suggested phase offset was 85°). Fortunately, neither of these should pose any problems, as this filter was only intended to provide the general effects of bandlimiting the signal, especially on the edges of the pulses. Therefore, the stopband did not need to be strictly enforced. The phase offset guidelines were not enforced, because they were intended to prevent crosstalk and distortion in the picture information [4]. The picture information from the simulated signals will not be used in this research. Thus, the emphasis was placed on ensuring a linear phase response, not how much phase offset was present. Additionally, it is believed that an implemented system would not only use a higher order filter, but a different type of filter as well. FIR filters induce ringing at discontinuities, known as the Gibbs phenomenon [37]. While this can be reduced by windowing (the Hamming window used in this filter, for example), it can never be eliminated in FIR filters. Other filters, such as infinite impulse response (IIR) filters, avoid this at the expense of increased processing [38].

The effects of this filter on the video signal are shown in Figure 3.5. It can be seen that, in general, minimal affects are imposed on the signal. As expected, the square corners of the analytical pulses impose slight ringing (highlighted in the "Synchronization Pulse Detail" plot in Figure 3.5), but the general pulse is still distinguishable (highlighted in the "Picture Detail" plot in Figure 3.5). Furthermore, the rest of the signal was not significantly degraded, and the bandwidth limitations did not change the overall envelope of the signal. Therefore, as the overall intent of these pulses is detection of similar pulses for TDOA navigation, not actual television

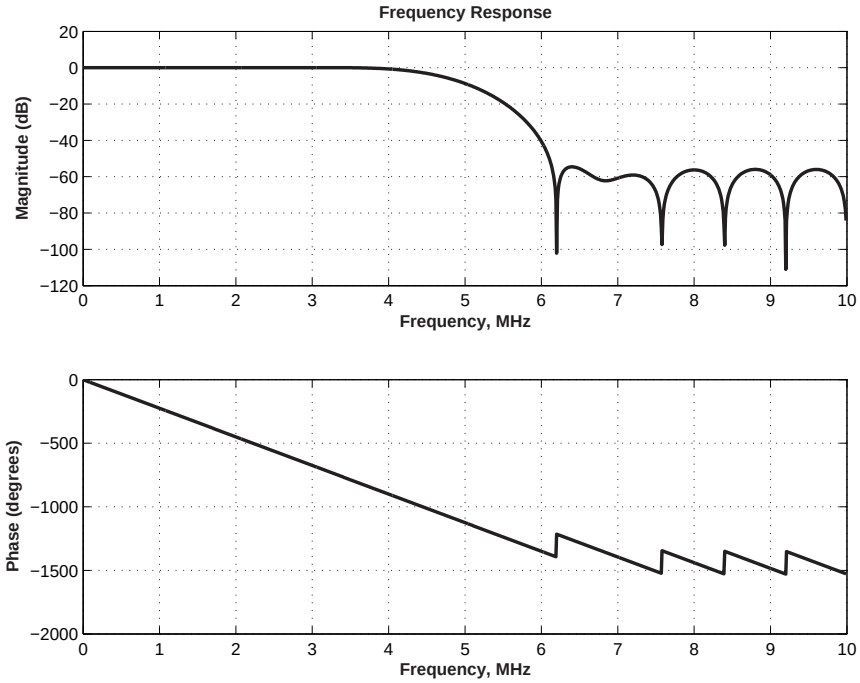

Figure 3.4: Magnitude and Phase Response of FIR Video Signal Filter

synchronization, these effects were deemed acceptable. It should be noted, however, that no investigation was made into the effects on the picture information. The fact that the phase response does not meet the suggested requirements could significantly impact the picture information, but, as previously mentioned, this part of the signal model will not be used so the potential impact can be ignored for the purposes of this research.

3.2.2 Validation. The previous section described how the analytical signal was created. Before this signal could be considered an accurate model, however, it needed to be validated. Specifically, the structure and timing near the synchronization pulses needed to be accurate for proper correlation. To accomplish this, video signal samples were gathered from various encoders and then compared to the analytical model. This section first validates the structure of the synchronization pulses using two of the video encoders and then validates the timing accuracy.

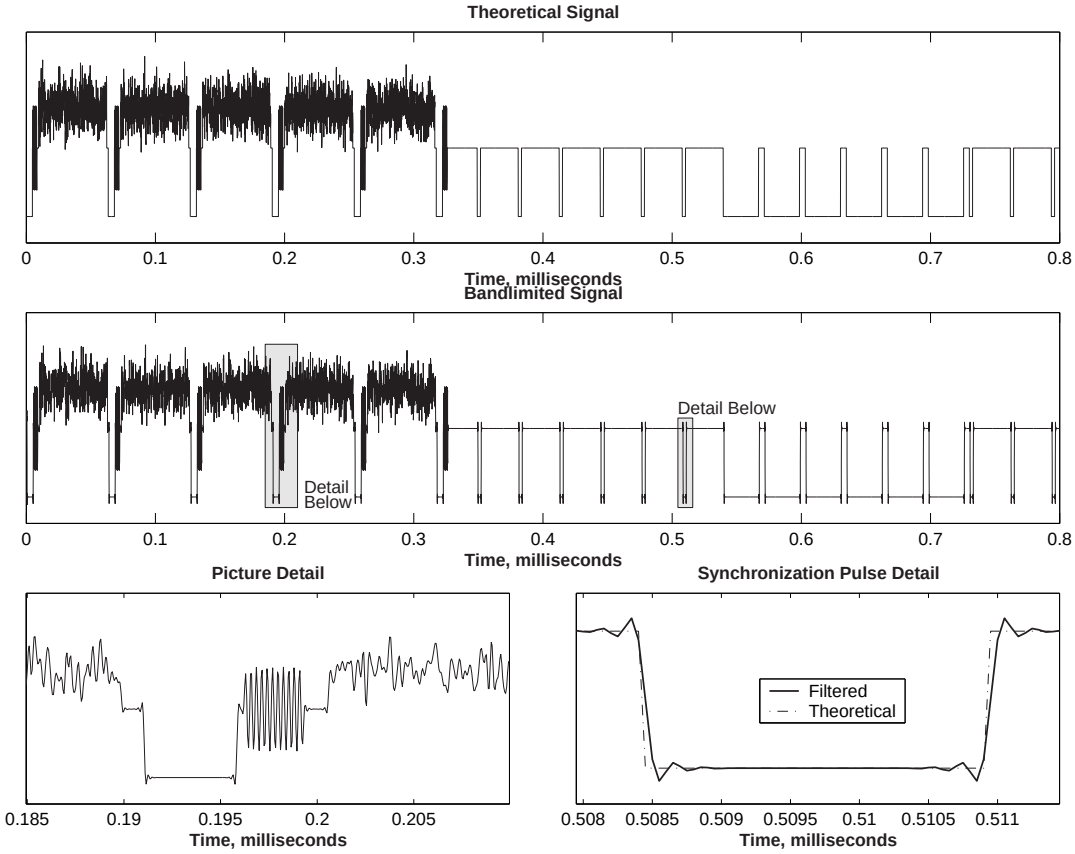

Figure 3.5: Effects of FIR Filter Bandlimiting the Video Signal

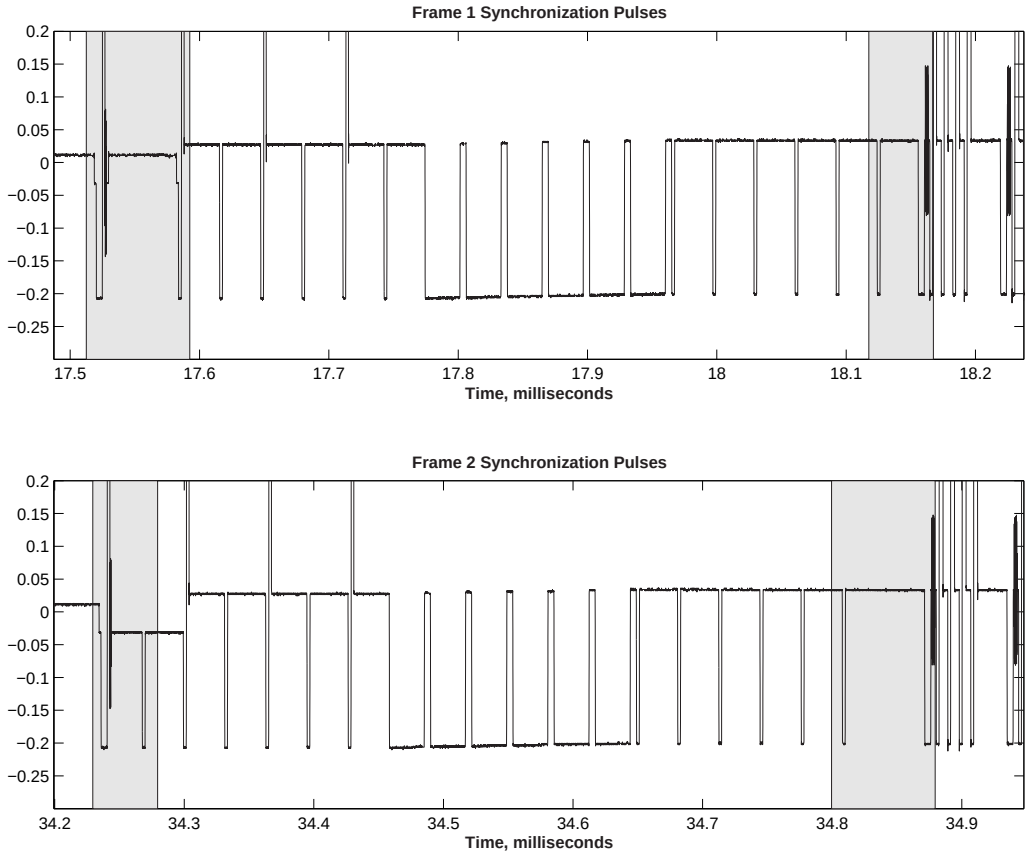

Figure 3.6: Comparison Between Sampled Frame 1 and Frame 2 Synchronization Pulses—DVD Video Encoder

3.2.2.1 Synchronization Pulse Structure. The most significant parts of the synchronization pulse structure to be validated were the distinctions between frame 1 and frame 2. Specifically, the implementation of the half picture line delay in the frame 2 synchronization pulses had to be verified. Figures 3.6 and 3.7 validated this delay using two successive synchronization pulses (one from frame 1, the other from frame 2) from both the DVD and VCR video encoders. The blanking level prior to the first pulse and after the last pulse is highlighted for ease of comparison.

It is seen that both encoders contain a full line delay prior to the frame 1 synchronization pulses and only a one-half line delay prior to the frame 2 synchronization pulses, as expected. The delays following the synchronization pulses were also as expected, a one-half line delay following the frame 1 synchronization pulses

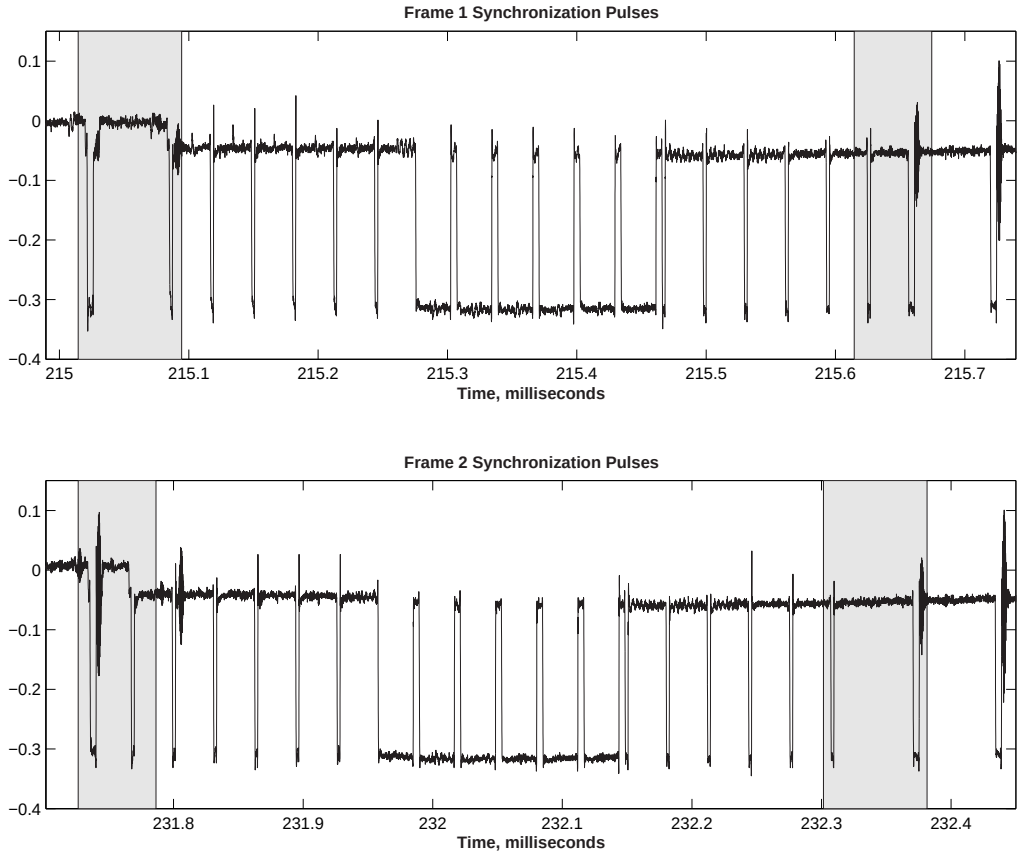

Figure 3.7: Comparison Between Sampled Frame 1 and Frame 2 Synchronization Pulses—VCR Video Encoder

and a full line delay following the frame 2 synchronization pulses. Thus, as compared to the last line of picture information, the frame 2 synchronization pulses were delayed by one-half a line. (Recall that the frame 2 synchronization pulses were delayed by inserting the first half of a line prior to the pulses. Therefore, the last picture line is the line prior to the half picture line shown.)

3.2.2.2 Timing Accuracy. While the structure of the synchronization pulses was validated above, that process did not validate the timing of the signals. For this, the synchronization pulses were isolated and aligned using the "hole punching" algorithm (the algorithm is discussed in Section 3.3.1.1, but all that remains of the signal are the parts of the synchronization pulses below the color burst), as shown in Figure 3.8. The top plot indicates, from a large scale perspective, the analytical and observed waveforms have consistent timing (the pulses seem to overlap for the entire plot). The two lower left plots detail the last vertical sync pulse and first equalizing pulse of the synchronization pulses. The upper of these plots shows how the observed pulses have a longer duration than the analytical model, but the general alignment is correct. The lower detail plot shows the difference in these plots; again, it is seen that the differences are limited to the pulse edges.

The histogram in Figure 3.8 categorizes the voltage differences between the two waveforms shown in the top plot. The number of occurrences in each bin is listed at the top of each bar (the vertical scale has been truncated for clarity). As over 99% of the data points are in the zero bin (which includes voltage errors between -62 and 65 millivolts), this chart clearly indicates the model's timing is accurate. Furthermore, over half of the points not in the zero bin have errors less than 0.5 volts. Many of these points are not caused by timing errors, but other distortions such as ringing in the model and slight deviations in the observed signal.

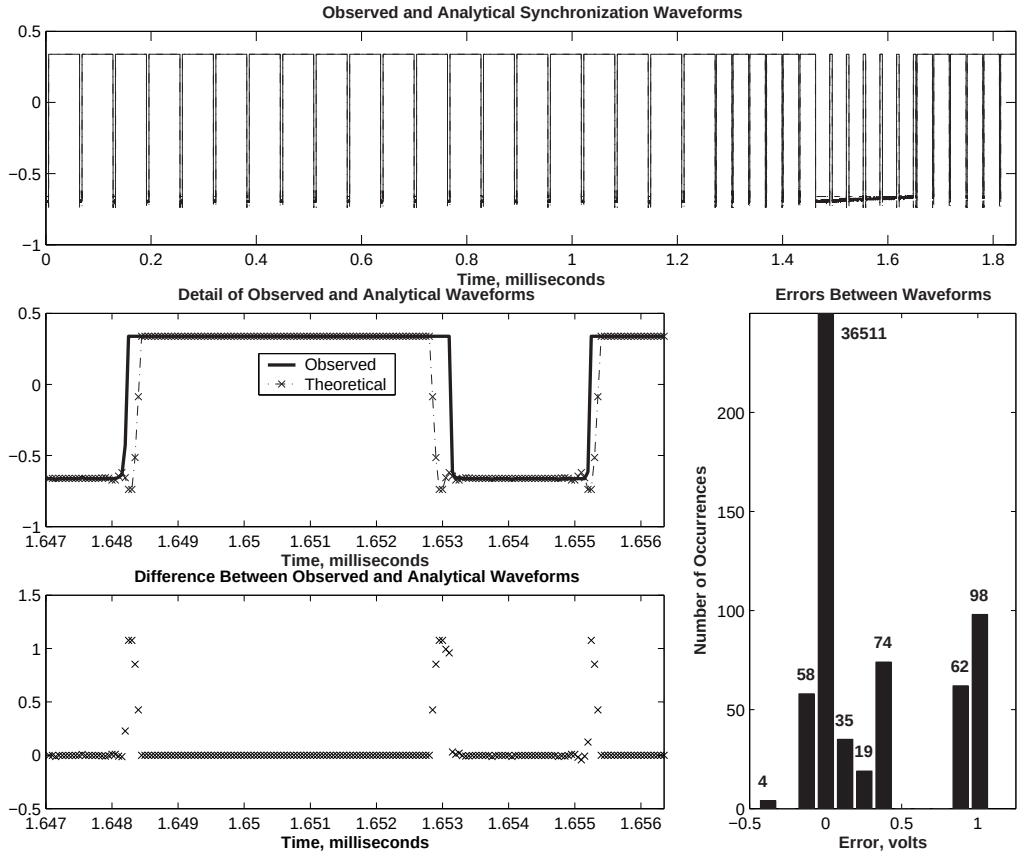

Figure 3.8: Timing Accuracy of the Analytical Model as Compared to the DVD Video Encoder

3.3 Algorithm Development

With an accurate model of the transmitted signal available, the first step towards potentially reducing the dataflow from the classic cross-correlation technique was to develop the algorithms for calculating time-of-arrival or extracting the desired portions of the signal. This section will outline the motivation and development of the waveforms and algorithms used in this research.

3.3.1 Correlation Waveform. The distinct structure and difference in amplitude of the synchronization pulses compared to the rest of the video signal made them desirable for use in a correlation waveform. Specifically, if the pulses could be separated from the remaining signal, the waveform would resemble a square wave with distinct timing patterns. Even if they couldn't be completely separated, however, their distinct amplitude and structure should still allow them to be detected. Thus, two potential correlation waveforms were developed. The first attempted to separate the synchronization pulses and correlate to find the desired structure, known as the "hole punching waveform". The second "searched" for the negative pulse amplitudes at the times where they theoretically should have been, known as the "zeroed pulse waveform". Each of these waveforms is developed below.

3.3.1.1 Hole Punching Waveform. The hole punching waveform performs a non-linear "hole punching" technique to remove all data above a set threshold [39]. This threshold was manually set to a value just below the bottom of the color burst for all waveforms used, and the removed data was set to zero. Then, to provide sharper peaks in the correlation waveform, a bias was subtracted from the entire waveform. As the particulars of the wavefom were not set, this bias was set to the mean of the synchronization pulses for frame 1 gathered from the DVD player video encoder.

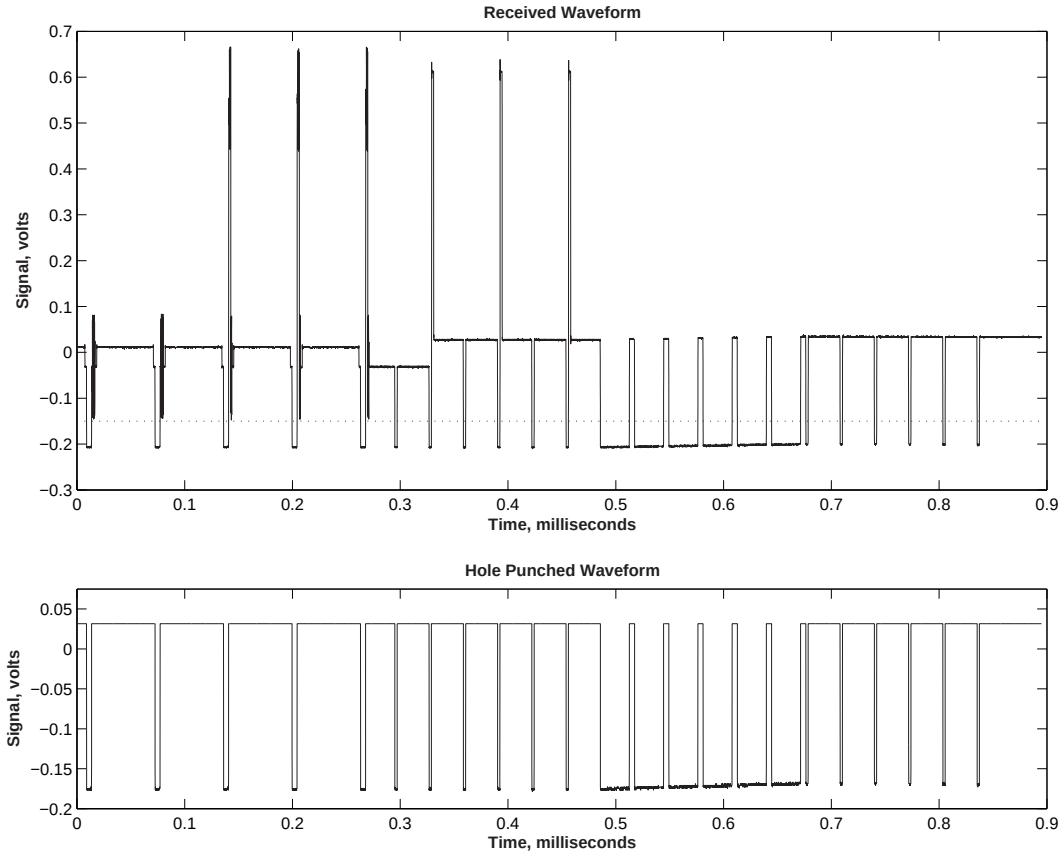

Figure 3.9: Example of Hole Punching Waveform

In some of the severely degraded signals, the bottom of the color burst extended below the synchronization pulses. In these cases, the threshold was set to the best possible level between upper and lower edges of the synchronization pulses.

An example of the hole punching waveform applied to a small section of data is shown in Figure 3.9. The upper plot shows the original data and the threshold used (indicated by the dotted line). The lower plot shows the waveform after "hole punching" and removing the mean.

After developing how the correlation waveform would be extracted from the data, the next step was developing what sections of the video signal were to be included in the waveform. For this, a series of analytic waveforms were correlated with a data set from the DVD player video encoder. The first waveform was the

synchronization pulses by themselves. Then, groups of ten picture lines were added to the front of these pulses to differentiate between frames 1 and 2 and reduce the correlation value of some of the sidepeaks, as shown in Figure 3.10. As expected, the synchronization pulses alone did not differentiate between frames 1 and 2. The additional picture lines did not produce the expected results, however. The correlation value of frame 2 synchronization pulses increased as the number of picture lines increased (after the initial drop from the first 10 picture lines). The alternating increase and decrease in correlation value of the alternate sidepeaks was also not expected. Thus, simply adding more picture lines did not seem to improve performance. The best performance occurred when either 10 or 20 picture lines were added to the synchronization pulses, depending on if the first or second sidepeaks were considered the most important. Ultimately, despite a slight decrease in correlation performance of frame 2 and the second sidepeak, 20 picture lines and the synchronization pulses were chosen as the correlation waveform. The longer waveform would have more stability when distortions affected the signal (i.e. the sidepeaks would stay less than the desired peak) and increased signal detection capabilities.

3.3.1.2 Zeroed Pulse Waveform. The zeroed pulse waveform was developed out of a desire to correlate without pre-processing or altering the received waveform. Thus, the fact that the synchronization pulses were the most negative part of the signal was exploited for correlation. Specifically, if the analytic waveform was negative during the intervals when the received waveform was negative, the "product integration" of the correlation process would cause the output to be positive (assuming no other points caused a subtraction). Furthermore, the more negative the received waveform, the larger the correlation value would become (assuming the analytic waveform was constant). Thus, the zeroed pulse waveform was made negative during all the synchronization pulses and zero elsewhere. This way, the correlation would be most positive when the analytic pulses aligned with the synchronization pulses.

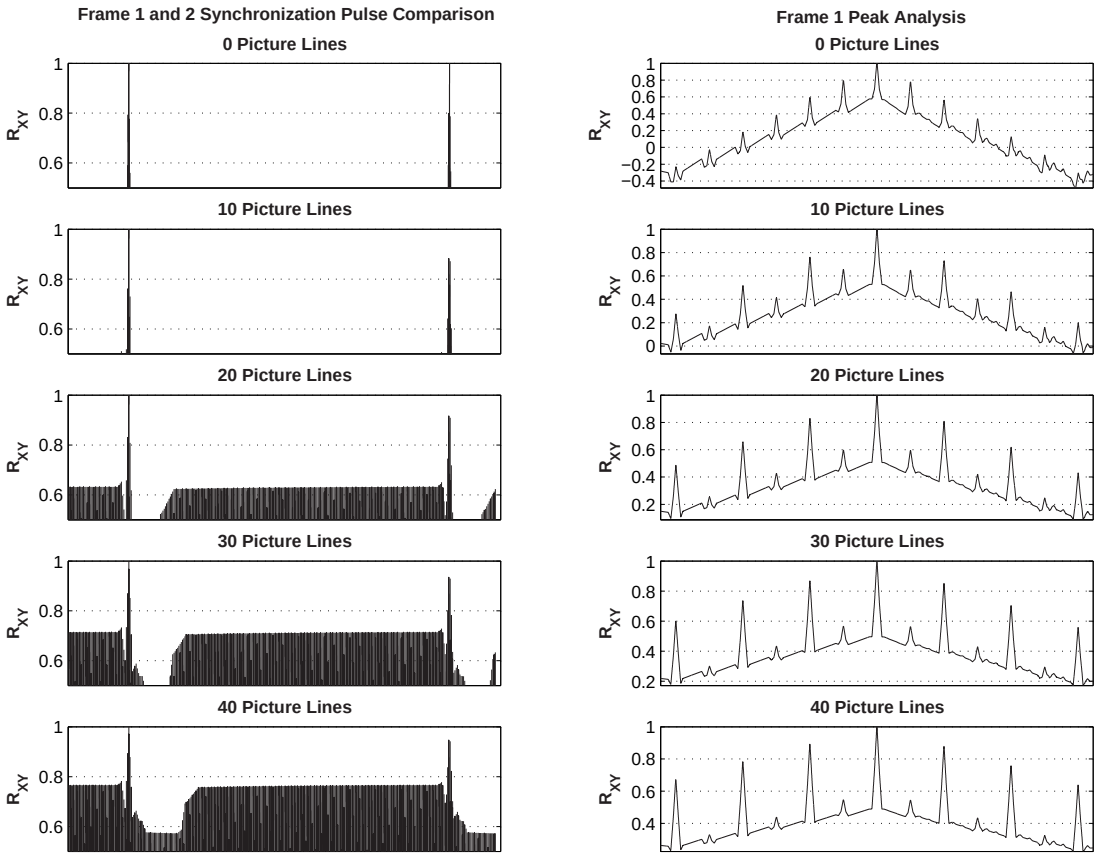

Figure 3.10: Waveform Development—Correlation Peak Analysis

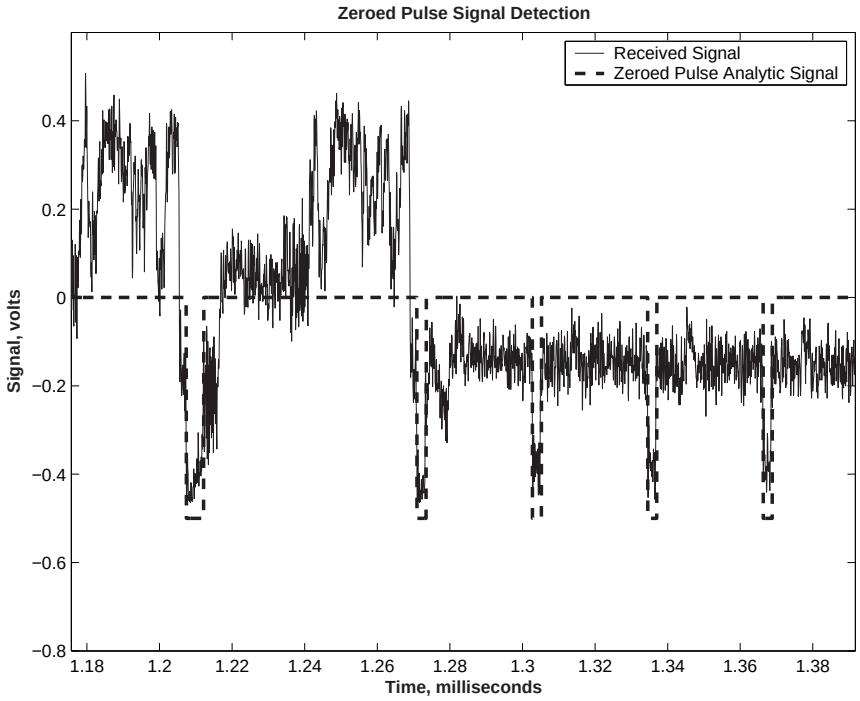

Figure 3.11: Zeroed Pulse Signal Detection

The elements of the the zeroed pulse waveform followed the efforts of the hole punching waveform in that 20 picture lines were added to the synchronization pulses. However, because this waveform would not eliminate the other portions of the signal, it was decided to add 20 picture lines before and after the synchronization pulses.

A portion of the zeroed pulse signal with a received signal is shown in Figure 3.11. From this figure, it can be seen how the zeroed pulse signal can accurately detect the received signal's TOA. If the alignment was slightly different, the smaller negative (or positive) value of the received signal would have a smaller output from the "product integration". Thus, when the zeroed pulse signal aligns with the synchronization pulses (theoretically the most negative part of the signal), the output of the correlator should be the greatest.

3.3.1.3 Calculating the TDOA Measurement. The waveforms to be correlated were discussed in the previous section. In this section, two methods of de-

termining the signal's TOA – or the resulting TDOA measurement (see Section 2.1.2) – are discussed: the linear fit estimator (as discussed in Section 2.3.2) and the center of mass estimator.

The correlation peaks, like those in Figure 3.10 above, contained 42 samples on each side of the peak value before the slope of the correlation peak changed. Unfortunately, the first two points on each side of the highest sample had a "round-off" effect, as opposed to a sharp intersection. Therefore, the linear fit estimator used the 40 remaining points on either side of the peak to estimate the actual correlation peak. These results, extrapolated for clarity, are shown in the upper plot of Figure 3.12.

The center of mass estimator investigated using much more of the correlation waveform for peak estimation in order to add stability in the presence of noise and other degradations. Specifically, the first six sidepeaks on each side of the main peak, along with the main peak, were used to calculate the center of mass. To allow for movement, a "floor" was set by averaging the samples just outside the desired interval, as shown by the shaded blocks in the lower plot of Figure 3.12. This floor was subtracted from all the samples so that, ideally, movement of the entire peak within this region would not affect the remaining correlation values. After removing this floor, all of the samples in between and including the shaded areas were processed to find the center of mass, shown by the vertical line. The deviation from the highest peak was caused by the asymmetry of the hole punching waveform and resulting correlation plot.

Despite not being aligned with the highest peak, the center of mass estimator could still be a viable time of arrival estimator. As long as the same method is used in both receivers, the difference between this method's estimate and the actual peak will be the same. Furthermore, the bias between this method and the linear fit estimator could prove to be very useful. As described in Section 2.4, multipath can either advance or delay the correlation peak estimate, depending on the multipath

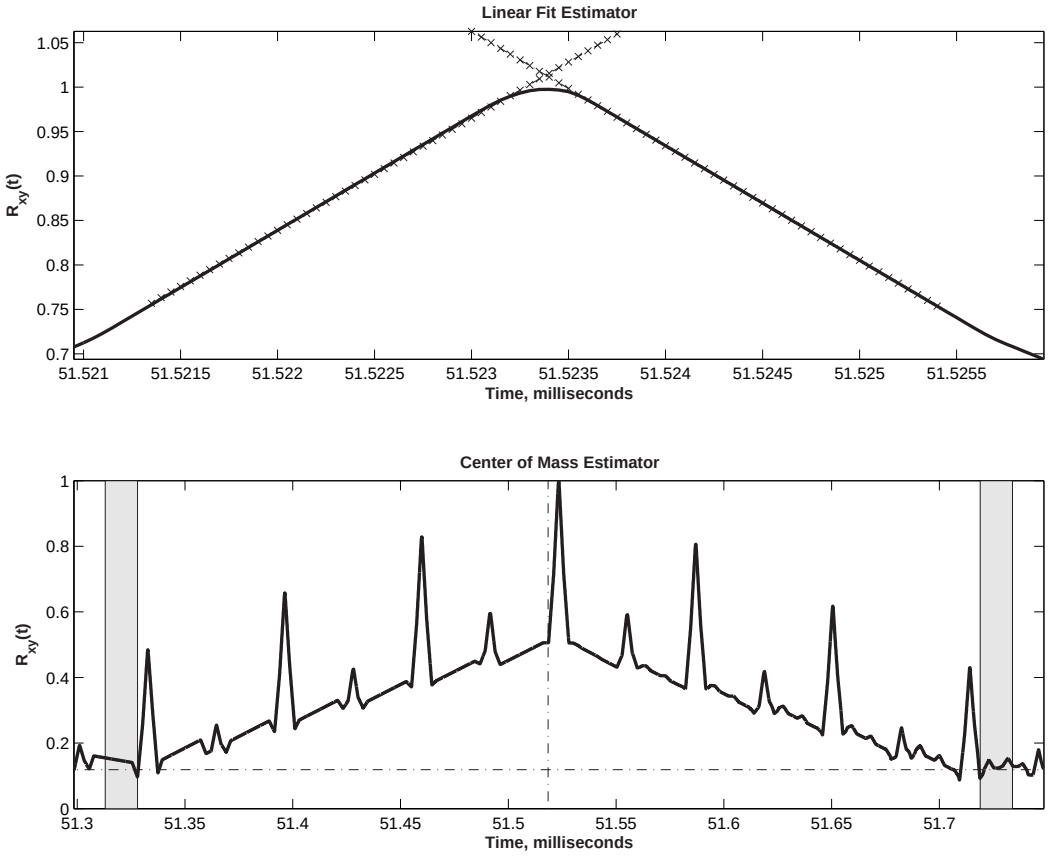

Figure 3.12: Illustration of Correlation Peak Estimators

and the peak estimator used. As these changes are caused by the addition of a delayed signal, the center of mass of the composite correlation waveform would also change. This change in bias between the center of mass estimator and linear fit peak estimator could serve as an indicator that multipath has degraded the signal.

3.3.2 Cross-Correlation Dataflow Reduction. The methods for calculating the individual TOAs were discussed in the previous section. This section, similar to the more classical cross-correlation method, develops how a subset of the received data was used in a cross-correlation algorithm to estimate the TDOA. A principal benefit to this approach, as motivated in Section 2.3.3, is that any random distortions common to both receivers would provide a much more distinctive peak (similar to impulse shown in Figure 2.12). The downside to this algorithm is that the reference

receiver must provide the time-tagged waveform to the target receiver, not just a single time-of-arrival. This may not be feasible in many practical applications.

The subset of the received waveform was generated by correlating the reference receiver waveform with the zeroed pulse waveform described in Section 3.3.1.2. The sample indices from the correlation peaks were then used to parse the received waveform into the sections containing the frame 1 synchronization pulses. These data sets were then correlated with the target receiver waveform to directly determine the TDOA measurement.

To reduce processing time, a shortcut was used in the target receiver correlation process. Because the clock bias was very near zero (the only potential bias was in the different hardware delays), the shift in data was limited to the actual distance separating the antennas. The hardware (specifically the cable lengths) used in this research only allowed a maximum separation of about 8 samples. Thus, the waveform from the reference receiver was expanded by 20 samples on either side and correlated to find the TDOA measurement. A fully implemented system would be able to perform a similar process once the approximate clock bias was known. Until that bias was known, however, the subset of data would have to be correlated over the entire target receiver data set, and an ambiguity resolution technique would have to be applied to all resulting peaks.

To justify this processing shortcut, the two potential ambiguities associated with this system are briefly discussed. First, the ambiguities from the successive synchronization pulses are shown in Figure 3.13. It is evident that the peaks occur at 60 Hz, thus the ambiguities equate to multiples of 5000 kilometers (3000 miles)–the distance between New York, NY and San Francisco, CA. The next ambiguity associated with this system is caused by the correlation sidepeaks shown in Figure 3.10. These peaks are separated by 63.5 microseconds, so the ambiguities are multiples of 19 kilometers (11 miles). While this ambiguity would be tougher to solve than that from the successive synchronization pulses, it would not be overly difficult. If an

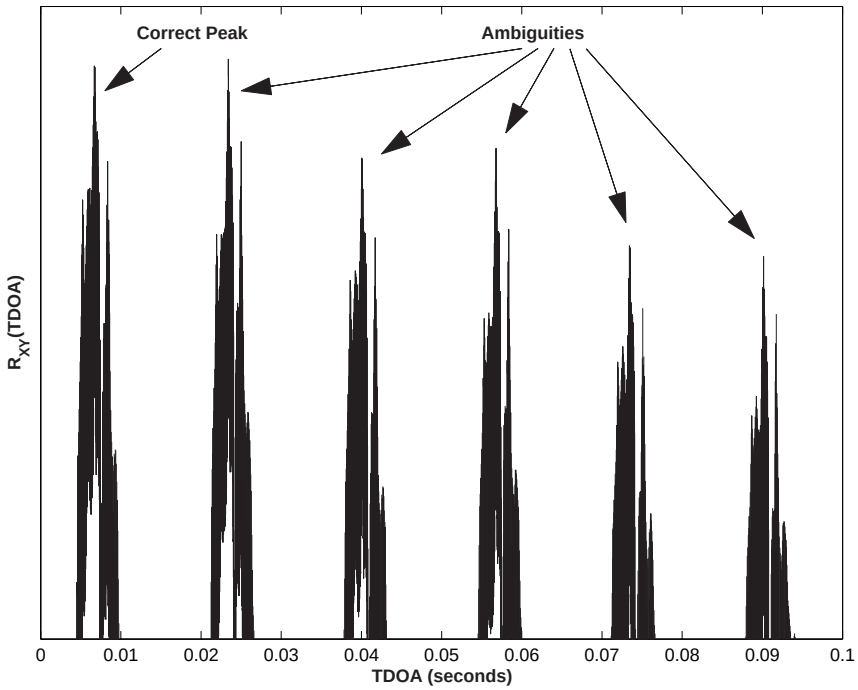

Figure 3.13: Potential Ambiguities From Successive Synchronization Pulses

initial position estimate with reasonable accuracy is available (i.e., significantly less than 19 kilometers), this would provide information to resolve all ambiguities. Even if an initial position estimate was not available, however, the separation is so large, ambiguity resolution techniques could quickly resolve the ambiguity. This process is outside the scope of this research and will be assumed possible.

3.3.2.1 Range Measurement Errors. The TDOA measurement process was outlined in Section 2.1.2, but only clock bias errors were discussed. There are many other potential sources of error in each TDOA measurement and resulting range estimate. To best understand these errors, it is convenient to start with the time measurement at each receiver with potential errors included.

$$t_{meas} = t_{true} + \varepsilon_{clk} + \varepsilon_{samp} + \varepsilon_{err} \tag{3.1}$$

where

t_{meas} is the signal's measured time of arrival
t_{true} is the signal's actual time of arrival
ε_{clk} is the error in the estimated clock bias
ε_{samp} is the discretization error
ε_{err} is the remaining error sources

Then, using Equation (2.3), the TDOA measurement is:

$$\begin{aligned} TDOA =& (t_{true_{TARGET}} - t_{true_{REF}}) + (\varepsilon_{clk_{TARGET}} - \varepsilon_{clk_{REF}}) + \\ & (\varepsilon_{samp_{TARGET}} - \varepsilon_{samp_{REF}}) + (\varepsilon_{err_{TARGET}} - \varepsilon_{err_{REF}}) \\ TDOA =& (t_{true_{TARGET}} - t_{true_{REF}}) + \Delta\varepsilon_{clk} + \Delta\varepsilon_{samp} + \Delta\varepsilon_{err} \end{aligned} \tag{3.2}$$

where

$t_{true_{TARGET}} - t_{true_{REF}}$ is the true time difference
$\Delta\varepsilon_{clk}$ is the differenced clock bias error
$\Delta\varepsilon_{samp}$ is the differenced discretization error
$\Delta\varepsilon_{err}$ is the differenced remaining error sources

Each of these error sources is discussed individually for the single time measurement below. Note that these errors will be differenced when forming the TDOA measurement, and this differencing would need to be taken into account if completely characterizing the TDOA measurement errors.

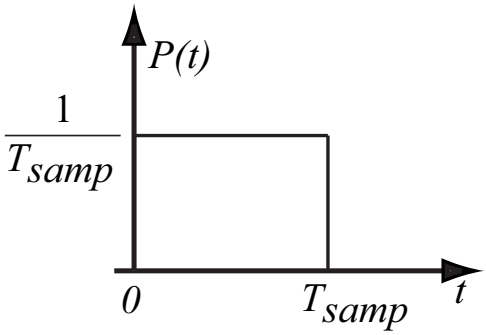

Figure 3.14: Probability Density of Discretization Error

Clock Bias Error. Equation (2.14) provides the clock bias estimate converted to meters, $c\hat{\delta}t$. Ignoring the speed of light scale factor, the clock bias error is:

$$\varepsilon_{clk} = \hat{\delta}t - \delta t \tag{3.3}$$

where

$\hat{\delta}t$ is the estimated clock bias

δt is the true clock bias

Thus, the clock bias error is the difference between the true clock bias and estimated clock bias.

Discretization Error. The NTSC broadcast signals are analog (continuous) signals; this research uses sampled versions of these signals. Therefore, the error associated with any time measurement is:

$$0 < \varepsilon_{samp} < T_{samp} \tag{3.4}$$

where T_{samp} is the sample period. Any event that happens between two samples will be measured at the later sample. Furthermore, as the actual sample times are independent of the signal being sampled (there is no synchronization), the probability of error is uniform between 0 and T_{samp}, as shown in Figure 3.14.

Remaining Error Sources. In addition to the clock bias and discretization errors, many other potential sources of error exist: multipath, interference from other signals, transmitter clock drift, receiver front end distortions, and antenna affects during both transmission and reception. Separately characterizing each of these parameters is outside the scope of this research, and they will be treated as a single error.

3.4 Test Environments

With all of the waveforms and algorithms for generating the TDOA measurement in place, system testing was the next step. This section will describe the two different test environments: (1) an open field to provide a low multipath environment, and (2) an area surrounded by buildings to provide a high multipath environment. Each of these areas are discussed below.

3.4.1 High Multipath Environment. The high multipath environment was an opening North of Building 194 on Wright-Patterson Air Force Base, Ohio (WPAFB), labeled "Test Area" in Figure 3.15. In this area, two different tests were performed. The first was a series of tests to investigate the multipath inside and in close proximity to the building (the area between lables "A" and "C") and is referred to as the "Indoor-Outdoor" test. The second test was in the field North of the building with antennas placed at the locations labeled "A","B", and "C" (the true coordinates for these locations are listed in Appendix A). The portion of the test with antennas placed at locations "A" and "C" is the "original" configuration, and the portion with antennas placed at "A" and "B" is the "perpendicular" configuration.

The "Indoor-Outdoor" test was divided into the three possible antenna combinations: (1) indoor-indoor, (2) indoor-outdoor, and (3) outdoor-outdoor, and are shown in Figure 3.16. The gray circles represent the antenna locations, the heavy

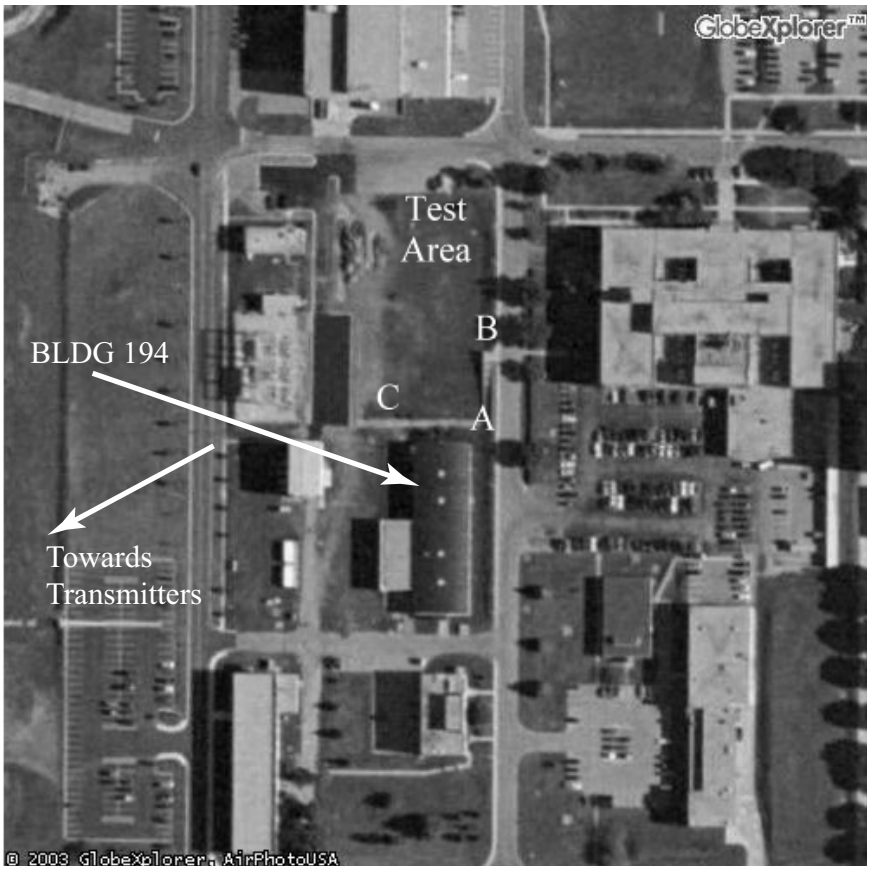

Figure 3.15: High Multipath Environment

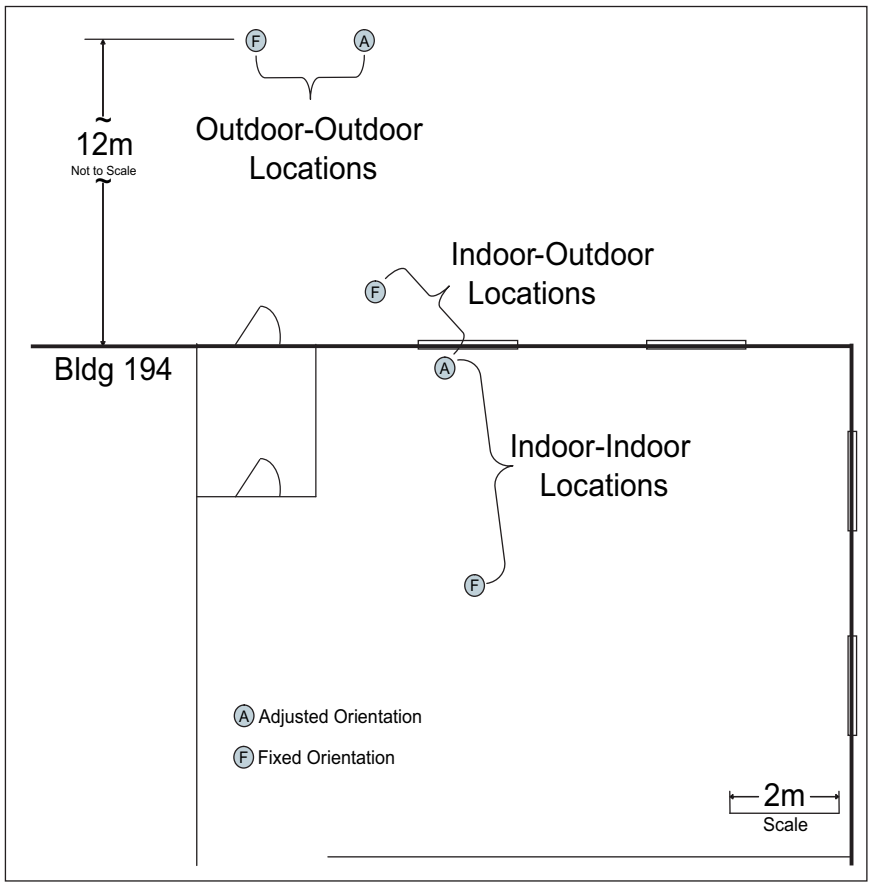

Figure 3.16: High Multipath Environment Test Diagram

lines represent the exterior (concrete-block) walls, the thin lines represent the inner walls (drywall covered metal studs), the boxes overlaying the exterior walls represent the windows (27 inches high, 57 inches wide), and the arcs represent doors (metal). The room where the indoor antennas were placed is 22 feet wide and 26 feet long. The ceiling of Building 194 is a drop ceiling with 2 feet by 4 feet ceiling tiles. Additionally, both of the exterior walls and the interior wall surrounding the indoor antenna locations were lined with computer desks and eleven powered on computers.

The adjusted indoor-indoor (and indoor-outdoor) antenna was placed on the cabinet of one of the computer desks about 6 inches below the bottom of the window. The fixed indoor-indoor antenna was placed on a printer stand about 4 feet above

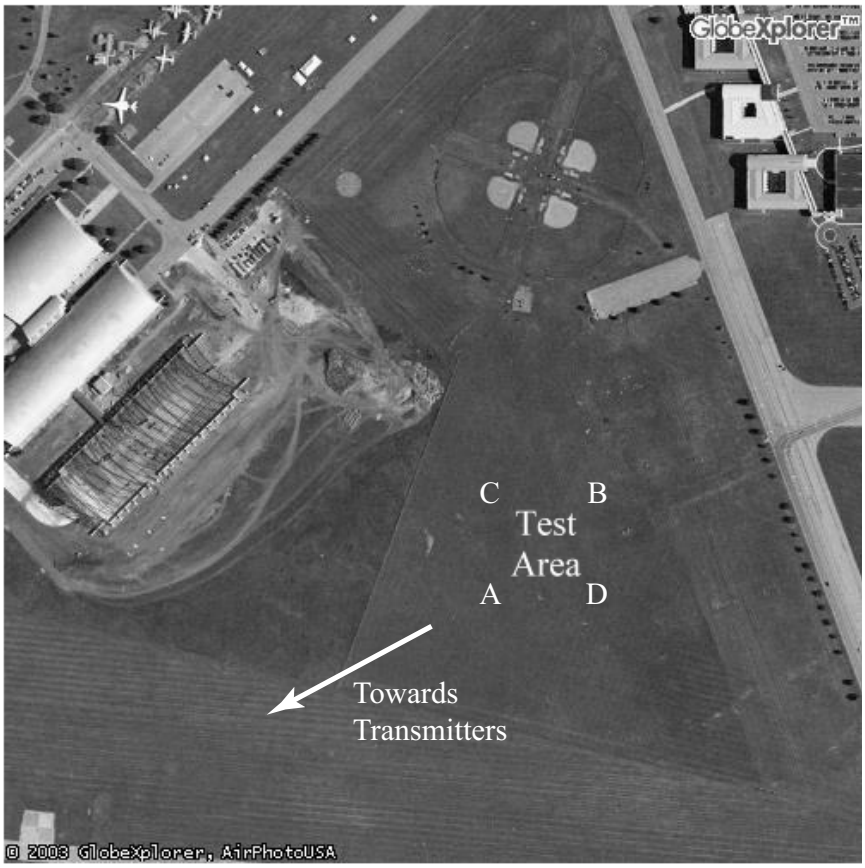

Figure 3.17: Low Multipath Environment

the floor. The fixed indoor-outdoor antenna was placed on an empty 12 inch wire-spool placed on the ground. Both of the outdoor-outdoor antennas were also placed on the wire-spools, again sitting on the ground.

3.4.2 Low Multipath Environment. The low multipath environment was a large open field Southeast of the United States Air Force Museum, WPAFB, as shown in Figure 3.17. At this location, the antennas were extended about the radial (inline with) the television transmitters (positions "A" and "B", known as the "original" and "switched" configurations) and perpendicular to the radial (positions "C" and "D", known as the "perpendicular" configuration). The true coordinates for these four locations are also given in Appendix A.

3.5 Summary

This chapter described the signal acquisition process. The sections on the NTSC broadcast signal and algorithm development described how the signals were exploited for navigation. The environments where system testing occurred were described.

IV. TDOA Measurement Results and Analysis

This chapter presents and analyzes the results from the tests conducted in the two test areas described in Section 3.4. Of particular interest is characterizing the error in each of the TDOA measurements and evaluating which algorithms consistently have the best performance. Additionally, TDOA measurements from one of the data sets are used to derive a position estimate using the TDOA algorithm derived in Section 2.1. Finally, an expanded system is simulated using actual television transmitter locations and the error characteristics derived in this research.

4.1 TDOA Measurement Analysis

A "zero baseline" test was conducted to measure the functionality of the test hardware, and then the spin test, short translation test, and long translation test were performed to evaluate the TDOA measurement accuracy. Each of these tests are described in the sections that follow.

4.1.1 Zero Baseline. The zero baseline test was designed to verify that the hardware and algorithms were working properly. In this test, the output of a single antenna was split and propagated through both sets of cables and VCRs to the ADC, as shown in Figure 4.1. The unique aspect of this test is that it performs just like having separate antennas, but the distance between them is known to be zero meters. Furthermore, because the same antenna is used, all errors inherent in the signal (propagation affects, multipath, and antenna phase delay) should be identical for both receivers. Any differences–both in signal structure and TDOA measurements–must be caused by a timing bias or inconsistencies in the hardware. This test was only performed with the antenna placed outdoors, North of Building 194.

The TDOA measurements calculated from four consecutive frame 1 synchronization fields using the hole punching waveform are shown in Table 4.1. Three

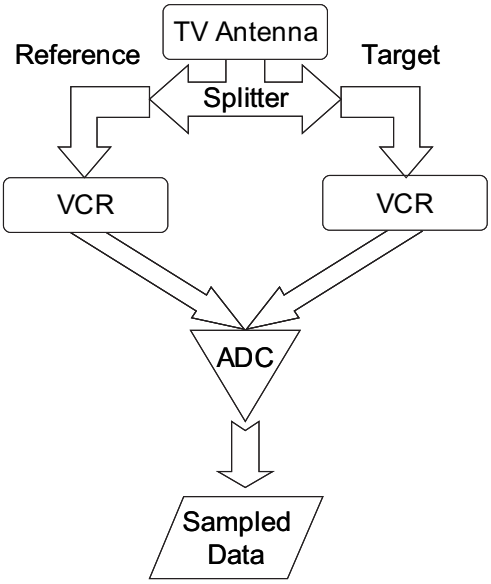

Figure 4.1: Zero Baseline Test Setup

Table 4.1: Zero-Baseline TDOA Measurement Errors (meters)

Sample Peak Estimator	Linear Fit Estimator	Center of Mass Estimator
0	0.01	2.09
0	-3.41	32.37
-14.99	-3.03	5.21
-14.99	-4.63	35.51

different measurement techniques were used–the sample peak estimator (discussed in Section 2.3.2), the linear fit estimator (discussed in Sections 2.3.2 and 3.3.1.3), and the center-of-mass estimator (discussed in Section 3.3.1.3). The only peak estimator that performed consistently was the linear fit estimator. While the sample peak estimator performed extremely well in two of the data points, it's lack of resolution makes it impractical. The center of mass estimator was also inconsistent in the four data points. Therefore, this data lead to dismissing both the sample peak and center of mass TDOA measurement estimators.

The consistently small error magnitude from the linear fit estimator supported the assumption that the timing bias and hardware delays were small (less than 5

meters in this case). While additional tests would be needed to verify the timing bias, this test proved both the hardware and basic algorithms were working as desired.

4.1.2 High Multipath Environment Tests. The second set of tests performed were the three combinations of indoor and outdoor antenna locations North of Building 194. The objective of these tests was to begin characterizing algorithm performance, and to determine the severity of multipath in this environment.

4.1.2.1 Spin Test. The spin test was first in a series of tests to analyze the severity and dynamic effects of multipath. For this test, one antenna remained fixed while the other was rotated to one of seven positions ranging 1/4 of a turn in either direction from the orientation of the fixed antenna. The seven positions are shown in Figure 4.3, where position 4 is the orientation of the fixed antenna. Additionally, this test was only performed using the rabbit-ears antenna; the wire antenna was assumed to be omnidirectional, so it would not benefit from this test.

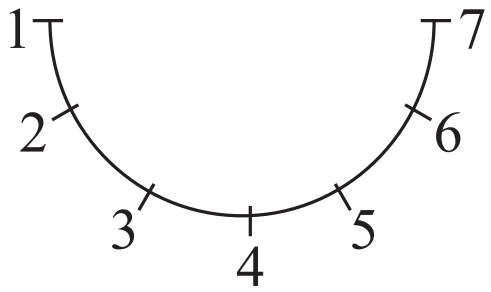

Figure 4.2: Spin Test Rotational Position Indicators

The resulting TDOA measurements from this test are shown in Table 4.2, where the cross-correlation algorithm is identified as "XCORR", the hole punching algorithm is identified as "HOLE", and the zeroed pulse algorithm is identified as "ZERO". (These algorithms are described in Sections 3.3.2, 3.3.1.1, and 3.3.1.2, respectively). The true TDOA measurement for each of location was 0 meters for the indoor-indoor test, 1 meter for the indoor-outdoor test, and 2 meters for the outdoor-

outdoor test. Thus, given the large magnitude of error in many of the measurements, the TDOA measurements themselves approximate the TDOA measurement errors.

This test demonstrates many interesting points. First, the general consistency among each of the groups of data (i.e., every position of a single algorithm) indicates that noise is not a dominant source of error. If errors from noise were present, the errors would have a random nature about the true values. Second, the wide variation in the number of data points at each position highlights a degradation in signal structure. Each data set contained 0.1 seconds of data; thus each group should, ideally, have three correlation peaks from the frame 1 synchronization pulses. However, given the data samples started at an arbitrary time, one of the synchronization pulses may have been too close to the starting or ending point to be processed. The groups containing more than three values processed either the frame 2 synchronization pulses or some of the sidepeaks along with the main peak from frame 1 (which was possible because a fixed normalized correlation threshold of 0.96 was used during processing). Finally, when looking at the data, the errors–whatever they may be–are greatly degrading system performance. Less than 1/4 of the data groups are within 10 meters of the true TDOA measurements; only three of these cases occurred during the indoor-outdoor test and none occurred in the outdoor-outdoor test.

When analyzing the total spread (the difference between the smallest and largest measurement) of the TDOA measurements over all antenna positions, the cross-correlation algorithm consistently outperformed the other methods. It's values were spread only 30 meters for the indoor-indoor test, compared to 100 meters for both of the other methods. The indoor-outdoor test had a spread of 15 meters, compared to 60 and 70 meters for the hole punching and zeroed pulse algorithms. Finally, the outdoor-outdoor test had a spread of 45 meters for the cross-correlation algorithm, compared to 75 and 80 meters for the other algorithms.

When analyzing the actual magnitude of the errors, all but one of the data sets were split such that the spread noted above was both above and below the true

Table 4.2: Indoor-Outdoor Rabbit-Ears Spin Test TDOA Measurements (meters)

Rotational Position	Indoor-Indoor True TDOA: 0 meters			Indoor-Outdoor True TDOA: 1 meter			Outdoor-Outdoor True TDOA: 2 meters		
	XCORR	HOLE	ZERO	XCORR	HOLE	ZERO	XCORR	HOLE	ZERO
1	14.50	47.60	66.32	0.52	-3.15	-7.10	-29.89	20.18	30.16
	14.43	52.97	66.16	0.58	-2.68	-7.65	-29.93	17.96	29.67
	14.46	51.33	67.56				-29.91	19.04	29.25
	14.43								
2	1.67	40.07	61.65	0.25	2.81	-2.13	-30.11	31.29	28.30
	1.59	41.35	61.26	0.26	2.75	-2.08	-30.13	28.42	27.36
	13.04	42.04	61.42	0.27	3.49	-2.18	-30.09	29.70	26.61
	1.65						0.10		
							-0.07		
3	-1.84	15.48	31.19	-0.58	2.00	-0.71	-29.67	25.32	28.32
	-1.80	18.57	30.41	-0.62	1.47	-0.79	-29.68	26.15	27.82
	-1.79	15.55	28.32	-0.65	0.90		-29.66	33.23	28.07
	-1.69								
	-1.63								
4	-15.35	-52.26	-41.42	-15.27	-49.84	-72.56	-29.82	-34.08	-23.38
	-15.39	-54.34	-41.09	-15.31	-55.23	-72.31	-29.88	-34.81	-24.15
	-15.54			-15.32	-54.32	-72.03	-29.83	-35.13	-23.38
5	-14.01	4.23	36.29	-14.15	-31.22	-39.97	14.73	26.82	46.16
	-14.01	13.30	38.40	-14.15	-32.64	-40.74	14.64	25.28	38.93
	-14.04	9.77	36.88	-14.15	-32.10	-39.85	14.61	26.43	38.54
	-13.97								
	-13.98								
6	-0.17	33.32	36.70	-0.39	-6.61	-16.35	-29.60	32.30	38.43
	-0.24	31.35	35.02	-0.38	-6.75	-15.64	-29.60	33.47	38.19
	-0.18	35.11	35.44				-30.01		38.22
	-0.20						-29.71		38.13
							-30.04		37.52
									37.86
7	1.29	31.20	46.55	0.09	-0.76	-6.62	-30.15	39.51	35.80
	1.22	31.75	45.33	-0.02	0.83	-6.00	-30.11	39.51	31.90
	1.26	27.96	44.61	-0.02		-5.81	-30.11	39.68	31.19
	1.21		43.72	0.10		-6.30			
	1.26		43.74	-0.07		-6.43			
				-0.07		-6.01			

TDOA measurement. The relatively large amounts of movement at the ends of the antenna and the in-phase out-of-phase shift pattern of multipath noted in Section 2.4 are strong indicators that multipath was a significant error source. (The antenna's gain pattern changes when the antenna is rotated, therefore the relative gain between the direct and multipath signals will change as the antenna is rotated. This change in relative gain can cause the effect seen in Table 4.2.)

4.1.2.2 Short Translation Test. While many insights were gathered from the previous test, including which algorithm seemed to be performing the best, the data could not confidently attribute the errors to a specific cause. To further explore the possibility of multipath causing the error without changing the direction of the antenna's gain pattern, the short translation test was performed for three different channels in the outdoor-outdoor test (a case where all algorithms performed to about the same level in the previous test). Again, one antenna remained fixed, but instead of rotating the second antenna, it was shifted sideways (i.e., "translated") on a line extending both directions from the starting point. Each translation was approximately 2 centimeters, except from position 3 to 4 where it was approximately 6 centimeters (see Figure 4.3). This test only moved the antenna slightly, so the received signal's incident angle should be nearly the same for all positions. Thus the antenna gains applied to each of the signals (whether they be direct or multipath signals) should not be different. This test was performed using both the rabbit-ears antenna and the wire antenna.

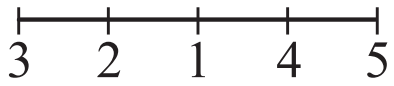

Figure 4.3: Short Translation Test Translational Position Indicators

Rabbit-Ears Antenna Short Translation Test. The TDOA measurements from the short translation test using the rabbit-ears antenna are shown

Table 4.3: Outdoor-Outdoor Rabbit-Ears Short Translation Test TDOA Measurements (meters)—True TDOA Measurement: 2 meters

Translational Position	Channel 2			Channel 7			Channel 26		
	XCORR	HOLE	ZERO	XCORR	HOLE	ZERO	XCORR	HOLE	ZERO
1	0.87	-9.41	-19.83	29.51	12.56	10.70	-164.33	-149.82	-151.08
2	0.94	-9.67	-16.14	29.52	18.75	15.02	-179.25	-149.27	-150.47
3	0.83	-8.56	-18.25	29.47	16.65	16.68	-179.26	-149.98	-151.32
4	0.90	-7.65	-15.21	29.66	18.22	15.15	-151.01	-144.32	-146.04
5	0.78	-7.37	-16.68	29.78	34.71	17.05	-151.41	-156.86	-157.41

in Table 4.3. Previously the spin test showed that each group of TDOA measurements was consistent to within a few meters. Therefore, the mean of each group is presented as the TDOA measurement for the remainder of this research. Before analyzing the data, it must be stated that channel 26 suffered from a very noticeable ghost image and was much noisier (i.e., the image had a large amount of "snow" with it). Thus, despite being included, it was expected that this data set would perform poorer than the others. The cross-correlation algorithm for channel 26 had a spread of 30 meters, as compared to 0.2 meters for channels 2 and 7. Additionally, channel 26 had a consistent general error of 150 meters across all three algorithms, whereas channels 2 and 7 had maximum error magnitudes between 15 and 30 meters.

Thus, this test proved that similar magnitudes of errors (very large) could affect the TDOA measurements without rotating the antenna. Large deviations from position to position in each channel during the spin test were not experienced. This was possibly explained by the small amounts of movement (opposed to the large movements of the spin test). This motivated the long translation test, which is described in Section 4.1.2.3.

Wire Antenna Short Translation Test. Continuing on the assumption that multipath was the dominant error source, the next test attempted to reduce (or mitigate) the errors. The rabbit-ears antenna had two different poles that extended over 1 meter wide. Thus, many different multipath signals could be

Table 4.4: Indoor-Indoor Antenna TDOA Measurements (meters) Comparison—True TDOA: 0 meters

(a) Rabbit-Ears Spin Test

Rotational Position	XCORR	HOLE	ZERO
1	14.50	47.60	66.32
2	1.67	40.07	61.65
3	-1.84	15.48	31.19
4	-15.35	-52.26	-41.42
5	-14.01	4.23	36.29
6	-0.17	33.32	36.70
7	1.29	31.20	46.55

(b) Wire Short Translation Test

Translational Position	XCORR	HOLE	ZERO
1	-14.11	9.83	10.23
2	-14.55	-0.15	0.03
3	-14.91	-3.79	-3.41
4	-13.90	4.32	6.14
5	-13.66	6.78	7.10

incident upon it at any given time. To reduce this, the wire antenna was used– it simply had less physical area for signal reception. It was known this antenna would have much less gain than the rabbit-ears antenna (probably losses), but this would only strengthen the argument that multipath was dominant if improvement was noted. This test was performed in both the indoor-indoor and outdoor-outdoor configurations; each are discussed below.

The indoor-indoor test was performed in order to compare with the indoor-indoor rabbit-ears spin test, and both of these data sets are shown in Table 4.4. Using the wire antenna the cross-correlation method, again, had much less of a spread in values (1 meter, compared to 18 meters for the other two algorithms). Unfortunately, despite being the most consistent, it also had the largest magnitude of error at -14 meters, compared to 10 meters for the other two algorithms.

When comparing results between the rabbit-ears spin test and wire antenna translation test, typically the hole punching algorithm and zeroed pulse algorithms reduced the error magnitudes by at least a factor of 4. The cross-correlation algorithm's error magnitude generally stayed the same for the two different antennas.

The outdoor-outdoor test was performed in order to compare with the outdoor-outdoor rabbit-ears short translation test (i.e., a direct comparison of antennas). Both data sets are shown together in Table 4.5. For the wire antenna, the cross-

correlation algorithm outperformed the other algorithms of both channels in both the spread and overall bias among the positions. The zeroed pulse algorithm performed the worst with a bias nearly double the hole punching algorithm in both channels. Comparing this test to the rabbit-ears data, the wire antenna reduced the cross-correlation bias in channel 7 from 29 meters to -1 meters (27 meter error to -3 meter error). Unfortunately, it more than doubled the bias for the hole punching and zeroed pulse algorithms of channel 2 (-9 and -18 meters to -25 and -40 meters, respectively).

Thus, the wire antenna often greatly reduced the magnitude and deviation of the errors. Also, compared to the rabbit-ears test, the cross-correlation algorithm using the wire antenna never suffered any significant degradations.

Spin Test Repeatability. One final test aimed at evaluating multipath effects involved repeating the indoor-indoor rabbit-ears spin test two more times using the same antenna locations as the first test. (The exact positions and rotations were marked during the first test). The first repeat occurred about 6 hours after the original data set (data set 2); the second occurred approximately 2 weeks later (data set 3). Because all major nearby reflectors were stationary, the multipath characteristics over these tests should have been similar. Some deviation was expected based on environmental differences (temperature, condensation, and precipitation), but the overall structure should not change. The results from this test are shown in Figure 4.4. As indicated by the legend, each data set has the same line style and each algorithm has the same symbol.

In Figure 4.4, it is evident that all algorithms for a given data set produce results with the same trend. However, there are few similarities when comparing across data sets. The most noticable similarity is the consistently improved performance of the cross-correlation (XCORR) algorithm (diamond symbol). When it is not performing better than the other algorithms, it's results are near those of

Table 4.5: Outdoor-Outdoor Antenna Long Translation TDOA Measurements (meters) Comparison—True TDOA Measurement: 2 meters

Translational Position	Rabbit-Ears Antenna						Wire Antenna					
	Channel 2			Channel 7			Channel 2			Channel 7		
	XCORR	HOLE	ZERO	XCORR	HOLE	ZERO	XCORR	HOLE	ZERO	XCORR	HOLE	ZERO
1	0.87	-9.41	-19.83	29.51	12.56	10.70	1.14	-24.62	-40.29	-1.02	-0.44	14.27
2	0.94	-9.67	-16.14	29.52	18.75	15.02	1.16	-28.17	-40.88	-0.81	3.65	18.56
3	0.83	-8.56	-18.25	29.47	16.65	16.68	1.03	-24.66	-42.96	-0.70	6.16	20.40
4	0.90	-7.65	-15.21	29.66	18.22	15.15	1.21	-26.92	-40.58	-1.27	3.68	23.60
5	0.78	-7.37	-16.68	29.78	34.71	17.05	1.18	-24.18	-38.83	-1.44	0.89	19.38

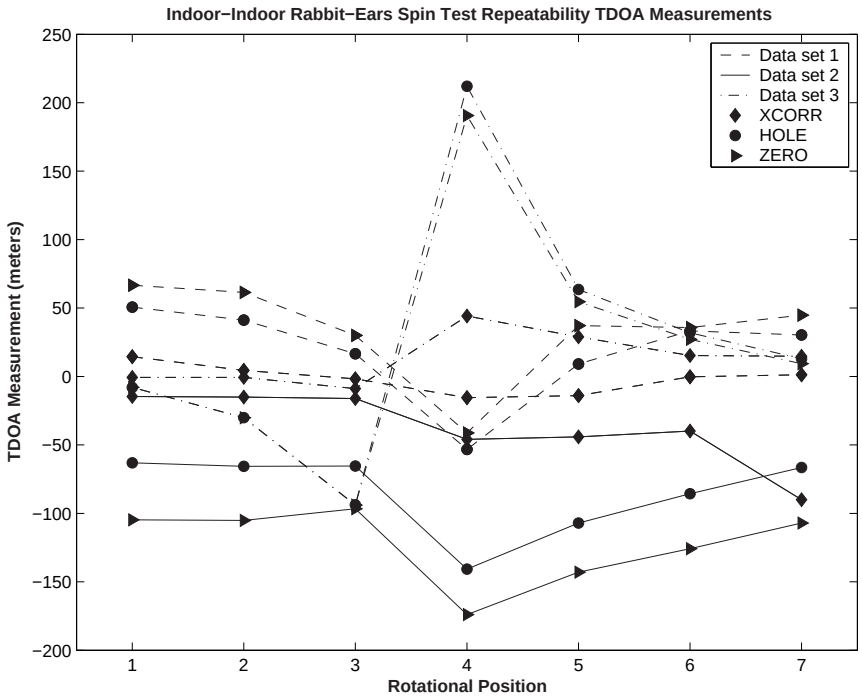

Figure 4.4: Indoor-Indoor Rabbit Ears Spin Test Repeatability TDOA Measurements (meters)—True TDOA: 0 meters

the other algorithms. Two additional trends that are noticeable are: (1) each algorithm produces a relative spike at position 4, and (2) the values at positions 1 and 7 are similar for each algorithm. Both of these support the claim that multipath is dominant error. The hypothesis is that at position 4 the antenna gain applied to a multipath signal (or signals) and the gain applied to the direct signal (or signals) were such that a large error occurred. The inconsistent direction of the spike can be explained by a change in phase of the multipath signal possible from changes in the reflecting surface (temperature, moisture, etc).

A summary of the indoor-outdoor tests thus far (excluding the spin test repeatability analysis) is presented in Figure 4.5. Each row of plots summarizes the TDOA measurements from one of the tests. Each bar is centered at the mean value for each group of TDOA measurements (all TDOA measurements at each position for a given algorithm) and has an amplitude equal to the spread within each group

of measurements. The heavy (or bold) data points indicate the cross-correlation algorithm, and show how much more consistent (less spread) that algorithm has compared to the other two. The heavy data points also show that, for the majority of the tests, the cross-correlation algorithm is more accurate (again, the TDOA measurement nearly equates to the measurement error because the true measurement is so small). The circled data points indicate the hole punching algorithm. It is seen that if there is a significant difference in the hole punching and zeroed pulse algorithms, the hole punching algorithm is more accurate (for all but one test).

As a result of the cross-correlation algorithm's improved performance, and the inconsistency and extreme errors noted in the other algorithms, the cross-correlation algorithm was the only algorithm used for the remainder of this research. While this eliminates the possibility of analyzing the performance of a system not using a cross-correlation approach, the waveform analysis performed in Section 4.1.4 provides insight into algorithm modifications needed to make that implementation feasible in future research.

4.1.2.3 Long Translation Test. The spin and short translation tests indicated that multipath could potentially cause large oscillatory type errors. To verify this was indeed caused by multipath (as opposed to antenna effects) the long translation test was performed. As before, one antenna remained fixed, and the other was translated along a linear path. Six translations (seven data points) of one-quarter wavelength were performed to analyze more of the long range multipath effects. The results for both antennas in the outdoor-outdoor test are shown in Table 4.6. The wire antenna TDOA measurement for position 3 of Channel 26 is marked with an asterisks because the original test location produced a signal that was not processable by the VCR. However, when the antenna was moved approximately 4 centimeters in any direction from that location, the signal was regained. While the exact cause of this is unknown, one conjecture is that multipath degradation (either constructive or destructive) is so severe that signal integrity is entirely lost. (However, it could

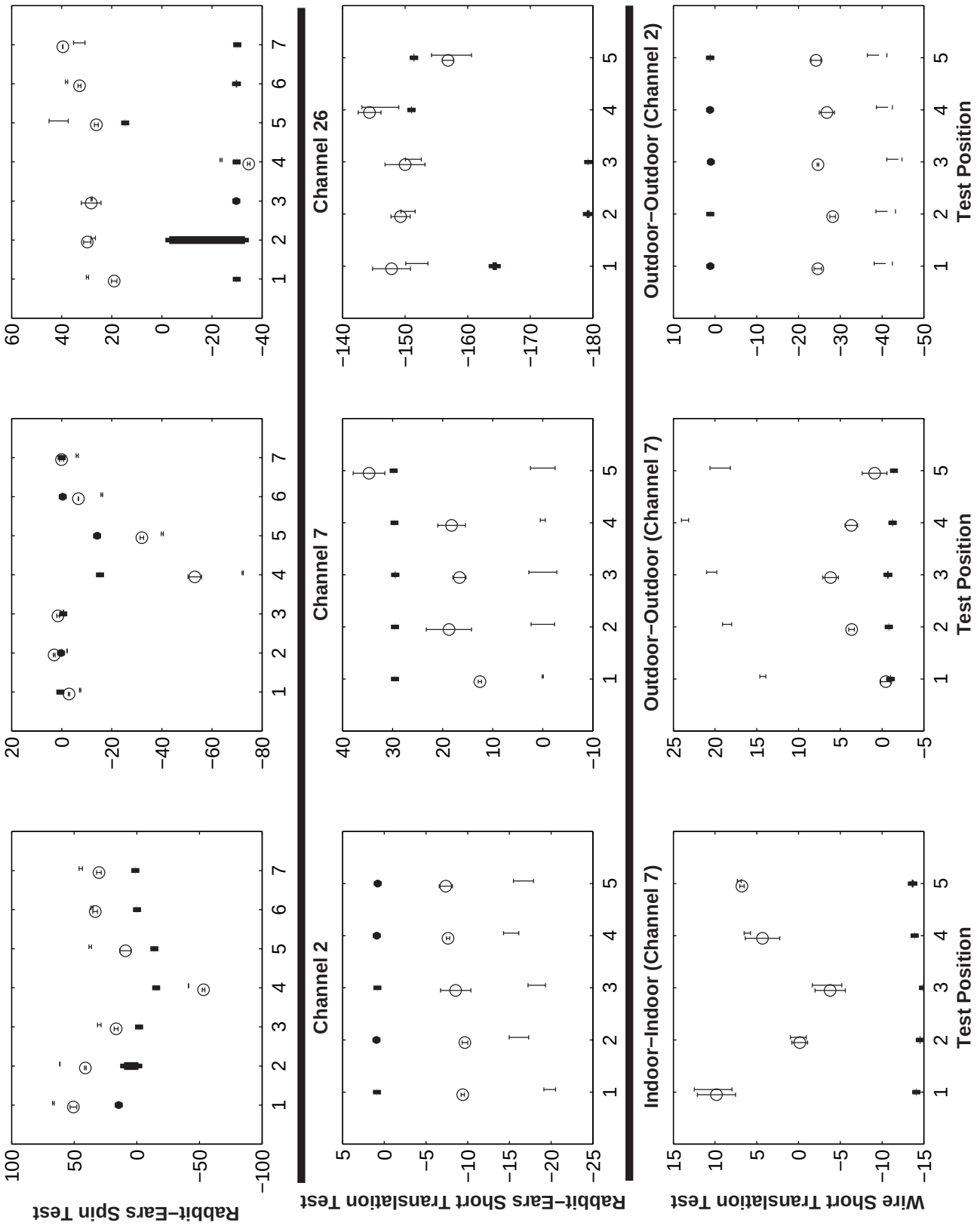

Figure 4.5: Summary of TDOA Measurements—Cross-Correlation Algorithm (thick line), Hole Punching Algorithm (circled data points with thin line), and Zeroed Pulse Algorithm (thin line)

Table 4.6: Long Translation Test TDOA Measurements (meters)

Position	Rabbit-Ears Antenna			Wire Antenna		
	Channel 2	Channel 7	Channel 26	Channel 2	Channel 7	Channel 26
1 True TDOA: 0.50 meters	-0.74	45.20	1.52	-0.56	29.98	-0.76
2 True TDOA: 1.00 meters	-1.75	0.63	45.63	-1.11	-15.88	5.59
3 True TDOA: 1.50 meters	-14.10	45.7	31.52	-15.08	14.18	*74.93
4 True TDOA: 2.00 meters	-14.21	14.78	45.71	-14.29	15.82	-89.13
5 True TDOA: 2.50 meters	-14.86	45.23	46.09	-13.20	53.71	-0.45
6 True TDOA: 3.00 meters	-14.05	44.76	45.06	-14.29	14.95	-76.69
7 True TDOA: 3.50 meters	1.01	60.42	28.67	-13.20	-299.83	89.61

*Antenna moved 4 centimeters to enable signal detection by VCR

simply be the result of a weak signal.) The wire antenna was presumed to have lower gain than the rabbit-ears antenna so it would perform poorer in this situation. Note that the rabbit-ears antenna did not perform well for this channel either.

In this test there were no significant differences between the two antennas. In regards to the multipath claim of Section 4.1.2.2, all channels experienced oscillations, had at least one jump greater than 10 meters, and contained similar patterns between antennas from position to position for channels 2 and 7. All of these support the claim that multipath is a dominant error. The following tests performed in both low and high multipath environments further aim to isolate multipath as an error.

4.1.3 Low and High Multipath Environment Comparisons. The previous sections used test repeatability and typical multipath errors to highlight that mul-

Table 4.7: Low Multipath Rabbit-Ears Spin Test TDOA Measurements (meters)

Rotational Position	Channel 2	Channel 22
1	-105.73	-127.63
2	-105.86	-120.10
3	-105.84	-119.88
4	-105.53	-120.15
5	-105.40	NO DATA
6	-105.61	-119.72
7	-105.81	-120.67

tipath was a potentially serious problem in the TDOA measurements. This section verifies the multipath effects by performing similar tests in low and high multipath environments. This section also provides a quantitative accuracy analysis of the range measurements by comparing the measurements to truth data created from precise GPS position estimates.

4.1.3.1 Low Multipath TDOA Measurements. The low multipath environment was the first part of the environment comparison test to demonstrate the effects of multipath. This location was in an open field with very few nearby multipath sources, but it would still exhibit non-multipath measurement errors, namely discretization and processing inconsistencies.

The results from the rabbit-ears spin test in the low multipath environment are shown in in Table 4.7. Position 5 of channel 22 failed to be collected due to an operator during data collection. Nonetheless, the consistency among all positions verifies that antenna effects are not causing the errors found in Table 4.2. As the only difference between the results of this test and those in Table 4.2 is location, environment based multipath must be the dominant error source. The accuracy of these measurements is analyzed below.

The results from the long translation test are shown in Table 4.8. Again, position 5 of channel 22 failed to be collected due to an operator error. The con-

Table 4.8: Low Multipath Long Translation Test TDOA Measurements (meters)

Translational Position	Rabbit Ears		Wire Antenna
	Channel 2	Channel 22	Channel 2
1	-105.92	-119.88	-105.24
2	-105.76	-119.82	-105.72
3	-105.94	-119.61	-105.80
4	-106.04	-119.42	-105.93
5	-106.20	NO DATA	-106.12
6	-106.20	-119.82	-106.45
7	-105.79	-119.83	-106.54

sistency among positions signifies the errors in the high multipath environment are indeed multipath. Additionally, the consistency between both antennas in the low multipath environment implies that improvement previously observed from the wire antenna in the high multipath environment is the result of multipath mitigation.

The first measurement accuracy analysis compares the measurements of Table 4.7 (the "original" data in Table 4.9) with measurements taken by switching the location of the antennas and all associated cables and hardware (the "switched" data in Table 4.9). In a perfect system the measurements should be equal and opposite. Note the inconsistent difference in TDOA measurements between the original and switched positions. Channel 2 has a difference of 14 meters, where channel 7 has a difference of 28 meters. Ideally, if the only error in each of the measurements was the timing bias, the difference of both channels would be the same. Realistically, however, that difference is a combination of many factors, including timing bias, propagation path differences, and hardware inconsistencies. While timing bias could potentially be a large factor, it is constant and ultimately removed in processing. The other factors are not compensated and are the true "errors" in the TDOA measurements. The most likely source of the error in this research is hardware inconsistencies. The VCRs used in signal acquisition were not designed for this purpose, and the tolerances necessary for accurate picture information are intuitively much less stringent than those needed for navigation purposes. This can

Table 4.9: Low Multipath Switched Antenna Comparison TDOA Measurements (meters)

Channel	Original	Switched
2	-105.68	118.96
22	-120.83	92.10

be highlighted if we consider both channels equally valid with equal timing biases for both the original and switched TDOA measurements. Thus, the actual timing bias can be estimated as half of the error stated: 7 and 14 meters for channels 2 and 7, respectively. The average of these values, 10.5 meters or 35 nanoseconds, is then used as the estimated overall timing bias. Thus, the actual hardware "error" associated with each of the measurements is 3.5 meters, or 11.7 nanoseconds. An error of that magnitude is, conceivably, far superior than would be required for picture integrity–the original objective of the video signal encoder. (In terms of picture information, 11.7 nanoseconds is less than 0.02% of the picture line duration.)

The GPS truth data was used to calculate the true TDOA measurement for both the "original" and "switched" configurations, as well as positions perpendicular to the radial–denoted as the "perpendicular" configuration. The measurement errors were calculated and shown in Table 4.10. If the difference between these measurements and the collected TDOA measurements is again considered a constant timing bias (previously rationalized to be 10.5 meters) plus error, the mean of all the TDOA measurement errors provides a second possible timing bias estimate. The mean of all the values in Table 4.10 is 1.6 meters. This suggests that either (1) the true timing bias is much less than originally anticipated, or (2) the process noise and hardware inconsistencies are much more dominant. Again, operating under the assumption that the hardware (namely the VCRs) is the source of error, the maximum error of 28.8 meters (96.1 nanoseconds) is only 0.15% of the picture line duration. Intuitively, consistencies of this magnitude are more than adequate in a television tuner, so it is likely that hardware inconsistencies between the two VCRs are to blame. Also,

Table 4.10: Field TDOA Measurement Errors (meters)

Channel	Original	Switched	Perpendicular
2	-13.1	27.6	-2.0
7	NO	26.1	4.9
22	-27.2	-0.7	-0.7
26	NO DATA	NO DATA	-0.4

the fact that the error was induced by switching the antenna locations is a further indication that the hardware (VCRs) is to blame. If it was a pure timing during ADC, then it would be consistent across all channels.

.

4.1.3.2 High Multipath TDOA Measurements. The final test performed was the high multipath portion of the environment comparison test. The TDOA measurements made were similar to those performed in the field (the low multipath environment), but now near Building 194 (the high multipath environment). The results of the indoor-outdoor tests performed in Section 4.1.2 suggested multipath would be a dominant error source, so a third channel was added. Additionally, as identified by Sections 4.1.2 and 4.1.3.1, the multipath errors were much greater than the timing bias error, thus the timing bias was neglected during this analysis.

GPS coordinates were again used to calculate the error in each of the TDOA measurements.[5] The errors from the rabbit-ears spin test are shown in Table 4.11. The VCRs could not process the signal at position 7 of channel 22. Still, it is again very clear that multipath creates very severe errors–the largest error was -192.20 meters.

The errors from the high multipath long translation test of both antennas are shown in Table 4.12. The three instances in channel 22 where data failed to be

[5]The true coordinates receiver coordinates are located in Appendix A, and the original TDOA measurements for this location are located in Appendix B.

Table 4.11: Building 194 Rotation Test TDOA Measurement Errors (meters)

Rotational Position	Ch 2	Ch 22	Ch 26
1	21.40	-96.90	-30.54
2	21.60	-96.30	-187.30
3	22.10	8.80	-22.10
4	-53.00	-96.60	-20.40
5	69.10	-112.90	-35.10
6	7.90	-112.00	-192.20
7	20.30	NO DATA	-188.00

collected were again caused by the VCRs not being able to process the data at those locations. These results not only show the severity of multipath errors again, but how much improvement the wire antenna makes. First, channel 2 had errors ranging from -50 to 24 meters using the rabbit-ears antenna, but a consistent error near 21 meters using the wire antenna. Similarly for channel 26, the peak error was reduced from -200 meters to -97 meters. Finally, despite having the highest magnitude of errors, the complete set of measurements for channel 22 using the wire antenna also indicates multipath mitigation. The rabbit ears antenna had three locations where the VCR could not process the video signal. Based on all of the previous results, the rabbit-ears antenna has better signal gain than the wire antenna. Therefore, a weak signal can not be argued as the reason for the blackout. Thus, as both antennas were placed at the same location, multipath so severe that the signal could not be processed is the most likely reason. These results also demonstrate that signal strength appears to have a very significant effect on measurement error. Performance can be consistently good with a strong signal (as in channel 2), but is very poor with a weak signal (as in channel 22).

For a final comparison, the errors from the measurements collected perpendicular to the radial are shown in Table 4.13. The results show the same characteristics as the errors in the nearby tests shown in Tables 4.11 and 4.12.

Table 4.12: Building 194 (High Multipath) Translation Test TDOA Measurement Errors (meters)

Translational Position	Rabbit Ears			Wire Antenna		
	Ch 2	Ch 22	Ch 26	Ch 2	Ch 22	Ch 26
1	24.10	-98.00	-6.40	21.30	-113.10	-97.10
2	22.30	-111.30	-21.80	21.00	-72.00	-21.50
3	23.80	-98.70	-35.30	21.20	-51.80	-21.10
4	-40.60	NO DATA	-200.80	21.00	-292.10	-7.00
5	-40.50	-111.60	-21.60	21.70	-201.80	-8.10
6	-39.80	NO DATA	-8.00	21.90	-277.50	-52.20
7	-51.70	NO DATA	-35.00	21.50	-82.30	-7.00

Table 4.13: Building 194 Perpendicular TDOA Measurement Errors (meters)

Channel	TDOA Measurement Error
2	12.2
7	13.3
22	-90.0
26	0.9

One other possible source of error that can not be dismissed is propagation affects. All of the signals used in this research originated from approximately the same location (shown later in Figure 4.10). No other propagation paths were used so there is no point of comparison. However, errors from propagation effects are unlikely because the transmitters were relatively close to the receivers, and a "line-of-sight" path from the receivers to the transmitters was often available.

4.1.4 Waveform Analysis. The previous sections identified multipath as a serious problem. It also noted that the cross-correlation algorithm consistently performed the best out of the three algorithms. This section explores the underlying causes of the errors by analyzing the received waveforms. First, to provide a comparison, a set of waveforms from the field (low multipath environment) are presented. Then, two data sets from the spin test repeatability test are presented: (1) position 1 from data set 2–which had -15 meters of error, and (2) position 1 from data set 3–which only had -1 meter of error. These two data sets should be very

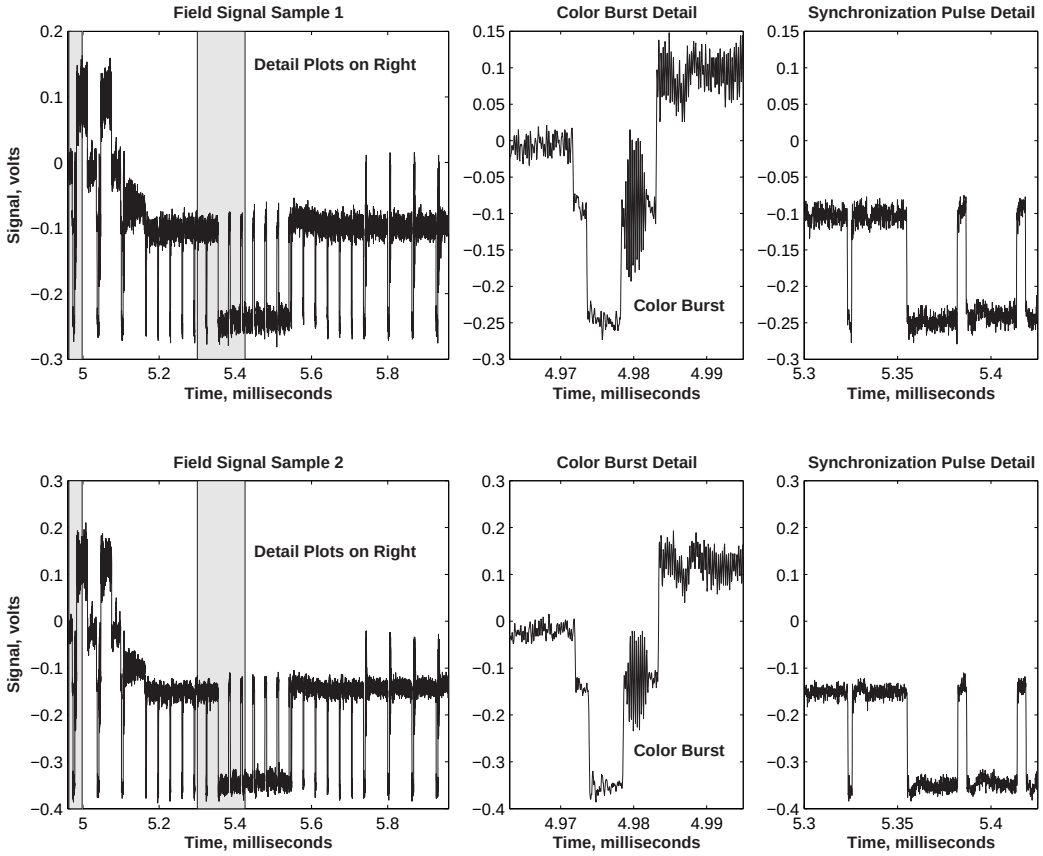

Figure 4.6: Field Signal Samples

similar because they were collected from precisely the same location; the differences should highlight the actual cause of TDOA measurement degradation.

The field waveforms are shown in Figure 4.6. Notice how well the signal structure as a whole resembles that of the analytical model shown in Figure 2.5. More importantly, notice how the lower level of the color burst (in the "Color Burst Detail" plot) remains above the bottom of the synchronization pulses (in the "Synchronization Pulse Detail" plot).

The waveforms from data set 2 of the spin test are shown in Figure 4.7. The lower plots again resemble the waveforms observed from the field data. The upper plots, however, have a severely degraded structure. Not only has the separation between the upper and lower levels of the synchronization pulses been comprimised,

but the lower level of the color burst and picture information extends to the same level as the synchronization pulses. This makes it impossible for the hole punching algorithm to place a threshold below the color burst and above the bottom of the synchronization pulses. Additionally, the distortions will degrade the zeroed pulse waveform. The very negative data points from the picture information and color-burst will increase the correlation peak for the times when the pulses shown in Figure 3.11 were aligned with these locations. Fortunately, the oscillatory nature of these sections will decrease the correlation peak to some extent, but the final level will still be much closer to the correlation level of the true peak (compared to a signal not suffering these degradations). Thus, the zeroed pulse algorithm should still have some resistance to these degradations, but the correlator output will be much flatter than a signal not suffering these degradations making the linear fit estimator more sensitive to other errors.

Finally, the waveforms from data set 3 are shown in Figure 4.8. (Recall how these waveforms performed better than those from data set 2). Again, signal degradation is apparent in the top plots (the "High Multipath Signal Sample"), but not nearly to the extent seen in Figure 4.7. First, there is still separation between the upper and lower edges of the synchronization pulses, and the picture information does not have the lower edge near the bottom of the synchronization pulses. The color burst, on the other hand, still does. Again, the color burst is oscillatory, so the correlation algorithm should maintain some resistance to this degradation. The "Low Multipath Signal Sample" appears to avoid the serious degradations present in the "High Multipath Signal Sample". However, if the signal is inspected closely, it might actually be the difference between constructive and destructive interference. The middle of the color burst narrows down close to the level of the signal where this signal is interjected. This is further evident if this color burst is compared to the color burst of "Field Signal Sample 2" in Figure 4.6.

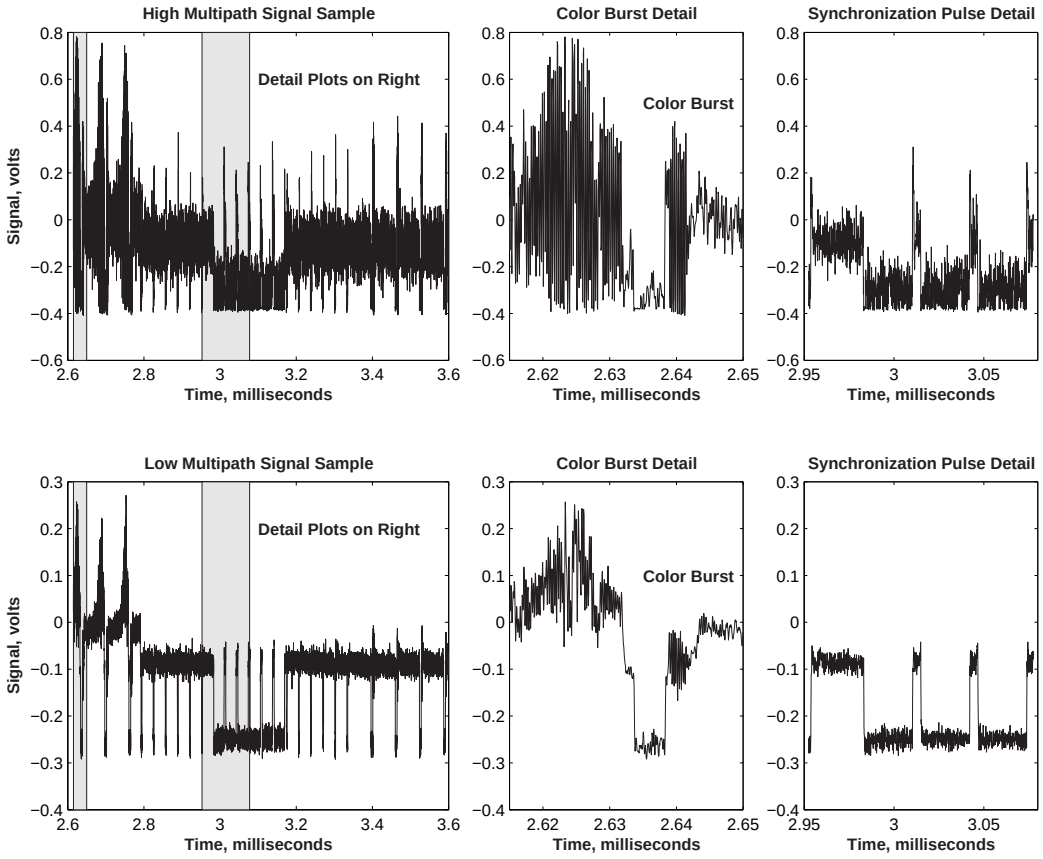

Figure 4.7: Low and High Multipath Signal Samples from Data Set 2

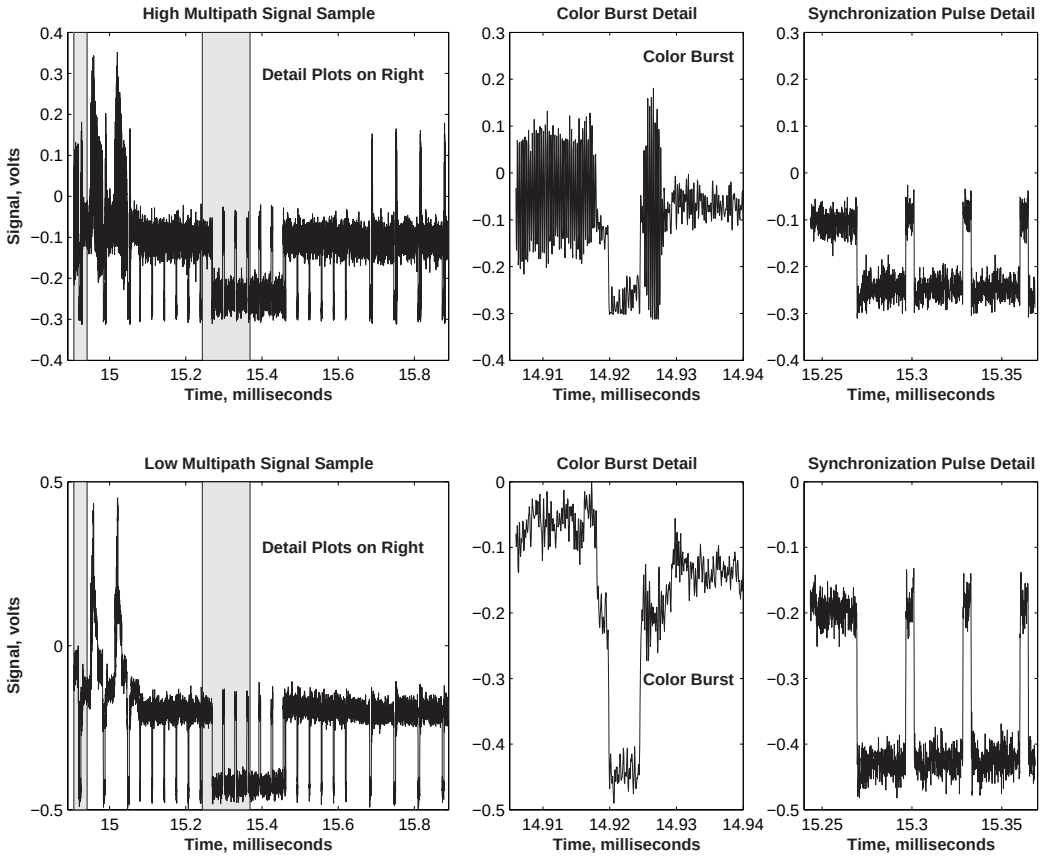

Figure 4.8: Low and High Multipath Signal Samples from Data Set 3

The above figures illustrate the degradations to each of the waveforms, and conceptually show how both the hole punching and zeroed pulse algorithms suffer from those degradations. The plots and analyses noted each of the waveforms as either a high or low multipath signal. It must be stated that beyond the rationale provided, this is an intuitive claim with no other evidence supporting it–there feasibly could still be other causes. However, oscillatory signals suffering constructive multipath will suffer increased amplitudes, as experienced in these waveforms, and oscillatory signals suffering destructive multipath will become negated, also as experienced in these waveforms. Finally, as signals not suffering from these degradations were consistently found in the field (low multipath test environment), this claim appears to have merit.

4.2 TDOA Processing

This section first processes the perpendicular TDOA measurements from the field (Table 4.9) to estimate the position of one of the receivers. Then, the error characteristics from Section 4.1 and actual television transmitter locations near Dayton, Ohio are used to determine the accuracy of a system with capabilities similar to that of the system used in this research. Finally, simulation is used to show the required accuracy of a TDOA system desiring position estimates with errors of 10 meters.

4.2.1 Processing the Perpendicular Field Data. Table 4.10 showed that the field radial data had small errors, so it was a good candidate to determine the accuracy of a system operating in the low multipath environment. Unfortunately, the geometry of the transmitters with respect to the receivers was very poor. Figure 4.9 shows that all four transmitters were tightly grouped Southwest of the receivers.[6] Thus, as described in Section 2.1.4, the horizontal position accuracy was expected to be very poor.

[6]All television transmitter information was collected from the FCC's TV database: www.fcc.gov/mb/video/tvq.html.

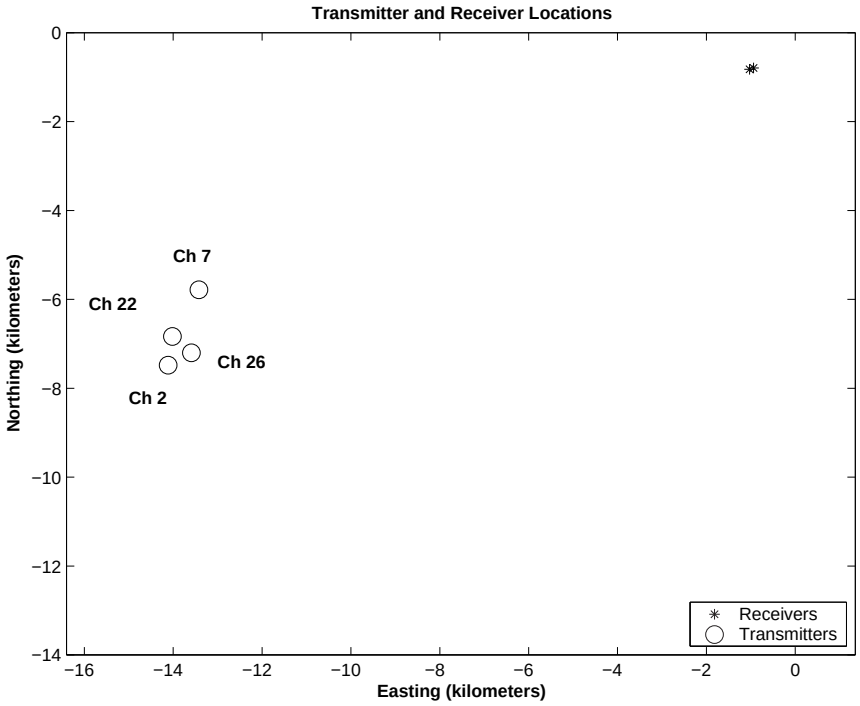

Figure 4.9: Dayton Television Transmitter Locations Used in Radial Data Position Estimates

The position estimates were calculated using two algorithms, one that assumed the timing bias was zero (a special circumstance for the system used in this research) and one that assumed an unknown bias. The results from both of these algorithms are shown in Figure 4.10. The estimates of the system assuming zero timing bias far exceed those of the system with an unknown bias. However, this was not all that surprising. Both systems used four measurements (repeating TDOA measurements from the other channels such that all eight TDOA measurements from channel 26 could be used, see Table B.2), but the unknown timing bias algorithm had three parameters to estimate (east and north position and timing bias), while the assumed bias algorithm only had to estimate the two position parameters. While neither algorithm performed exceptionally well, the assumed timing bias system had errors similar to GPS before Selective Availability (SA) was turned off [5]. Additionally, the unknown timing bias algorithm grossly miscalculated the timing bias. This has the affect of extending the measurement outward from the transmitter. Recalling the

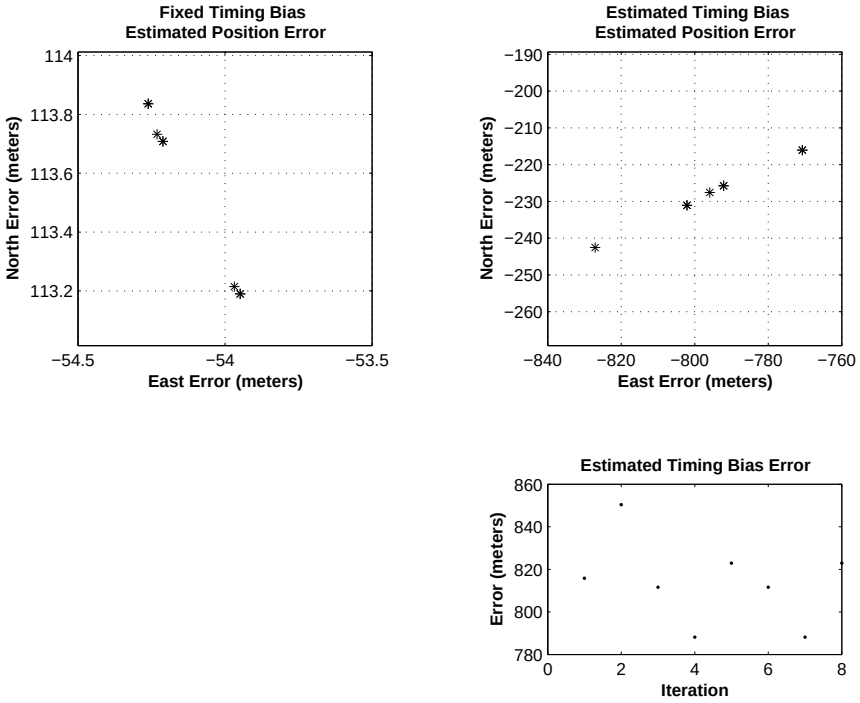

Figure 4.10: Dayton Four Station Position Estimation Error

geometry shown in Figure 4.10, the large East error and increased North error make sense. It also emphasizes the necessity of good geometry for a practical system that needs to estimate the timing bias. The errors in each of the TDOA measurements (although small) produced a position estimate that–in the Least-Squares algorithm–had a smaller overall error at a position where all the range estimates were biased by 800. If even one of the transmitters was positioned in a different direction from the receivers, it would be enough to prevent an error of this sort.

Both of these systems represent a worst-case scenario. Signal acquisition in this research was restricted to signals strong enough for accurate television reception. A positioning system would be able to use many more signals that were too weak for television reception because of the correlation techniques. Thus, the following section analyzes a simulated system capable of processing many more signals from eight transmitters near Dayton, Ohio.

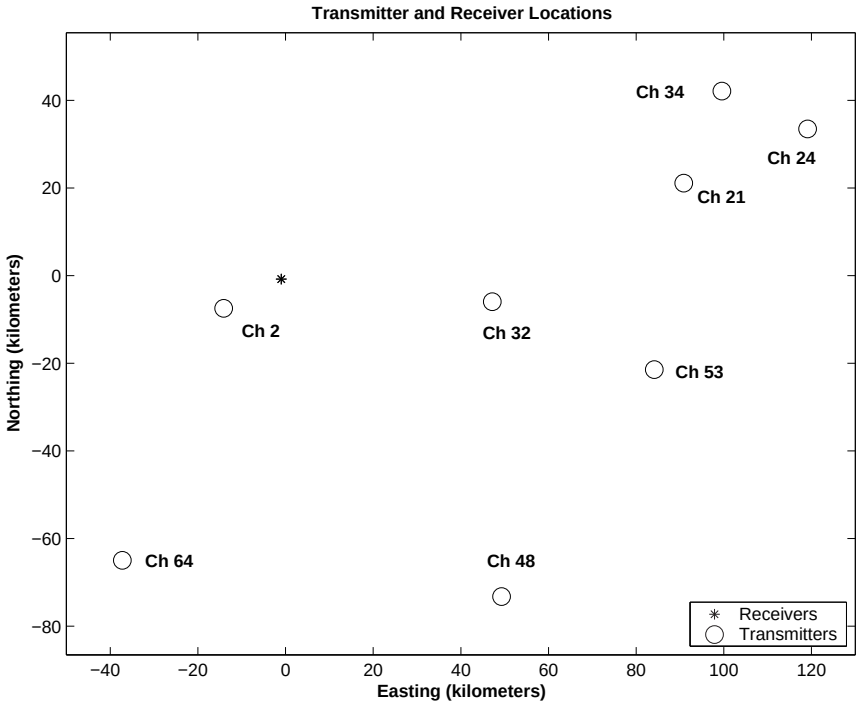

Figure 4.11: Expanded Dayton Area Television Transmitter Locations

4.2.2 Accuracy of a Simulated Reception System. The television transmitters used for this portion of the analysis were restricted to those within 150 kilometers that had maximum radiated transmission power of at least 1000 kW. The location of the eight channels used and the receiver positions are shown in Figure 4.11. While the geometry of this scenario is much better than that of the field perpendicular data, it still is not ideal–no transmitters are located in the Northwest quadrant relative to the receivers.

The first simulation analyzed a system with characteristics similar to those of the field data, the most accurate data gathered in this research. Table 4.10 indicates a maximum TDOA measurment error of nearly 30 meters. Thus the first simulation used 30 meters as the TDOA measurement accuracy which was implemented using a uniformly distributed error probability ranging between -30 and 30 meters. The position and timing bias estimate errors of this simulation are shown in Figure 4.12.

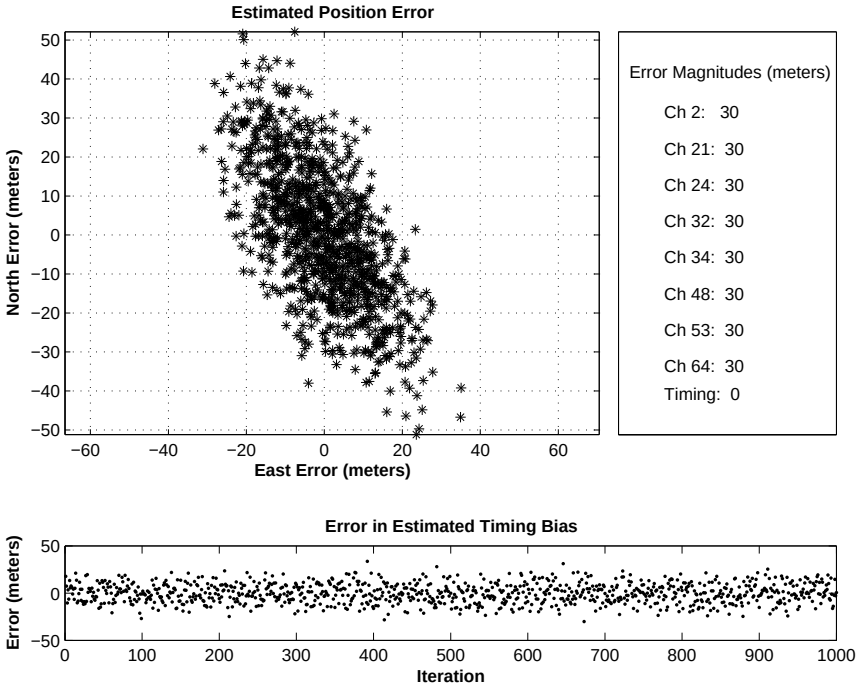

Figure 4.12: Simulated Position Estimation Error, Field-like Errors

Also noted in the figure are the TDOA measurement error magnitudes and the true timing bias affecting the system.

The estimated position error plot shows that both the north and east accuracies are very similar, with the majority of the errors being less than 40 meters in any direction. However, errors in both directions are highly correlated; the errors to the south are also to the east. The timing bias errors indicate a random error with maximum amplitude near 30 meters. This coincides with the specified measurement accuracy because the portion of the TDOA measurement error similar to all of the TDOA measurements would be estimated as a timing bias and removed from the measurements.

The next two simulations analyzed a system experiencing large amounts of error (e.g., a high multipath environment). The magnitude of the error was determined from the indoor-outdoor test results summarized in Figure 4.5. The absolute

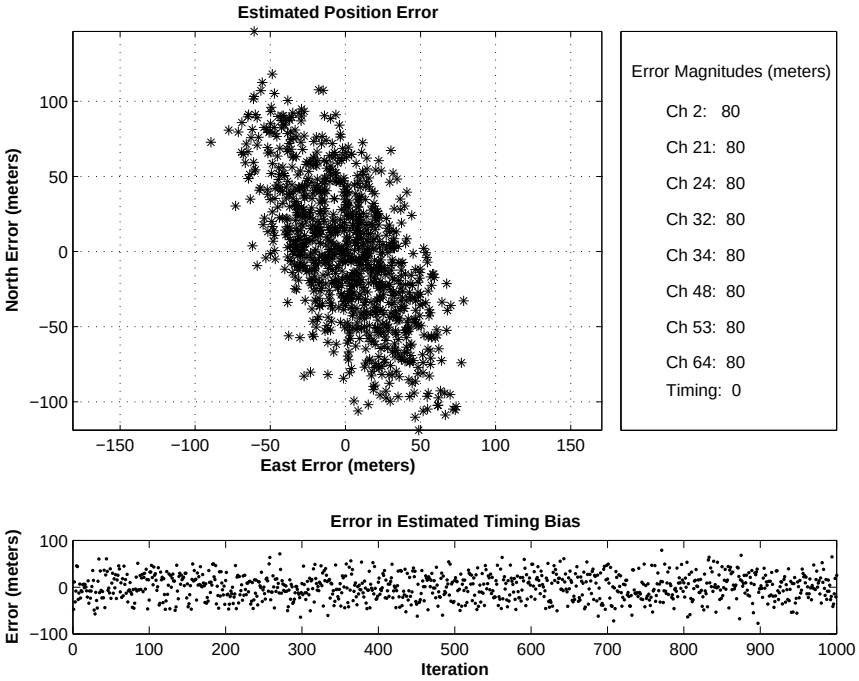

Figure 4.13: Simulated Position Estimation Error, High Multipath Errors and 0 Meter Timing Bias

worst case of 180 meter errors was not used because it was assumed that additional forms of multipath mitigation (either active or passive) would be able to reduce this error. Excluding the worst case results in Figure 4.5, all errors were less than 80 meters; thus this value was used as the maximum error magnitude. The results from a simulation using this error magnitude and zero meter timing bias–a system similar to the one used in this research–is shown in Figure 4.13. Again, the position errors are very correlated in the South and East directions, but the position errors are much greater. Fortunately, the errors are not so large the system would be unusable; they again mimic the capability of GPS prior to SA being turned off. The timing bias errors again are randomly distributed with a maximum magnitude of 80 meters.

The results of the second simulation using the large multipath TDOA measurement errors the shown in Figure 4.14. The only difference in this simulation from the previous one was the addition of a 25 meter timing bias. As expected, this system's performance was nearly identical to the previous one without a timing bias

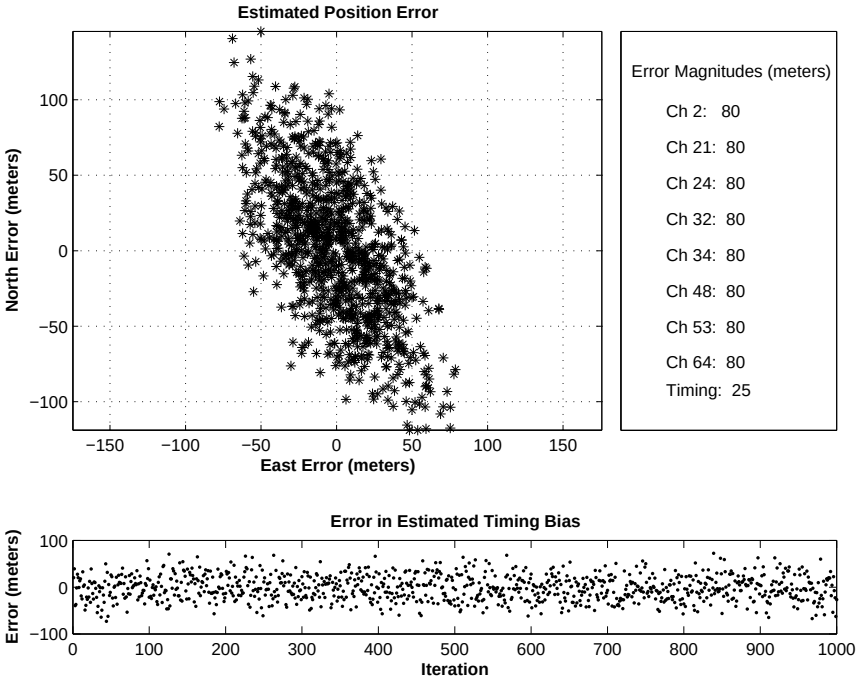

Figure 4.14: Simulated Position Estimation Error, High Multipath Errors and 25 Meter Timing Bias

(the algorithm estimates this error so it should have no effect–assuming all resulting ambiguities can be properly resolved).

4.2.3 Determining TDOA Measurement Accuracy Requirements. This section determines how accurate the TDOA measurements must be to provide a position estimate with errors less than 10 meters (the performance of a readily available single frequency GPS receiver). Section 4.2.2 demonstrated that measurement errors of 30 meters produced position estimate accuracies of 40 meters. Therefore, the measurement accuracy for a 10 meter position accuracy must be better than 30 meters. As the overall system accuracy was 10 meters, this value (10 meters) was chosen as the measurement accuracy in this initial simulation. The results are shown in Figure 4.15.

This system did not meet the desired position error of 10 meters. Fortunately, the majority of the position estimate errors were less than 5 meters (noted by the

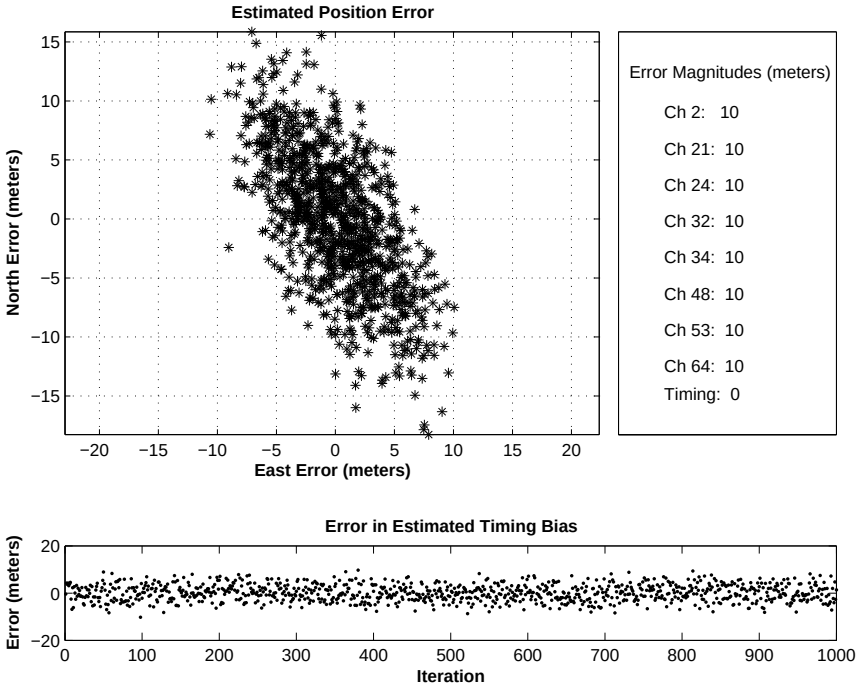

Figure 4.15: Simulated Position Estimation Error, 10 Meter Errors

dense collection of datapoints within 5 meters). Additionally, the error spread in the Southwest to Northeast direction suggests that a system with better geometry among the transmitters and receivers would meet the 10 meter error requirement. Nonetheless, the TDOA measurement error magnitudes were reduced to 5 meters. Figure 4.16 shows that the error in any direction was indeed always less than 10 meters in both directions.

While the results of Figure 4.16 met the desired position accuracies of 10 meters, it is not probable that all TDOA measurements would have the same accuracy. The errors would be different for each transmitter (including multipath and propagation effects), thus giving varying accuracies. A final simulation using both 5 and 10 meter accuracies was performed, and the position errors are shown in Figure 4.17. The East error again meets the desired 10 meter accuracy, but the North error occasionally exceeds this value. Nonetheless, these error values approximate

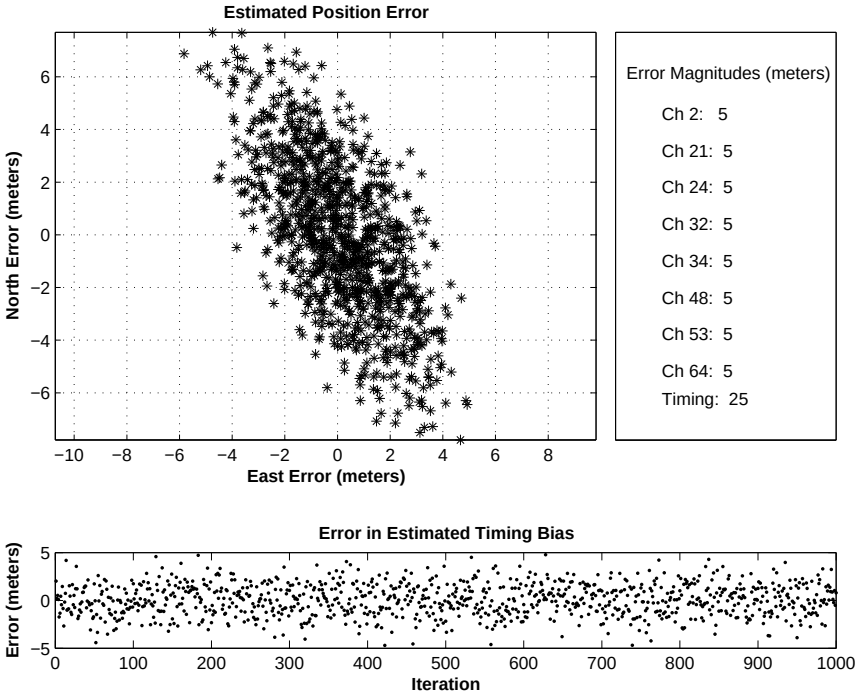

Figure 4.16: Simulated Position Estimation Error, 5 Meter Errors

the requirements of a system in this geometry to provide position estimates with 10 meter accuracy.

4.3 Summary

This chapter started by verifying functionality of the hardware and algorithms. Once confident the system was working, tests began to explore the effects of multipath and ways in which it can be mitigated. A final series of tests compared and quantified the errors from low and high multipath environments. One of these data sets and the resulting error characteristics were then used in TDOA positioning algorithms to analyze position estimate errors from actual transmitter locations near Dayton, Ohio.

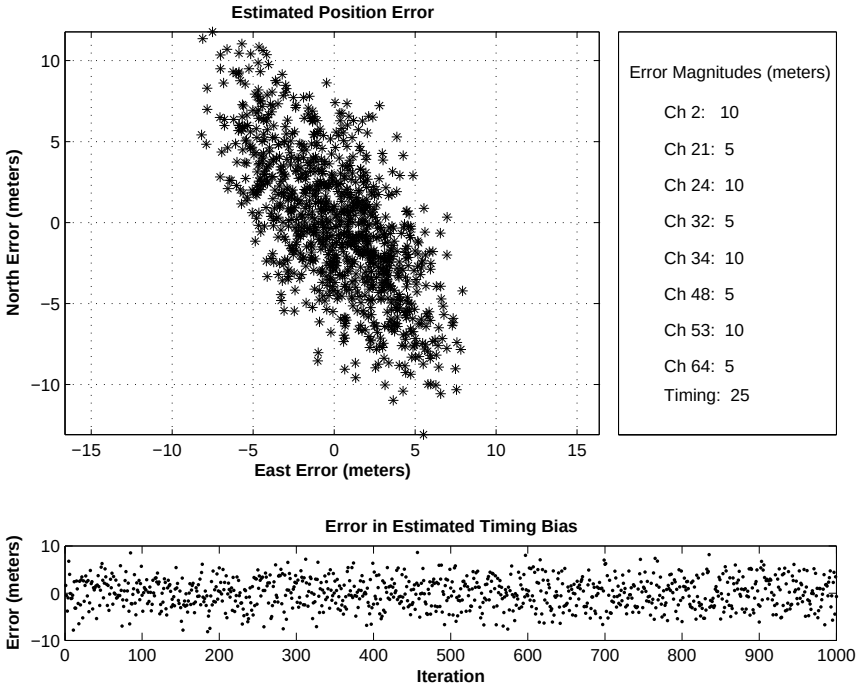

Figure 4.17: Simulated Position Estimation Error, Mixed 5 and 10 Meter Errors

V. Conclusions and Recommendations

This chapter summarizes the research results of the navigation potential of the NTSC broadcast. Following this, future work is recommended to support fielding a navigation system using television signals.

5.1 Summary of Results

This section summarizes the test results presented in Chapter IV. Attention is focused on system level outcomes and techniques developed in this research.

- **Measurement Consistency** The consistency within each group of measurements suggests that algorithm noise (or inconsistencies) is not affecting system performance. Not only does this consistency permit isolation of external error sources (namely multipath and hardware inconsistencies) as the dominant error sources, it signifies the future potential for very accurate position estimates once the dominant error sources are removed.
- **TDOA Measurement Errors** The TDOA measurement errors indicate a strong correlation with the multipath environment and signal strength. The high strength signals in the low multipath environment provided TDOA measurement errors as low as 1 meter and as high as 30 meters. The consistency of the larger errors, however, suggests that other correctable error sources (namely timing bias) are likely causes. Signals with low signal strength or from high multipath environments have considerably larger errors, with a peak error of 300 meters experienced in this research.
- **TDOA Positioning Results** The TDOA position estimates provided position accuracies similar to GPS with Selective Availability activated. The limited geometry of the television transmit towers available for this research is the principal cause of this error.

- **System Performance Requirements** A 30 meter TDOA measurement accuracy is required to maintain position errors less than 40 meters. To reduce the position error to 10 meters, a TDOA measurement accuracy between 5 and 10 meters is needed. However, the correlated error patterns suggest these requirements could be reduced with improved system geometry.

5.2 Future Work

The future work recommendations are divided into two sections: (1) system development, and (2) system testing. Each of these are discussed below

5.2.1 System Development. After developing and analyzing the results, many suggestions for improving the system and expanding the research are available. The principal areas requiring additional development are:

- Improved Receivers
- Adaptive Algorithms
- Minimized Hardware Requirements
- Center of Mass Technique

- **Improved Receivers** The most significant receiver improvement would be designing and building a navigation-focused receiver. A navigation system is much more sensitive to errors than a television system. Therefore, different design trade-offs could be made (with the understanding that the final cost would increase as the sensitivity is increased). Furthermore, a custom receiver could incorporate additional features to aid navigation. The carrier signal should be maintained and processed for additional measurements (similar to a GPS receiver which uses code measurements as well as carrier-phase measurements). Also, both passive and active techniques could be employed to reduce the biggest error source revealed in this research, multipath. Lastly, the receiver could estimate the SNR for each signal and evaluate the accuracy of the associated measurements accordingly.

- **Adaptive Algorithms** Section 4.1.4 revealed significant information about the signal's integrity through a simple visual inspection of the waveform. Adaptive algorithms could be employed to exploit the information available in the signal's structure. Furthermore, many signal effects have been characterized and algorithms for mitigating these effects can be developed and implemented.
- **Minimized Hardware Requirements** The hardware used in this research was designed to evaluate maximum system performance. Unfortunately, processing and memory requirements inherent with this hardware make it impractical for an operational system. Additional research should explore the degradations from lesser sampling rates and fewer quantization bits.
- **Center of Mass Technique** The center of mass technique was dismissed after results indicated it was inconsistent, even within a controlled test. However this technique has potential to provide valuable information. Additional development could focus on whether the changes discernable from the center of mass technique are correlated with system errors. If correlation exists, it can be used in conjunction with the adaptive algorithms to minimize the errors.

5.2.2 System Testing. This section outlines additional testing to further research presented in this Thesis. It is restricted to hardware and algorithms similar to those currently available. The four main areas to expand upon are:

- Long Baselines
- Different Locations
- Omnidirectional Antennas
- Fixed Antennas

- **Long Baselines** Additional testing could be conducted with longer baselines. In these tests, each antenna could be placed in a different environment to remove the correlated errors inherent with shorter baselines. The biggest obstacle

is synchronizing the receivers to keep the duration of test data at manageable levels.

- **Different Locations** The conclusions of this research are based on using four television stations near Dayton, Ohio. Additional geometries at varied locations could be used to validate results presented.
- **Omnidirectional Antennas** This research used a crude, lossy omnidirectional antenna to validate some initial results. Antennas designed with greater signal gain for the frequency band of interest could greatly improve performance.
- **Fixed Antennas** Approximately 0.1 second data sets were collected in this research. Many system level insights would be available by analyzing signals collected over longer periods from fixed antennas for maximized repeatability.

Appendix A. GPS Truth Coordinates

This appendix contains the true coordinates of both the receivers and transmitters used in this research. Positions denoted by "Field" are the low multipath environment (see Figure 3.17), positions denoted by "Bldg194" are the high multipath environment (see Figure 3.15), and positions denoted by "TX" are the television transmitters (see Figures 4.10 and 4.11).

Table A.1: Test Location True Coordinates

Location	ECEF			Local Level	
	X	Y	Z	East	North
Field A	504268.950	-4882654.614	4059265.481	-1028.88	-820.84
Field B	504356.743	-4882627.689	4059285.409	-938.78	-794.17
Field C	504280.407	-4882617.931	4059305.456	-1013.71	-767.52
Field D	504331.106	-4882674.219	4059233.375	-969.07	-862.08
Bldg194 A	505255.996	-4882051.402	4059899.536	15.02	-14.66
Bldg194 B	505253.168	-4882025.635	4059929.119	14.86	24.66
Bldg194 C	505207.677	-4882025.635	4059902.531	-32.29	-4.54
TX 2	491721.031	-4888516.390	4054379.093	-14113.55	-7480.31
TX 7	492301.52	-4887386.801	4055699.177	-13419.86	-5785.13
TX 22	492226.509	-4888305.780	4054607.953	-13589.07	-7203.68
TX 26	491771.825	-4888069.436	4054855.955	-14017.01	-6832.71
TX 21	594223.856	-4859038.901	4075921.635	90879.15	21084.72
TX 24	621470.975	-4847796.770	4085066.324	119138.78	33472.87
TX 32	552587.756	-4881136.577	4055461.972	47189.50	-5960.26
TX 34	601469.163	-4844584.496	4091928.471	99573.89	42108.29
TX 48	559060.064	-4923359.353	4003430.862	49281.03	-73245.14
TX 53	590315.013	-4886840.694	4043280.218	84129.16	-21437.23
TX 64	472452.468	-4927136.908	4009923.884	-37255.33	-64955.01

Appendix B. Low and High Multipath Environment TDOA Measurements and Truth Data

B.1 Low Multipath Environment

This section provides the complete set of TDOA measurements taken at the Field test location (the low multipath environment) along with the true TDOA measurements. Table B.1 contains the measurements from the rotation and long translation tests taken in the "original" configuration (locations "A" and "B" in Figure 3.17). Table B.2 contains the TDOA measurements taken in the "switched" and "perpendicular" configurations of the low multipath environment. Table B.3 contains the true TDOA measurements all of the locations in this environment.

B.2 High Multipath Environment

This section provides the complete set of TDOA measurements taken at locations "A","B", and "C" North of Building 194 (the high multipath environment) along with the true TDOA measurements. Table B.4 gives the TDOA measurements for the "original" configuration (locations "A" and "C" in Figure 3.15). Table B.5 gives the TDOA measurements for the "perpendicular" configuration (locations "B" and "C" in Figure 3.15). Finally, Table B.6 gives the true TDOA measurements for both of the data sets.

Table B.1: Field Test TDOA Measurements (meters)

Position	Rabbit Ears Rotation		Rabbit Ears Long Translation		Wire Long Translation
	Ch 2	Ch 22	Ch 2	Ch 22	Ch 2
1	-105.73	-121.95	-105.92	-119.92	-105.24
	-105.71	-133.30		-119.85	-105.25
	-105.75			-119.88	-105.24
2	-105.88	-120.17	-105.76	-119.89	-105.71
	-105.87	-120.05	-105.75	-119.82	-105.72
	-105.82	-120.07		-119.87	-105.72
				-119.71	
3	-105.84	-119.89	-105.90	-119.57	-105.80
	-105.84	-119.87	-106.04	-119.60	-105.82
	-105.84	-119.89	-105.87	-119.67	-105.79
		-119.89			
		-119.84			
4	-105.52	-120.13	-106.05	-119.46	-105.93
	-105.52	-120.15	-106.03	-119.45	-105.94
	-105.55	-120.16	-106.04	-119.35	
		-120.14			
5	-105.40	NO	-106.20	NO	-106.12
	-105.40	DATA	-106.20	DATA	-106.11
	-105.38		-106.20		-106.12
6	-105.61	-119.77	-106.23	-119.85	-106.43
	-105.61	-119.73	-106.20	-119.82	-106.44
	-105.61	-119.67	-106.16	-119.80	-106.47
			-106.21		-106.45
					-106.44
7	-105.81	-120.71	-105.79	-119.84	-106.53
	-105.83	-120.64	-105.81	-119.75	-106.53
	-105.80	-120.65	-105.77	-119.74	-106.55
				-119.83	
				-119.88	
				-119.87	
				-119.80	
				-119.96	

Table B.2: Field Test Comparison TDOA Measurements (meters)

Channel	Perpendicular	Switched
2	1.06	118.95
		118.96
		118.96
7	-1.43	119.60
	-1.37	119.61
	-1.42	119.61
22	-0.27	92.22
	-0.26	92.13
	-0.23	92.08
		92.02
		92.03
		92.13
26	-1.18	NO
	-1.19	DATA
	-1.16	
	-1.15	
	-1.16	
	-1.16	
	-1.15	
	-1.16	

Table B.3: Field True TDOA Measurements (meters)

Channel	Original	Perpendicular
2	-92.40	3.05
7	-93.54	-6.30
22	-92.80	0.36
26	NO DATA	-0.83

Table B.4: Building 194 Test Area TDOA Measurements (meters)

Position	Rabbit Ears Rotation			Rabbit Ears Long Translation			Wire Long Translation		
	Ch 2	Ch 22	Ch 26	Ch 2	Ch 22	Ch 26	Ch 2	Ch 22	Ch 26
1	-15.46	-134.52	-73.00	-12.82	-135.60	-44.34	-15.58	-150.76	-134.99
	-15.47	-134.63	-73.01	-12.83	-135.54	-44.29	-15.61	-150.61	-134.89
	-15.49	-134.44	-72.99	-12.76	-135.55	-44.21	-15.61	-150.59	
			-61.60						
			-61.59						
2	-15.28	-133.95	-225.14	-14.58	-148.87	-59.75	-15.90	-134.95	-59.35
	-15.31	-133.82	-225.17	-14.57	-148.89	-59.73	-15.91	-134.54	-59.41
	-15.29	-133.96	-225.20	-14.52	-148.95	-59.72	-15.87	-59.40	
						-59.71			
						-59.73			
						-59.71			
						-59.70			
						-59.69			
3	-14.83	-28.78	-60.00	-13.14	-136.22	-73.14	-15.74	-59.70	-59.13
	-14.78	-28.80	-60.00	-13.10	-136.30	-73.19	-15.75	-59.61	-58.94
	-14.77	-28.75	-60.07		-136.25	-73.26	-15.73	-148.95	-58.84
			-60.03						
			-60.03						
			-59.99						
			-60.00						
			-30.02						
4	-89.93	-134.29	-58.18	-77.51	NO	-238.69	-15.89	-329.80	-44.94
	-89.92	-134.24	-58.20	-77.54	DATA	-238.68	-15.87	-329.69	-44.85
	-89.93	-134.23	-58.37	-77.52		-238.71	-15.87	-329.67	
							-15.87		
5	32.23	-150.44	-72.97	-77.44	-149.31	-59.48	-15.25	-239.49	-45.90
	32.15	-150.54	-72.98	-77.37	-149.22	-59.49	-15.22	-239.51	-45.95
	32.16	-150.53	-73.00	-77.32	-149.18	-59.55	-15.24	-239.18	-46.06
6	-29.09	-149.61	-226.10	-76.74	NO	-45.93	-14.97	-315.08	-90.11
	-29.05	-149.53	-226.31	-76.69	DATA	-45.88	-15.00	-315.09	90.08
	-29.04	-149.57	-237.90	-76.65			-14.98	-315.03	-90.16
									-90.11
									-90.08
									-90.10
7	-16.65	NO	-225.86	-88.55	NO	-72.84	-15.36	-119.91	-44.75
	-16.64	DATA	-225.86	-88.58	DATA	-72.87	-15.36	-119.99	-44.93
	-16.64		-225.85	-88.60		-72.99	-15.37	-119.85	-44.94
			-225.94						

Table B.5: Building 194 Perpendicular Test TDOA Measurements (meters)

Channel	TDOA Measurement
2	30.52
	30.50
	30.50
7	28.71
	28.69
	28.67
22	-75.65
	-75.62
	-75.62
	-75.63
	-75.63
	-75.61
26	16.09
	16.19
	16.15

Table B.6: Building 194 True TDOA Measurements (meters)

Channel	Original	Perpendicular
2	-36.90	18.28
7	NO DATA	15.43
22	-37.63	17.44
26	-37.9	17.10

Appendix C. NTSC Analytical Model Generation Code

This appendix contains the core Matlab® code used to create the analytical NTSC Broadcast Signal Model.

Listing C.1: Frame 1 Synchronization Pulses. (appendix3/synchpulses.m)

```
function [waveform, t_rem] = synch_pulses(Fs,t_rem_in,...
    data_vals)
%This will build up the synchronizing sections of the ...
    fields
% Subfunctions are: low_pulses, high_pulses
% Inputs are:
%   Fs = the sampling frequency (Hz)
%   t_rem_in = remaining time (thus far) of signal time, to...
    number of
%              samples
%   data_vals = a structure containing the output values

if nargin==3
    low_pulse = data_vals.low_pulse;
    high_pulse = data_vals.high_pulse;
else
    low_pulse = -200;
    high_pulse = 30;
end

waveform = [];
t_rem = t_rem_in;
for index = 1:6
    [waveform2, t_rem] = low_pulses(Fs, t_rem,low_pulse,...
        high_pulse);
    waveform = [waveform,waveform2];
end
for index = 1:6
    [waveform2, t_rem] = high_pulses(Fs, t_rem,low_pulse,...
        high_pulse);
    waveform = [waveform,waveform2];
end
for index = 1:6
    [waveform2, t_rem] = low_pulses(Fs, t_rem,low_pulse,...
        high_pulse);
```

```
30      waveform = [waveform,waveform2];
    end

    function [waveform, t_rem] = low_pulses(Fs,t_rem_in,...
        low_pulse,high_pulse)
    %start with low part of pulse
35  waveform = [];
    %t = 2.45e-6+t_rem_in;
    t = .04*63.5e-6+t_rem_in;
    num_samps = floor(t*Fs);
    t_rem = mod(t,1/Fs);
40  waveform = [waveform, low_pulse*ones(1,num_samps)];
    %add plateau prior to next pulse
    t=.46*63.5e-6+t_rem;
    num_samps = floor(t*Fs);
    t_rem = mod(t,1/Fs);
45  waveform = [waveform,high_pulse*ones(1,num_samps+1)];

    function [waveform, t_rem] = high_pulses(Fs,t_rem_in,...
        low_pulse,high_pulse)
    waveform = [];
    %start with low part of pulse
50  t=.43*63.5e-6+t_rem_in;
    num_samps = floor(t*Fs);
    t_rem = mod(t,1/Fs);
    waveform = [waveform,low_pulse*ones(1,num_samps)];
    %add plateau prior to next pulse
55  t=.07*63.5e-6+t_rem;
    num_samps = floor(t*Fs);
    t_rem = mod(t,1/Fs);
    waveform = [waveform, high_pulse*ones(1,num_samps)];
```

Listing C.2: Frame 2 Synchronization Pulses. (appendix3/synchpulses2.m)

```
function [waveform, t_rem] = synch_pulses2(Fs,t_rem_in,...
    data_vals)
%This will build up the synchronizing sections of field 2
% it will first add the 1/2 line segment to produce the ...
    shift. It will
% also extend the plateau of the last pulse by 1/2 line to ...
    restore the
% proper time synchronization.
% sub functions are: low_pulses, high_pulses, ...
    half_blanking_line,
%                    half_plateau
% Inputs are:
%   Fs = the sampling frequency (Hz)
%   t_rem_in = remaining time (thus far) of signal time, to...
    number of
%              samples
%   data_vals = a structure containing the output values

if nargin==3
    low_pulse = data_vals.low_pulse;
    high_pulse = data_vals.high_pulse;
    burst_amp = data_vals.burst_amp;
else
    low_pulse = -200;
    high_pulse = 30;
    burst_amp = 110;
end
[waveform, t_rem] = half_blanking_line(Fs, t_rem_in,...
   low_pulse,high_pulse,burst_amp);
for index = 1:6
    [waveform2, t_rem] = low_pulses(Fs, t_rem,low_pulse,...
       high_pulse);
    waveform = [waveform,waveform2];
end
for index = 1:6
    [waveform2, t_rem] = high_pulses(Fs, t_rem,low_pulse,...
       high_pulse);
    waveform = [waveform,waveform2];
end
for index = 1:6
```

```
        [waveform2, t_rem] = low_pulses(Fs, t_rem,low_pulse,...
            high_pulse);
        waveform = [waveform,waveform2];
end
    [waveform2, t_rem] = half_plateau(Fs, t_rem,low_pulse,...
        high_pulse);
    waveform = [waveform,waveform2];

    function [waveform, t_rem] = low_pulses(Fs,t_rem_in,...
        low_pulse,high_pulse)
%start with low part of pulse
    waveform = [];
    %t = 2.45e-6+t_rem_in;
    t = .04*63.5e-6+t_rem_in;
    num_samps = floor(t*Fs);
    t_rem = mod(t,1/Fs);
    waveform = [waveform, low_pulse*ones(1,num_samps)];
    %add plateau prior to next pulse
    t=.46*63.5e-6+t_rem;
    num_samps = floor(t*Fs);
    t_rem = mod(t,1/Fs);
    waveform = [waveform,high_pulse*ones(1,num_samps)];


    function [waveform, t_rem] = high_pulses(Fs,t_rem_in,...
        low_pulse,high_pulse)
waveform = [];
    %start with low part of pulse
    t=.43*63.5e-6+t_rem_in;
    num_samps = floor(t*Fs);
    t_rem = mod(t,1/Fs);
waveform = [waveform,low_pulse*ones(1,num_samps)];
    %add plateau prior to next pulse
    t=.07*63.5e-6+t_rem;
    num_samps = floor(t*Fs);
    t_rem = mod(t,1/Fs);
waveform = [waveform, high_pulse*ones(1,num_samps)];


    function [waveform, t_rem] = half_blanking_line(Fs,t_rem_in...
        ,low_pulse,high_pulse,burst_amp)
    %start with low part of pulse
```

```
waveform = [];
t = .075*63.5e-6+t_rem_in;
num_samps = floor(t*Fs);
t_rem = mod(t,1/Fs);
waveform = [waveform, low_pulse*ones(1,num_samps)];
%add small delay prior to color burst
t = .006*63.5e-6+t_rem;
num_samps = floor(t*Fs);
t_rem = mod(t,1/Fs);
waveform = [waveform,high_pulse*ones(1,num_samps)];
%insert color burst
F = 3.5795e6; %frequency of color burst
t = .048*63.5e-6+t_rem;
num_samps = floor(t*Fs);
phase_offset = t_rem*2*pi;
t_rem = mod(t,1/Fs);
t_vec = [0:num_samps]/Fs;
waveform = [waveform,[burst_amp*sin(2*pi*F*t_vec+...
    phase_offset)+high_pulse]];
%add flat line to end of blanking
t = .368*63.5e-6+t_rem;
num_samps = floor(t*Fs);
t_rem = mod(t,1/Fs);
waveform = [waveform,high_pulse*ones(1,num_samps+3)];

function [waveform, t_rem] = half_plateau(Fs,t_rem_in,...
    low_pulse,high_pulse)
t = .5*63.5e-6+t_rem_in;
num_samps = floor(t*Fs);
t_rem = mod(t,1/Fs);
waveform = high_pulse*ones(1,num_samps);
```

Listing C.3: Picture Line Structure. (appendix3/pictureline.m)

```
function [waveform, t_rem] = pictureline(Fs,t_rem_in,...
    data_vals)
%This function builds the picture line
% It requires the function picturedata.m
% Inputs are:
%   Fs = the sampling frequency (Hz)
%   t_rem_in = remaining time (thus far) of signal time, to...
    number of
%              samples
%   data_vals = a structure containing the output values

if nargin==3
    low_pulse = data_vals.low_pulse;
    high_pulse = data_vals.high_pulse;
    burst_amp = data_vals.burst_amp;
    pic_mean = data_vals.pic_mean;
else
    low_pulse = -200;
    high_pulse = 30;
    burst_amp = 110;
    pic_mean = 230;
end
persistent last_index Pic_Data
if isempty(last_index)
    last_index = 0;
end

%start with low part of pulse
waveform = [];
t = .075*63.5e-6+t_rem_in;
num_samps = floor(t*Fs);
t_rem = mod(t,1/Fs);
waveform = [waveform, low_pulse*ones(1,num_samps)];
%add small delay prior to color burst
t = .006*63.5e-6+t_rem;
num_samps = floor(t*Fs);
t_rem = mod(t,1/Fs);
waveform = [waveform,high_pulse*ones(1,num_samps)];
%insert color burst
F = 3.5795e6; %frequency of color burst
t = .048*63.5e-6+t_rem;
```

```
40 num_samps = floor(t*Fs);
   phase_offset = t_rem*2*pi;
   t_rem = mod(t,1/Fs);
   t_vec = [0:num_samps]/Fs;
   waveform = [waveform,[burst_amp*sin(2*pi*F*t_vec+...
      phase_offset)+high_pulse]];
45 %add delay prior to picture information
   t=.02*63.5e-6+t_rem;
   num_samps = floor(t*Fs);
   t_rem = mod(t,1/Fs);
   waveform = [waveform,high_pulse*ones(1,num_samps)];
50 %add picture information
   t=0.831*63.5e-6+t_rem;
   num_samps = floor(t*Fs);
   t_rem = mod(t,1/Fs);

55 if last_index+num_samps>length(Pic_Data)
       %not enough sample points, must append to the array!
       [last_index, Pic_Data]=picturedata(Fs,last_index,...
          Pic_Data);
   end

60 first_index = last_index+1;
   last_index=last_index+num_samps;

   waveform=[waveform,Pic_Data(first_index:last_index)'+...
      pic_mean];

65 %add small portion after picture information
   t=.02*63.5e-6+t_rem;
   num_samps = floor(t*Fs);
   t_rem = mod(t,1/Fs);
   waveform = [waveform,high_pulse*ones(1,num_samps)];
```

Listing C.4: Time Correlated Picture Information for Picture Line. (appendix3/picturedata.m)

```
function [last_index, Picture_Data] = picture_data(Fs, ...
    prev_index, prev_data, data_vals)
%This function will append more samples to the picture ...
    information vector and trim
%out the 'old stuff'
% It requires the simulink model 'TV_picture.mdl'
% Inputs are
%   Fs = sampling frequency (Hz)
%   prev_index = the index where the last use of picture ...
    information
%                stopped (in the prev_data array)
%   prev_data = the picture information vector as it is now...
    (to be extended
%                and old stuff trimmed from)
%   data_vals = the structure containing the necessary ...
    data_values
if nargin==4
    rand_strength = data_vals.rand_strength;
else
    rand_strength = 155e7;
end

h = msgbox('Generating Picture Data');
t=0.639*63.5e-6;
num_samps = floor(t*Fs)*525;
Rand_vector_local = 1*155e7*randn(1,num_samps)';
t_vec = [1/Fs:1/Fs:(num_samps)/Fs];
Rand_vector_local = [t_vec',Rand_vector_local];
%requires a method of generating First-order Gauss-Markov
%Simulink model used (and called) here
assignin('base','Rand_vector',Rand_vector_local)
sim('TV_picture',t_vec);
Picture_Data = [prev_data(prev_index+1:end);Picture_Data];
last_index = 0;
try
    close(h) %if the generating data window is open, it ...
        will close it. If closed, will not stop execution.
catch
end
```

Listing C.5: Blanking Line. (appendix3/blankingline.m)

```
function [waveform, t_rem] = blanking_line(Fs,t_rem_in,...
    data_vals)
%This function builds the blanking line
% Inputs are:
%   Fs = the sampling frequency (Hz)
%   t_rem_in = remaining time (thus far) of signal time, to... number of
%              samples
%   data_vals = a structure containing the output values

if nargin==3
    low_pulse = data_vals.low_pulse;
    high_pulse = data_vals.high_pulse;
    burst_amp = data_vals.burst_amp;
else
    low_pulse = -200;
    high_pulse = 30;
    burst_amp = 110;
end
%start with low part of pulse
waveform = [];
t = .075*63.5e-6+t_rem_in;
num_samps = floor(t*Fs);
t_rem = mod(t,1/Fs);
waveform = [waveform, low_pulse*ones(1,num_samps)];
%add small delay prior to color burst
t = .006*63.5e-6+t_rem;
num_samps = floor(t*Fs);
t_rem = mod(t,1/Fs);
waveform = [waveform,high_pulse*ones(1,num_samps)];
%insert color burst
F = 3.5795e6; %frequency of color burst
t = .048*63.5e-6+t_rem;
num_samps = floor(t*Fs);
phase_offset = t_rem*2*pi;
t_rem = mod(t,1/Fs);
t_vec = [0:num_samps]/Fs;
waveform = [waveform,[burst_amp*sin(2*pi*F*t_vec+...
    phase_offset)+high_pulse];
%add flat line to end of blanking
t = .871*63.5e-6+t_rem;
```

```
    num_samps = floor(t*Fs);
40  t_rem = mod(t,1/Fs);
    waveform = [waveform, high_pulse*ones(1,num_samps-1)];
```

Bibliography

1. E. Hepsaydir, "Mobile positioning in cdma cellular networks," in *Vehicular Technology Conference*, vol. 2. IEEE, Fall 1999, pp. 795–799.
2. W. Connelly, "Telenav: A precision navigation system based upon television signal reception," *Navigation: Journal of The Institute of Navigation*, vol. 33, no. 2, pp. 109–122, Summer 1986.
3. R. Prasad and T. Ojanpera, "An overview of cdma evolution toward wideband cdma," *IEEE Communications Surveys*, vol. 1, no. 1, pp. 2–29, 1998.
4. K. B. Benson, *Television Engineering Handbook*. New York: McGraw-Hill Book Company, Inc, 1985.
5. P. Misra and P. Enge, *Global Positioning System: Signals, Measurements, and Performance*. Massachusetts: Ganga-Jamuna Press, 2001.
6. G. M. Siouris, *Aerospace Avionics Systems, A Modern Synthesis*. San Diego, California: Academic Press, Inc, 1993.
7. A. Brown, D. Reynolds, D. Roberts, and S. Serie, "Jammer and interference location system - design and initial test results," in *Proceedings of the ION GPS '99*. ION, September 1999, pp. 137–142.
8. J. M. Beukers, "Loran-c system characterization," Wild Goose Association (currently the International Loran Association (ILA)), Tech. Rep. 1, Septempber 1976.
9. I. Jami, M. Ali, and R. F. Ormondroyd, "Comparison of methods of locating and tracking cellular mobiles," *IEE Colloquium on Novel Methods of Location and Tracking of Cellular Mobiles and Their System Applications*, vol. 1999/046, pp. 1/1–1/6, 1999.
10. L. Cong and W. Zhuang, "Hybrid tdoa/aoa mobile user location for wideband cdma systems," *IEEE Transactions on Wireless Communications*, vol. 1, pp. 439–447, July 2002.
11. D. Adamy, *EW 101: A First Course in Electonic Warfare*. Norwood, Massachusetts: Artech House, 2001.
12. N. Thomas, D. Cruickshank, and D. Lauernson, "Performance of a tdoa-aoa hybrid mobile location system," in *Second International Conference on 3G Mobile Communication Technologies*, March 2001, pp. 216–220.
13. N. Thomas and D. Cruickshank, "A passive mobile location system for umts," *UMTS Terminals and Software Radio, IEE Colloquium on*, pp. 10/1–10/6, April 1999.

14. P. J. Bennett, "The use of digital map data for airborne operations," *IEE Colloquium on Serious Low Flying*, pp. 2/1–2/10, February 1998.

15. P. S. Maybeck, *Stochastic Models, Estimation and Control*, R. Bellman, Ed. Arlington VA: Navtech Book and Software Store, 1994, vol. 1.

16. P. Oxley, "Terrain following and terrain avoidance algorithms," *IEE Colloquium on Navigation, Guidance and Control on Aerospace*, pp. 2/1–2/3, November 1989.

17. L. Coelho and M. Campos, "Pose estimation of autonomous dirigibles using artificial landmarks," in *Proceedings of the XII Brazillian Symposium on Computer Graphics and Image Processing*, 1999, pp. 161–170.

18. J. F. Raquet and M. Giebner, "Navigation using optical measurements fo objects and unknown locations," in *Proceedings of the ION 59th Annual Meeting*. ION, June 2003.

19. A. Yasuda, W. Wei, P. Zhu, K. Yamashita, and M. Kawamura, "Positioning system using tv broadcasting from geostationary satellites," in *Proceedings of the 1994 IEEE National Telesystems Conference*. IEEE, 1994, pp. 107–110.

20. M. Rabinowitz and J. James J. Spilker, "A new positioning system using television synchronization signals," March 2003.

21. M. Rabinowitz and J. James J. Spilker, "The rosum technology television positioning technology," in *Proceedings of the ION 59th Annual Meeting/CIGTF 22nd Guidance Test Symposium*. ION, June 2003.

22. H. Torii and Y. Takechi, "Vehicle location using gps in urban areas," in *Proceedings of the ION GPS '92*. ION, 1992, pp. 1153–1158.

23. E. Molloy and W. Pannett, *Radio and Television Engineers' Reference Book*. London: George Newnes Limited, 1955.

24. S. Amos and D. Birkinshaw, *TELEVISION ENGINEERING Principles and Practices*. London: Iliffe and Sons, Ltd., 1953, vol. 1.

25. G. M. Glasford, *Fundamentals of Television Engineering*, F. E. Terman, Ed. New York: McGraw-Hill Book Company, Inc, 1955.

26. K. A. Fisher, "Signals to navigate and their exploitation," Air Force Institute of Technology, Tech. Rep., December 2002.

27. B. Sklar, *Digital Communications*. New Jersey: Prentice Hall, 2001.

28. K. Shanmugan and A. Breipohl, *Random Signals: Detection,Estimation and Data Analysis*. New York: John Wiley and Sons, Inc, 1988.

29. A. El-Saigh and R. Macario, "A review of anti-multipath techniques, past and present," in *IEE Colloquium on Multipath Countermeasures*. IEE, May 1996, pp. 2/1–2/6.

30. A. Burr, "The multipath problem: An overview," in *IEE Colloquium on Multipath Countermeasures*. IEE, May 1996, pp. 1/1–1/7.

31. M. Bucher, "Simulation of multipath fading/ghosting for analog and digital television transmission in broadcast channels," in *IEEE Transactions on Broadcasting*, vol. 38. IEEE, Dec 1992, pp. 256–262.

32. R. Grosskopf, "Field strength prediction in the vhf and uhf range including multipath propagation," in *Seventh Internation Conference on Antennas and Propagation*, vol. 2. IEE, Apr 1991, pp. 965–967.

33. Y. Horiki and E. Walton, "A study of automatic null steering for suppression of ghosts in tv reception," in *Antennas and Propagation Society International Symposium*, vol. 2. IEEE, 2002, pp. 116–119.

34. R. Eggert, J. Gutierrez, and J. Raquet, "Code and phase multipath characterization for beam-steering receivers," in *Proceedings of the ION NTM '04*. ION, Jan 2004.

35. R. Sherratt, "Identification and minimization of iir tap coefficients for the cancellation of complex multipath in terrestrial television," in *IEEE Transactions on Circuits and Systems for Video Technology*, vol. 6. IEEE, Dec 1996, pp. 703–706.

36. J. Lourens and W. de Waal, "On the tv ghost image model," in *IEEE Transactions on Broadcasting*, vol. 40. IEEE, Sep 1994, pp. 125–131.

37. E. P. Cunningham, *Digital Filtering: An Introduction*. John Wiley and Sons, Inc., 1995.

38. S. K. Mitra, *Digital Signal Processing, A Computer Based Approach*, 2nd ed. McGraw-Hill, 2001.

39. J. M. Anderson, M. A. Temple, W. M. Brown, and B. L. Crossley, "A nonlinear suppression technique for range ambiguity resolution in pulse doppler radars," in *Proceedings of the 2001 IEEE National Radar Conference*. Atlanta, GA: IEEE, May 2001, pp. 141–146.

REPORT DOCUMENTATION PAGE	Form Approved OMB No. 074-0188

1. REPORT DATE *(DD-MM-YYYY)*	2. REPORT TYPE	3. DATES COVERED *(From – To)*
23-03-2004	Master's Thesis	Feb 2003 – Mar 2004

4. TITLE AND SUBTITLE
EVALUATING THE NAVIGATION POTENTIAL OF THE NATIONAL TELEVISION SYSTEM COMMITTEE BROADCAST SIGNAL

5a. CONTRACT NUMBER

5b. GRANT NUMBER

5c. PROGRAM ELEMENT NUMBER

6. AUTHOR(S)

Eggert, Ryan J., 2d Lt, USAF

5d. PROJECT NUMBER

5e. TASK NUMBER

5f. WORK UNIT NUMBER

7. PERFORMING ORGANIZATION NAMES(S) AND ADDRESS(S)

Air Force Institute of Technology
Graduate School of Engineering and Management (AFIT/EN)
2950 Hobson Way, Building 640
WPAFB OH 45433-7765

8. PERFORMING ORGANIZATION REPORT NUMBER

AFIT/GE/ENG/04-08

9. SPONSORING/MONITORING AGENCY NAME(S) AND ADDRESS(ES)

AFRL/MNGI
Virgil E. Zetterlind, 1st Lt
101 West Eglin Parkway
EGLIN AFB, FL 32542 (850) 882-3946 x2360
VIRGIL.ZETTERLIND@EGLIN.AF.MIL

10. SPONSOR/MONITOR'S ACRONYM(S)

11. SPONSOR/MONITOR'S REPORT NUMBER(S)

12. DISTRIBUTION/AVAILABILITY STATEMENT
APPROVED FOR PUBLIC RELEASE; DISTRIBUTION UNLIMITED

13. SUPPLEMENTARY NOTES

14. ABSTRACT

The accuracy and worldwide availability of the Global Positioning System (GPS) make it the dominant system for navigation and precise positioning. Unfortunately, many situations arise in which GPS may not be adequate, e.g., urban navigation. This research evaluates the navigation potential of the National Television System Committee (NTSC) broadcast signal using a time-difference-of-arrival (TDOA) algorithm. TDOA measurements are made using NTSC broadcast signals collected from low and high multipath environments. These measurements are then used to evaluate the severity and dynamic effects of NTSC broadcast multipath signals. Three data reduction algorithms were developed--one that modifies the classical cross-correlation TDOA approach, and two that difference the signals' time-of-arrival at each receiver. Each algorithm was evaluated for consistency and accuracy in each environment. Multipath mitigation was demonstrated using a locally fabricated antenna.

Collected NTSC broadcast signal samples reveal TDOA measurement errors ranging from 1 to 200 meters, with typical errors between 10 and 40 meters. Multipath was shown to be the dominant error source. However, errors due to the particular hardware configuration used in this research were also significant. Simple multipath mitigation techniques were able to reduce these errors, and analyses of the received waveforms provide the foundation for developing additional active multipath mitigation techniques.

Simulations using eight television station locations near Dayton, Ohio reveal 40 meter position accuracy with the typical range errors found in this research. Extreme measurement errors from high multipath areas reduced this accuracy to 100 meters. Additionally, using the same transmitter geometry, simulation results showed that TDOA measurement accuracies of 5 to 10 meters were required to provide position estimates with 10 meter accuracy--the accuracy of readily available single frequency GPS receivers.

15. SUBJECT TERMS
Surface Navigation, TDOA Navigation, Radio Navigation, Position Finding, TDOA, Multipath Transmission, NTSC, Television Systems, Indoor Navigation

16. SECURITY CLASSIFICATION OF:			17. LIMITATION OF ABSTRACT	18. NUMBER OF PAGES	19a. NAME OF RESPONSIBLE PERSON
REPORT	ABSTRACT	c. THIS PAGE			Dr. John F. Raquet, AFIT/ENG
U	U	U	UU	150	19b. TELEPHONE NUMBER *(Include area code)* (937) 255-6565, ext 4580; e-mail: john.raquet@afit.edu

Standard Form 298 (Rev: 8-98)
Prescribed by ANSI Std. Z39-18